



PhD-FSTC-2018-65
The Faculty of Sciences, Technology and Communication

DISSERTATION

Defence held on 18/10/2018 in Luxembourg

to obtain the degree of

DOCTEUR DE L'UNIVERSITÉ DU LUXEMBOURG

EN PHYSIQUE

by

Patrick Seamus HAUGHIAN

Born on 4 February 1992 in Troisdorf (Germany)

TRANSPORT AND THERMODYNAMICS
IN DRIVEN QUANTUM SYSTEMS

Dissertation defence committee

Dr Thomas Schmidt, dissertation supervisor
Associate Professor, Université du Luxembourg

Dr Christoph Bruder, Vice Chairman
Professor, Universität Basel

Dr Andreas Michels, Chairman
Associate Professor, Université du Luxembourg

Dr Andreas Nunnenkamp
Royal Society Research Fellow, University of Cambridge

Dr Massimiliano Esposito
Professor, Université du Luxembourg

Abstract

This thesis studies the nonequilibrium properties of quantum dots with regard to electrical conduction as well as thermodynamics. The work documented here shows how these properties behave under the influence of time-dependent drive protocols, pursuing two main lines of inquiry. The first concerns the interplay between nanomechanics and drive: In nanomechanical systems with strong coupling between the charge and vibrational sectors, conductance is strongly suppressed, an effect known as Franck-Condon blockade. Using a model Hamiltonian for a molecular quantum dot coupled to a pair of leads, it is shown here that this blockade can be exponentially lifted by resonantly driving the dot. Moreover, a multi-drive protocol is proposed for such a system to facilitate charge pumping that enjoys the same exponential amplification. The second line of inquiry moves beyond charge transport, examining the thermodynamics of a driven quantum dot coupled to a lead. Taking a Green's function approach, it is found that the laws of thermodynamics can be formulated for arbitrary dot-lead coupling strength in the presence of dot and coupling drive, as long as the drive protocol only exhibits mild non-adiabaticity. Finally, the effects of initial states are studied in this situation, proving that the integrated work production in the long-time limit conforms to the second law of thermodynamics for a wide class of initial states and arbitrary drive and coupling strength.

Contents

Introduction	3
1 Background and methods	6
1.1 Molecular quantum dots	6
1.2 Non-equilibrium Green's functions	10
1.2.1 Keldysh technique	10
1.2.2 Occupation of a single level coupled to a lead	13
1.2.3 From Keldysh to current	21
1.3 Floquet expansion for driven systems	25
1.4 Open quantum systems and master equations	27
1.4.1 From von Neumann to Lindblad	27
1.4.2 A note on Markovianity	29
1.5 Quantum thermodynamics: An overview	32
1.5.1 Open quantum systems and weak-coupling thermodynamics	33
1.5.2 Stochastic thermodynamics	34
1.5.3 Hamiltonians of mean force	36
2 Results	38
2.1 Lifting the Franck-Condon blockade in carbon nanotube quantum dots	38
2.1.1 Introduction	38
2.1.2 Model	40
2.1.3 Polaron tunneling approximation	43
2.1.4 Born-Markov analysis	49
2.1.5 Conclusion	55
2.1.6 Appendix: Details on the NEGF approach	57
2.1.7 Appendix: Tunneling rates for Fock vibron state	60
2.2 Charge pumping in strongly coupled molecular quantum dots	62
2.2.1 Introduction	62
2.2.2 Model	63
2.2.3 Floquet Green's functions	65
2.2.4 Current under bias	68
2.2.5 Polaron pumping	69

2.2.6	Conclusion	73
2.2.7	Appendix: Bare Green's functions	74
2.2.8	Appendix: Self-energy	76
2.3	Quantum thermodynamics of the resonant-level model with driven system-bath coupling	77
2.3.1	Introduction	77
2.3.2	Resonant-level model	79
2.3.3	Thermodynamic definitions and first law	82
2.3.4	Link to equilibrium	83
2.3.5	Second law	85
2.3.6	Comparison with exact numerical results	87
2.3.7	Conclusions	88
2.3.8	Appendix: Adiabatic limit	90
2.3.9	Appendix: Quasi-adiabatic expansion	91
2.4	Initial states in quantum thermodynamics	93
2.4.1	Introduction	93
2.4.2	Model	94
2.4.3	Work production	96
2.4.4	Long-time limit	98
2.4.5	Conclusion	99
2.4.6	Appendix: Expectation values	100
3	Summary	104
	Bibliography	107
	Acknowledgments	121
	List of publications	122

Introduction

In one way or another, transport physics serves as the foundation for much of modern civilization. Technical processes and machines that depend on precise engineering of electrical, heat and matter currents are innumerable, and the ever-increasing sophistication of tomorrow's technology relies upon today's research. Among the many aspects of the theory of transport, the ones under investigation in this thesis are those connected with the quantum regime and thermodynamics.

Quantum mechanics is the blockbuster discovery of 20th century physics: It has revolutionized our understanding of the microscopic world, and its implications reach far beyond academic studies, into everyday life. What started out as an attempt by Planck to understand black-body radiation [1] has since evolved into a comprehensive theory, leading to a torrent of inventions such as the laser, the transistor, and modern medical imaging, just to name three. The sub-field of condensed matter physics, which has as its subject the study of interacting quantum many-particle systems, has proven to be particularly fruitful in terms of applications to engineering and materials science. In the evolution of modern condensed matter physics, two convergent directions have been apparent: On the one hand, with increasing development of the theory and powerful computational tools, our conceptual understanding of quantum systems has grown to include ever more complex and large many-particle systems. On the other hand, the evolution of our experimental capabilities have afforded us more and more precise control over ever smaller objects, even down to single-atom devices [2]. These developments have converged to form the burgeoning field of nanoscale physics, where quantum theory, simulation, and experiments are used in concert to build the devices of the future. Some of these devices have already reshaped the technology of the present: Decades of miniaturization efforts have placed the current state of transistor development firmly into the nanoscale, and modern solar cells and LEDs would be unthinkable without knowledge of nanoscale physics. The nanoscale is home to a remarkable wealth of phenomenology, including electronics as well as optical and mechanical effects, all of which may interact in ways too numerous to list. Equipped with such a large toolkit, the research directions available to today's nanoscientists are as boundless as the possible technologies that may grow from their work.

The beginnings of thermodynamics lie further in the past [3] than those of quantum mechanics. Developed in the 19th century as a framework for the under-

standing of heat, work, temperature and energy, thermodynamics is invaluable in the design of machines and work cycles and provided the scientific underpinning of the industrial revolution. Its laws were first formulated in a phenomenological manner, without reference to any microscopic theory. Even though it was later understood to arise from statistical mechanics in the limit of large particle number, this limit lies on the scale of Avogadro's constant $N_A \approx 6 \times 10^{23}$, and therefore classical thermodynamics cannot be expected to hold at all scales. Nonetheless, thermodynamics and its laws have long since become a mainstay not only in engineering and physics, but also in computer science, where the theory of information makes extensive use of entropy and related concepts [4, 5, 6].

Fluxes and currents are natural objects in thermodynamics. Therefore, the connections between transport theory and thermodynamics, such as the effect of current flowing as a result of temperature gradients [7], have been explored early on. The path between thermodynamics and quantum mechanics is far less traveled: Since the former has its classical applications in macroscopic systems, and the domain of the latter are chiefly microscopic systems, a vast difference in scale has kept the two theories relatively separated, with only occasional historical overlap, such as the early proposal for a quantum engine [8] and the analysis of thermodynamics in a certain class of open systems [9].

In recent decades, the advent of nanoscale physics has led to a change in perspective: The range of device sizes accessible in experiments has been extended down to a regime where quantum effects are paramount. These devices hold great promise in many regards, such as the miniaturization of electronic components, the design of innovative measurement schemes and quantum machines, as well as in the context of quantum computation. Heat production has emerged as a serious bottleneck for the performance of these systems, and so a consistent theory of quantum thermodynamics has become extremely desirable. Such a theory would need to re-formulate the laws of thermodynamics for quantum systems while as much as possible of the generality of their classical counterpart. Moreover, due to the prominence of non-stationary effects at the nanoscale, quantum thermodynamics needs to remain valid far from the equilibrium or adiabatic settings common in macroscopic settings. Considerable progress has already been achieved in this endeavor, both in terms of conceptual foundations, and regarding the behavior of certain model systems, but an overarching framework is still lacking.

The work documented in this thesis is performed on the frontier of nanoscale physics, at the confluence of fields of transport theory, quantum mechanics, and thermodynamics. The presentation is structured as two parts: First, Ch. 1 is used to lay out the methods and provide context for the research to be viewed in. Second, the results are laid out in Ch. 2. The beginning of the expository chapter gives a short historical overview of the relevant nanodevices in Sec. 1.1. There, the focus lies on quantum dots, meso- or nanoscale structures that combine the quantized energy structure of quantum systems with the ability to be integrated into electrical circuits. Systems of this kind provide a versatile platform for device development and are studied under various aspects in the remainder of this work. Next, the meth-

ods used to this end are laid out in Secs. 1.2 to 1.4. The exposition concludes in Sec. 1.5 with a sketch of the current state of quantum thermodynamics and the challenges that still need to be addressed. The first two sections of the results concern themselves with using time-dependent driving potentials to manipulate the electric transport through a strongly coupled nanomechanical quantum dot: In Sec. 2.1 it is shown that by driving the quantum dot resonantly with its vibrational mode, its conductance can be increased exponentially, thus lifting the transport blockade inherent in strongly coupled electromechanical systems. Then, in Sec. 2.2, a more complex drive protocol is proposed to pump charge in either direction across such a nanomechanical quantum dot. It is shown that the current pumped in this way also enjoys the exponential amplification discovered in the previous section. The third and fourth result sections are devoted to quantum thermodynamics: Sec. 2.3 shows how to use nonequilibrium Green's functions to establish the laws of thermodynamics in a model of a quantum dot coupled with arbitrary strength to a metallic lead, subject to a multi-drive protocol. Lastly, Sec. 2.4 adds the initial state of the setup to the consideration, and links the quantum thermodynamics of such a model system with the general framework of stochastic thermodynamics. This connection is used to show that the work produced under a general drive protocol behaves according to the second law of thermodynamics for a wide class of initial states, as long as the long-time limit is considered. Finally, a summary discussion is provided in Ch. 3, reviewing the documented findings and pointing out directions for future research.

Chapter 1

Background and methods

1.1 Molecular quantum dots

Quantum dots are mesoscopic structures with individually spaced energy levels. A plethora of different implementations of such systems have emerged over the past decades, with applications ranging from display technology [10] over medical imaging [11] to proposals for quantum computation [12].

This thesis concerns itself with the transport properties of quantum dots. Since our results build upon many years' worth of insight obtained previously, this chapter will be used to give an outline of this body of knowledge.

The physics of quantum dots has its beginning in the study of semiconductor nanocrystals [13, 14], where individual quantum states can be examined even in systems consisting of several thousand atoms. Their properties are evocative of zero-dimensional quantum systems, hence the name *quantum dot*. The optical and electronic features of quantum dots were soon realized and spurred a flurry of research. This led to the development of various platforms to realize quantum dots, as well as various ways of embedding them into electrical circuits, thus bringing into focus their conductive properties [15]. In order to probe the conductance of a quantum dot, it is connected to a number of leads, across which voltages can be applied. A schematic representation of such a setup is given in Fig. 1.1. The physics that manifests in such a setup strongly depends on its parameters and energy scales [16]. These include the lead temperature T , the applied potentials V_α , the tunneling rates Γ_α between the dot and the leads, as well as the internal properties of the lead, such as its quantum level spacing Δ and the strength of the interaction between electrons on the dot. Signatures of the quantization of the energies on the dot can only be observed if these energies are spaced sufficiently far apart, in particular further than typical thermal fluctuations in energy. This dictates the condition $\Delta > k_B T$, where k_B denotes the Boltzmann constant. Moreover, the level spacing Δ needs to be compared to the tunneling rates Γ_α . The case $\Delta \gg \Gamma_\alpha$ is known as weak coupling. In this case, the energy levels on the dot still exhibit clear peak signatures, with a width on the scale of Γ acquired by hybridization to the energies in the

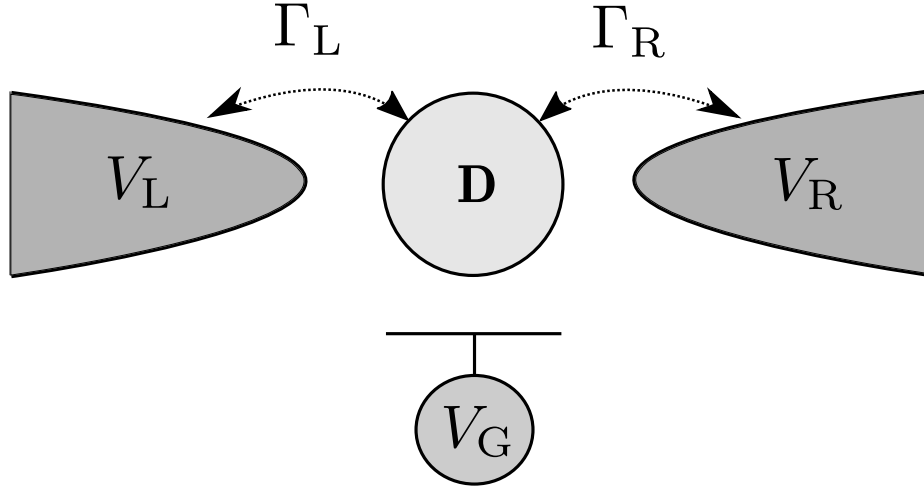


Figure 1.1: Quantum dot (D) connected to a pair of leads at the respective potentials V_L and V_R . The tunneling rates into the leads are given by Γ_L and Γ_R , respectively. The potential of the dot can be tuned by means of the gate voltage V_G .

lead. The transport physics of this configuration is well-established [17, 16, 18]; the features most relevant to this thesis will be outlined below, largely following [15].

As a result of the small tunneling rates, electrons can “hop” and populate localized states on the dot. Because of Coulomb repulsion among the dot electrons, as well as potential jumps in the single particle spectrum of the dot, this hopping requires energy. Neglecting the latter contribution, one obtains an approximating charging energy of $E_C = e^2/(2C)$, with the elementary charge e , and C denoting the capacitance of the dot. For these individual charge number states to be well-separated, it is required that $E_C \gg k_B T$, which for most semiconductor setups corresponds to the sub-1K regime. For the setup from Fig. 1.1, it can be shown that, in this regime, electron transport only occurs if there are available states on the dot within the energy window defined by the bias $V_L - V_R$. Since the dot energy levels can be moved by changing the gate voltage V_G , the conductance of the dot can be described by a diagram of the type seen in Fig. 1.2. The resulting pattern is referred to as *Coulomb diamonds* and is understood as follows: If there is no dot state available in the bias window, no conduction occurs, and the electron number on the dot is fixed to a constant N . By increasing the bias (y axis), the window expands and eventually comes to include a level so that current can flow. Alternatively, changes in the gate voltage (x axis) may move a level into the window. In the semi-classical *constant-interaction model* [19], the charging energy does not vary

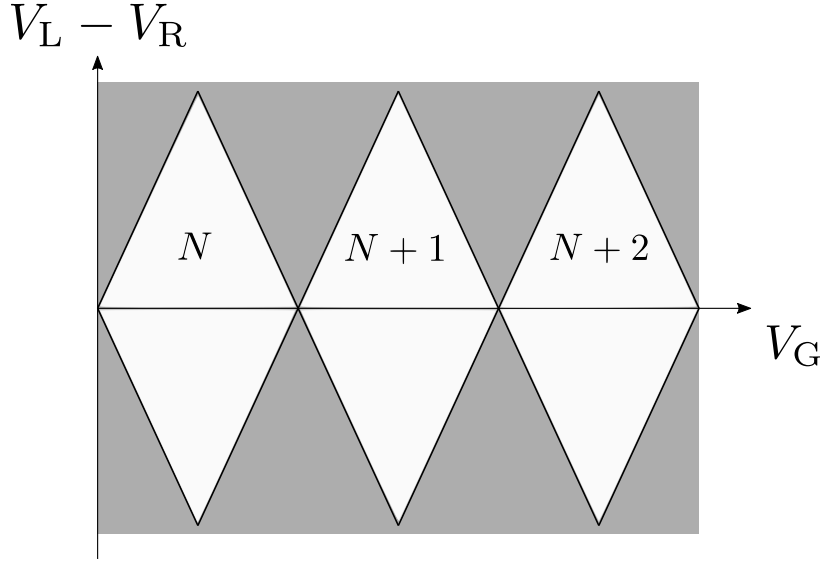


Figure 1.2: Conductance of the setup from Fig. 1.1 as a function of the bias and gate voltages, assuming equally spaced energy levels on the quantum dot. The non-conducting regions, distinguished by constant particle number on the dot and the lack of a dot energy level within the bias window of size $V_L - V_R$, are indicated in white. The pattern formed in this way is known as Coulomb diamonds.

as a function of the dot electron number and any further structure resulting from the internal level spacing Δ is ignored. Using this approximation, the conductance pattern is periodic as in Fig. 1.2.

More realistic theories have been developed to take into account a wide variety of further effects, such as asymmetry in the coupling, the influence of higher electronic states, as well as strong-coupling effects and a more sophisticated treatment of electron interaction. Moreover, the physics of quantum dots is not limited to purely electronic phenomena: As in any material, charge on a quantum dot may couple to its vibrations. This is of particular importance in single-molecule junctions [20, 21, 22, 23] and other strongly vibrating quantum dot platforms such as carbon nanotubes [24, 25]. Novel fabrication techniques have been developed for some quantum dots, which allow a precise tuning of the coupling between vibrational modes and the charge sector [26]. In this way, the rich physics of nano-electromechanical systems (NEMS) has become more experimentally accessible, opening up a path to various applications such as innovative sensor design and data processing schemes [27].

Charge transport through NEMS is strongly dependent of the vibrational degrees of freedom of the device in question. In particular, tunneling processes that excite vibrations may be favored compared to purely electronic transitions. These

manifest in vibrational sidebands in the Coulomb diamond pattern which contain information about the vibrational modes of the quantum dot and their coupling to the charge sector. Furthermore, strong electromechanical coupling leads to exponential suppression of purely electronic tunneling, a phenomenon termed Franck-Condon blockade. It has been observed in experiments with single-molecule junctions [28, 29] and carbon nanotubes [30]. A great variety of theoretical work on these systems has been performed as well, on both nanotubes [31, 32, 33] and single-molecule junctions [20, 21, 22, 23, 34, 35], exploring the vibrational spectrum, the conductance, and the transfer statistics of such devices. The novel contribution presented in this thesis concerns the interplay between these electromechanical effects and time-dependent drive, documented in Secs. 2.1 and 2.2.

Quantum dots also can be used as a platform for nanoscale heat engines, considering that they do not suffer from the miniaturization issues of other techniques and can be operated at high efficiency [36, 37]. Specifically, a quantum dot connected between two reservoirs may enable particle and heat flow across a bias as a function of temperature gradients [38, 39, 37]. Setups of this kind hold promise for purposes of cooling nanoscale electronics and for harvesting energy in solar cells. Secs. 2.3 and 2.4 of this thesis use a model system to examine the thermodynamics of quantum dots, taking into account non-stationary and strong-coupling effects.

1.2 Non-equilibrium Green's functions

In this chapter, we give an overview of the nonequilibrium Green's function technique, which is the main tool employed in our work. The use of Green's functions in quantum theory provides a systematic way of relating the known dynamics of a non-interacting system to those in the presence of an interaction.

Generally speaking, a *Green's function* is a particular solution to a given boundary value problem for a differential operator, which can be used to construct solutions to this problem given arbitrary source terms. In the context of the quantum theory of many-particle systems, the term is used to describe certain expectation values of the operators used to model that system. These expectation values are found to solve equations of motion and can be used as building blocks for the full dynamics of the system, and the observables associated with it. [40]

1.2.1 Keldysh technique

Originally applied to systems in equilibrium only, the Green's function formalism can be modified to treat nonequilibrium settings as well [41]. This version of the formalism is commonly referred to as *nonequilibrium Green's function (NEGF) technique*, or *Keldysh formalism*. In the following, we give an introduction to the formalism, as far as it will be used in the remainder of this thesis. Our main reference in doing so is the recent review article [42]; other comprehensive accounts of the topic include the textbooks [43, 44, 45].

Let us consider an arbitrary quantum system, the state of which at time t is described by its density matrix $\rho(t)$. The time evolution of ρ is governed by the system Hamiltonian H in accordance with the von Neumann equation

$$\partial_t \rho(t) = -i[H, \rho(t)]. \quad (1.1)$$

Here and throughout this thesis, we set $\hbar = k_B = 1$. The equation can be formally solved by writing

$$\rho(t) = U(t, t_0) \rho(t_0) U^\dagger(t, t_0), \quad (1.2)$$

where t_0 denotes some initial time, and $U(t, t_0)$ is called the *evolution operator* or *propagator*, which solves the Schrödinger equation

$$\begin{cases} i\partial_t U(t, t_0) &= H U(t, t_0) \quad \forall t > t_0 \\ U(t_0, t_0) &= 1. \end{cases} \quad (1.3)$$

Next, we introduce an operator O whose expectation value we want to calculate. Choosing the Schrödinger picture, we assume the operator to be time-independent, with the entire time-dependence of the system encoded in the density matrix. The desired expectation value is defined as a trace,

$$\begin{aligned} \langle O(t) \rangle &\equiv \text{tr} [\rho(t) O] = \text{tr} [U(t, t_0) \rho(t_0) U^\dagger(t, t_0) O] \\ &= \text{tr} [\rho(t_0) U^\dagger(t, t_0) O U(t, t_0)] = \text{tr} [\rho(t_0) O_H(t)], \end{aligned} \quad (1.4)$$

making use of the cyclicity of the trace operation. In the last step we introduced the Heisenberg picture, where any time dependence is absorbed into the operator,

$$O_H(t) \equiv U^\dagger(t, t_0) O U(t, t_0). \quad (1.5)$$

Analogously, for a pair of Heisenberg operators, we define the expectation value

$$\langle A(t) B(t') \rangle \equiv \langle A_H(t) B_H(t') \rangle = \text{tr}[\rho(t_0) U^\dagger(t, t_0) A U(t, t') B U(t', t_0)], \quad (1.6)$$

making use of the group property of the propagator, $U(t, t_0) U^\dagger(t', t_0) = U(t, t')$. $\langle A(t) B(t') \rangle$ is also referred to as the correlator of $A(t)$ and $B(t')$, without explicit mention of the Heisenberg picture.

As our goal is to describe interaction effects, we write the Hamiltonian as

$$H = H_0 + V(t), \quad (1.7)$$

with a bare Hamiltonian H_0 , and a possibly time-dependent interaction Hamiltonian $V(t)$. In this setting, it will prove convenient to use the interaction picture, i.e. to absorb only the time dependence induced by the bare Hamiltonian into the operators,

$$\hat{O}(t) = e^{iH_0(t-t_0)} O e^{-iH_0(t-t_0)}. \quad (1.8)$$

In the following, we will indicate operators in the interaction picture with a hat. The expectation value is then written as

$$\langle O(t) \rangle = \text{tr}[\rho(t_0) S^\dagger(t, t_0) \hat{O}(t) S(t, t_0)], \quad (1.9)$$

with the S-matrix (or scattering matrix) operator $S(t, t_0) = e^{iH_0(t-t_0)} U(t, t_0)$ obeying a Schrödinger equation that only features the interaction Hamiltonian,

$$i\partial_t S(t, t_0) = \hat{V}(t) S(t, t_0). \quad (1.10)$$

This equation can be solved by introducing the time-ordered exponential

$$S(t, t_0) = \mathcal{T} e^{-i \int_{t_0}^t ds \hat{V}(s)}, \quad (1.11)$$

where the time-ordering symbol \mathcal{T} moves operators evaluated at later times to the left,

$$\mathcal{T}[O_1(t_1) O_2(t_2)] = \theta(t_1 - t_2) O_1(t_1) O_2(t_2) \pm \theta(t_2 - t_1) O_2(t_2) O_1(t_1), \quad (1.12)$$

with θ denoting the Heaviside step function, and the signs “+” for bosonic and “-” for fermionic operators, respectively. The time-ordered exponential in Eq. (1.11) is then to be understood as a time-ordered infinite series. Analogously, the inverse evolution operator is found to be

$$U^\dagger(t, t_0) = \tilde{\mathcal{T}} e^{i \int_{t_0}^t ds \hat{V}(s)}, \quad (1.13)$$

introducing the anti-time ordering symbol $\tilde{\mathcal{T}}$, which orders operators in the reverse fashion to Eq. (1.12),

$$\tilde{\mathcal{T}}[O_1(t_1)O_2(t_2)] = \theta(t_2 - t_1)O_1(t_1)O_2(t_2) \pm \theta(t_1 - t_2)O_2(t_2)O_1(t_1). \quad (1.14)$$

The expectation value from Eq. (1.9) therefore reads

$$\langle O(t) \rangle = \text{tr} \left[\rho(t_0) \tilde{\mathcal{T}} e^{i \int_{t_0}^t dt' \hat{V}(t')} \hat{O}(t) \mathcal{T} e^{-i \int_{t_0}^t dt' \hat{V}(t')} \right]. \quad (1.15)$$

The time-ordered expectation value will be of special interest. Starting from Eq. (1.6), we find

$$\begin{aligned} \langle \mathcal{T} A(t) B(t') \rangle &= \text{tr} [\rho(t_0) S^\dagger(t, t_0) \mathcal{T} [S(t, t_0) \hat{A}(t) \hat{B}(t')]] \\ &= \text{tr} \left[\rho(t_0) \tilde{\mathcal{T}} e^{i \int_{t_0}^t dt' \hat{V}(t')} \mathcal{T} \left[e^{-i \int_{t_0}^{t'} dt' \hat{V}(t')} \hat{A}(t) \hat{B}(t') \right] \right]. \end{aligned} \quad (1.16)$$

The two time-ordered exponentials can thus be merged into a single one as follows:

$$\langle \mathcal{T} A(t) B(t') \rangle = \text{tr} \left[\rho(t_0) \mathcal{T}_C \left[e^{-i \int_C dt' \hat{V}(t')} \hat{A}(t_-) \hat{B}(t'_-) \right] \right]. \quad (1.17)$$

Here, the times are defined to lie on the contour C , as in Fig. 1.3, meaning that times are defined on either branch of C , with the subscripts $+$ and $-$ indicating the upper and lower branches, respectively. The place of time ordering has been taken by contour ordering, denoted by \mathcal{T}_C , which orders times along C , with operators evaluated at times lying later along the contour being moved to the left. It is worth emphasizing that we do not assign an imaginary part to the times at this point. Rather, the introduction of the contour corresponds to doubling the time axis, and is the main structural difference between the equilibrium and nonequilibrium Green's function formalisms. By employing this scheme, we can avoid making a statement about the state in the infinite future, which in the equilibrium case is simply assumed to be non-interacting, but may not be well-defined out of equilibrium.¹

When dealing with this contour, we adopt the convention of using Latin letters to denote times whose branch is specified and Greek ones for times that may live on either branch.

Finally, we define the contour-ordered expectation of a pair of operators as

$$\langle \mathcal{T}_C A(\tau) B(\tau') \rangle = \text{tr} \left[\rho(t_0) \mathcal{T}_C \left[e^{-i \int_C d\sigma \hat{V}(\sigma)} \hat{A}(\tau) \hat{B}(\tau') \right] \right], \quad (1.18)$$

which takes different values depending on which branch the times τ and τ' lie on. As we will see in detail below, all relevant Green's functions arise from Eq. (1.18) in this manner, making it the basic building block of NEGF. The exponentiated contour integral will be abbreviated as

$$S_C \equiv \mathcal{T}_C e^{-i \int_C d\sigma \hat{V}(\sigma)}, \quad (1.19)$$

in analogy to the expression for the S-matrix given in Eq. (1.11).

¹From a technical point of view, extending the contour from the largest of the times t and t' to positive infinity does not result in additional contributions to the expectation value since the upper branch of the extension always cancels with the lower branch.

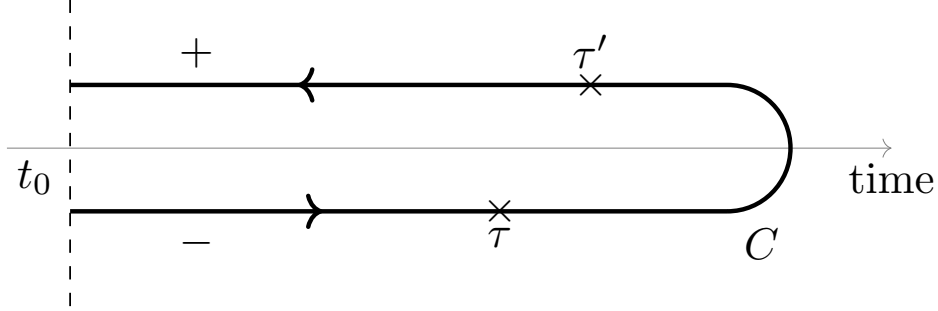


Figure 1.3: Keldysh integration contour C with times τ and τ' , running from t_0 to ∞ in the lower half plane, before returning to t_0 in the upper half plane.

1.2.2 Occupation of a single level coupled to a lead

The expectation value in Eq. (1.18) is amenable to modified versions of the quantum field-theoretical methods used in the equilibrium formalism. We will now use an example to outline which modifications need to be made: Considering a single electron level coupled to a lead, we will calculate its steady-state occupation. We choose the bare Hamiltonian as

$$H_0 = \epsilon d^\dagger d, \quad (1.20)$$

where d^\dagger and d are fermionic creation and annihilation operators, respectively, and fulfill the anticommutation relations $\{d, d^\dagger\} = 1$. H_0 thus describes a non-interacting spinless fermion at the single-particle energy ϵ . Before introducing the interaction term, let us calculate the bare Green's function required in the NEGF formalism. This Green's function is given by

$$D_0(\tau, \tau') \equiv -i \langle \mathcal{T}_C d(\tau) d^\dagger(\tau') \rangle_0, \quad (1.21)$$

where the subscript 0 indicates that the time evolution of the operator in the Heisenberg picture is governed by the bare Hamiltonian,² according to the equations of motion

$$\begin{aligned} \partial_\tau d(\tau) &= -i\epsilon d(\tau) \\ \partial_\tau d^\dagger(\tau) &= i\epsilon d^\dagger(\tau). \end{aligned} \quad (1.22)$$

Hence, the time-evolved operators are given by

$$\begin{aligned} d(\tau) &= e^{-i\epsilon(\tau-\tau_0)} d(\tau_0) \\ d^\dagger(\tau) &= e^{i\epsilon(\tau-\tau_0)} d^\dagger(\tau_0), \end{aligned} \quad (1.23)$$

²In the presence of an interaction Hamiltonian, the subscript 0 will thus indicate the interaction picture.

where the initial condition $d(\tau_0)$ may remain unspecified here. The times τ and τ' are defined on the contour C from Fig. 1.3. As a result of contour ordering, the value of $D_0(\tau, \tau')$ depends on which of the two branches each of the times sits. The Green's function in each of these four cases are commonly grouped together using matrix notation,³

$$\begin{aligned} \underline{D}_0(\tau, \tau') &= \begin{pmatrix} D_0^{--}(\tau, \tau') & D_0^{-+}(\tau, \tau') \\ D_0^{+-}(\tau, \tau') & D_0^{++}(\tau, \tau') \end{pmatrix} \\ &= \begin{pmatrix} -i \langle \mathcal{T} d(\tau) d^\dagger(\tau') \rangle_0 & i \langle d^\dagger(\tau') d(\tau) \rangle_0 \\ -i \langle d(\tau) d^\dagger(\tau') \rangle_0 & -i \langle \tilde{\mathcal{T}} d(\tau) d^\dagger(\tau') \rangle_0 \end{pmatrix}. \end{aligned} \quad (1.24)$$

The four components of $\underline{D}(\tau, \tau')$ can be calculated using Eq. (1.22), for instance,

$$\begin{aligned} D_0^{--}(\tau, \tau') &= -i \left[\theta(\tau - \tau') \langle d(\tau) d^\dagger(\tau') \rangle_0 - \theta(\tau' - \tau) \langle d^\dagger(\tau') d(\tau) \rangle_0 \right] \\ &= -i e^{i\epsilon(\tau' - \tau)} [\theta(\tau - \tau')(1 - N_0) - \theta(\tau' - \tau)N_0] \\ &= -i e^{i\epsilon(\tau' - \tau)} [\theta(\tau - \tau') - N_0]. \end{aligned} \quad (1.25)$$

Here, the initial occupation number N_0 was introduced, i.e.

$$\langle d^\dagger(\tau_0) d(\tau_0) \rangle_0 \equiv \text{tr}[\rho(t_0) d^\dagger(\tau_0) d(\tau_0)] = N_0, \quad (1.26)$$

without making any assumptions about its value.⁴ The other three Green's functions are obtained analogously,

$$\begin{aligned} D_0^{-+}(\tau, \tau') &= i e^{i\epsilon(\tau' - \tau)} N_0 \\ D_0^{+-}(\tau, \tau') &= -i e^{i\epsilon(\tau' - \tau)} (1 - N_0) \\ D_0^{++}(\tau, \tau') &= -i e^{i\epsilon(\tau' - \tau)} [\theta(\tau' - \tau) - N_0]. \end{aligned} \quad (1.27)$$

Next, an interaction term is introduced as follows. Imagine the single particle previously modeled by H_0 is coupled to a metallic lead, which is a system of many effectively non-interacting particles, with spatial extent L . We describe the lead by the Hamiltonian

$$H_B = \sum_k \epsilon_k c_k^\dagger c_k, \quad (1.28)$$

where the index k enumerates the lead modes. Thus, we expand the bare Hamiltonian to

$$H_0 = \epsilon d^\dagger d + \sum_k \epsilon_k c_k^\dagger c_k. \quad (1.29)$$

³occasionally referred to as a Keldysh matrix

⁴Equivalently, the initial state $\rho(t_0)$ is unspecified.

The coupling of the single particle to the lead will be treated as an interaction,

$$V = \sum_k \frac{\gamma_k}{\sqrt{L}} d^\dagger c_k + \text{h. c.}, \quad (1.30)$$

with h. c. denoting the Hermitian conjugate. Each mode of the lead is coupled to the single particle with a time-independent tunneling amplitude γ_k . In the following, we quantify the effect of the coupling by calculating the contour-ordered Green's function

$$D(\tau, \tau') \equiv -i \langle \mathcal{T}_C d(\tau) d^\dagger(\tau') \rangle, \quad (1.31)$$

which differs from its bare counterpart in the fact that the expectation value is calculated with respect to the Hamiltonian $H = H_0 + V$. We employ the expression from Eq. (1.18) to do so, expanding the interaction exponential in powers of V . After performing the leading-order expansion of $D(\tau, \tau')$, we have

$$\begin{aligned} D(\tau, \tau') &= -i \left\langle \mathcal{T}_C e^{-i \int_C d\sigma \left[\sum_k \frac{\gamma_k}{\sqrt{L}} d^\dagger(\sigma) c_k(\sigma) + \text{h.c.} \right]} d(\tau) d^\dagger(\tau') \right\rangle_0 \\ &= D_0(\tau, \tau') - \frac{i}{2} \int_C d\sigma \int_C d\sigma' \sum_{kq} \left[\frac{\gamma_k \gamma_q^*}{L} \langle \mathcal{T}_C d^\dagger(\sigma) c_k(\sigma) c_q^\dagger(\sigma') d(\sigma') d(\tau) d^\dagger(\tau') \rangle_0 \right. \\ &\quad \left. + \frac{\gamma_k^* \gamma_q}{L} \langle \mathcal{T}_C c_k^\dagger(\sigma) c(\sigma) d^\dagger(\sigma') c_q(\sigma') d(\tau) d^\dagger(\tau') \rangle_0 \right] + O(V^4). \end{aligned} \quad (1.32)$$

Here, we assumed an initial state of the factorized form $\rho(t_0) = \rho_D(t_0) \otimes \rho_B(t_0)$, meaning the coupling only affects the system as it starts to evolve. With this choice, the expectation values $\langle c_q d^\dagger \rangle_0$ and $\langle c_q^\dagger d \rangle_0$ both vanish, leading to the disappearance of all odd-ordered terms in Eq. (1.32). Furthermore, we work with a thermal initial state for the lead, $\rho_B(t_0) = e^{-\beta H_B}$ with an inverse temperature $\beta = 1/T$. This allows us to drop terms that will evaluate to zero because of $\langle c_k c_k \rangle = \langle c_k^\dagger c_k^\dagger \rangle = 0$. In order to reduce the higher-order correlators in this expansion to products of Green's functions, Wick's theorem is employed, the validity of which extends to nonequilibrium correlators [42]. This procedure results in

$$\begin{aligned} D(\tau, \tau') &= D_0(\tau, \tau') + \int_C d\sigma \int_C d\sigma' \sum_k \frac{\gamma_k \gamma_k^*}{L} D_0(\tau, \sigma) G_{0,k}(\sigma, \sigma') D_0(\sigma', \tau') \\ &\quad + O(V^4), \end{aligned} \quad (1.33)$$

where we used the absence of off-diagonal correlators in the initial state ρ_B of the lead to drop the sum over q . Moreover, considerable simplification is brought about by the fact that fermion operators in contour-ordered expectation values freely anticommute. Eq. (1.33) does not just give the second-order result in perturbation theory, but its structure also allows to deduce $D(\tau, \tau')$ to all orders: By iterating, we see that the exact Green's function is obtained by substituting $D(\sigma', \tau')$ in place

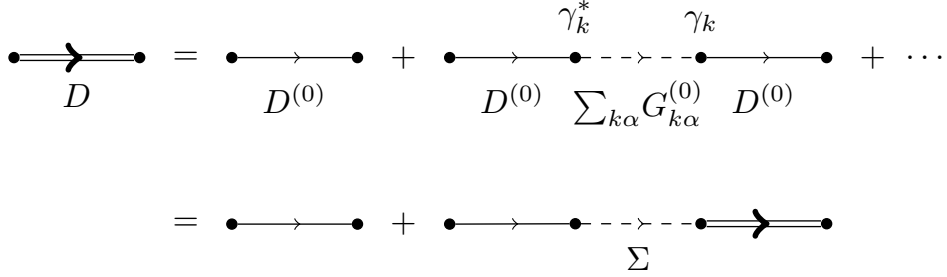


Figure 1.4: Feynman diagrams contributing to the exact dot Green's function $D(\tau, \tau')$. The linearity of the diagrams allows us to re-sum the perturbation series by defining the self-energy $\Sigma(\sigma, \sigma')$ as in Eq. (1.35).

of $D_0(\sigma', \tau')$ in the convolution term above. We thus obtain a Dyson equation for the contour-ordered Green's function,

$$D(\tau, \tau') = D_0(\tau, \tau') + \int_C d\sigma \int_C d\sigma' D_0(\tau, \sigma) \Sigma(\sigma, \sigma') D(\sigma', \tau'), \quad (1.34)$$

with the self-energy

$$\Sigma(\sigma, \sigma') = \sum_k \frac{\gamma_k \gamma_k^*}{L} G_{0,k}(\sigma, \sigma'). \quad (1.35)$$

The simple structure of Eq. (1.34) is a consequence of the coupling \hat{V} being merely quadratic in the operators. In the language of Feynman diagrams, this means that all terms in the expansion of Eq. (1.18) correspond to linear diagrams that can be re-summed upon introduction of the self-energy, as illustrated in Fig. 1.4.

In order to calculate the coupling corrections to the individual components of \underline{D} , i.e. the coupling corrections to the Green's functions in Eqs. (1.25) and (1.27), we need to specify the branches of the contour where the time arguments τ and τ' are defined. Evaluating the contour-ordered integrals is then done by splitting the contour integral into “forward” and “backward” parts along the real line: For any function f we have

$$\int_C d\tau f(\tau) = \int_{t_0}^{\infty} dt^- f(t^-) - \int_{t_0}^{\infty} dt^+ f(t^+), \quad (1.36)$$

meaning every integration over the positive branch of the contour comes with a minus sign. Here and in the following, times on the contour are denoted by Greek letters and times on the real line by Latin ones. For instance, the $-+$ component of the Green's function is obtained by defining τ to lie on the negative branch of C

and τ' on the positive one. Using Eq. (1.36) to split the integrals yields

$$\begin{aligned}
D^{-+}(t, t') &= D_0^{-+}(t, t') + \int_{t_0}^{\infty} ds \int_{t_0}^{\infty} ds' D_0^{--}(t, s) \Sigma^{--}(s, s') D^{-+}(s', t') \\
&\quad - \int_{t_0}^{\infty} ds \int_{t_0}^{\infty} ds' D_0^{-+}(t, s) \Sigma^{+-}(s, s') D^{-+}(s', t') \\
&\quad - \int_{t_0}^{\infty} ds \int_{t_0}^{\infty} ds' D_0^{--}(t, s) \Sigma^{++}(s, s') D^{++}(s', t') \\
&\quad + \int_{t_0}^{\infty} ds \int_{t_0}^{\infty} ds' D_0^{-+}(t, s) \Sigma^{++}(s, s') D^{++}(s', t'). \quad (1.37)
\end{aligned}$$

Here, the components of the self energy are defined by taking the corresponding component of $G_{0,k}(\sigma, \sigma')$ in Eq. (1.35). This result, together with the other three components, can be written more compactly in terms of matrices along the lines of Eq. (1.24),

$$\underline{D}(t, t') = \underline{D}_0(t, t') + \int_{t_0}^{\infty} ds \int_{t_0}^{\infty} \underline{D}_0(t, s) \underline{\Sigma}(s, s') \underline{D}(s', t'). \quad (1.38)$$

Note that the self-energy matrix is defined so as to include the negative signs arising from the contour integration,

$$\underline{\Sigma}(s, s') = \begin{pmatrix} \Sigma^{--}(s, s') & -\Sigma^{-+}(s, s') \\ -\Sigma^{+-}(s, s') & \Sigma^{++}(s, s') \end{pmatrix}. \quad (1.39)$$

When calculating transport properties of a system below, we will also make use of the *retarded* and *advanced* Green's functions. These are defined by

$$\begin{aligned}
D^R(t, t') &\equiv -i\theta(t - t') \langle \{c(t), c^\dagger(t')\} \rangle, \\
D^A(t, t') &\equiv i\theta(t' - t) \langle \{c(t), c^\dagger(t')\} \rangle = [D^R(t', t)]^*, \quad (1.40)
\end{aligned}$$

$$(1.41)$$

respectively. It is easily verified how these Green's functions are related to the previous definitions,

$$\begin{aligned}
D^R(t, t') &= D^{--}(t, t') - D^{-+}(t, t') \\
D^A(t, t') &= D^{--}(t, t') - D^{+-}(t, t'). \quad (1.42)
\end{aligned}$$

These Green's functions play a central role, among other things, in determining the excitation spectrum of a system and its response to external influences. On the other hand, information about its distributional properties is encoded in D^{-+} and D^{+-} , which are often referred to as the lesser and greater Green's functions, respectively. As an alternative, these properties can be summarized in the so-called *kinetic* (or *Keldysh*) Green's function

$$D^K(t, t') = D^{-+}(t, t') + D^{+-}(t, t'). \quad (1.43)$$

In the following, we modify the matrix Green's function by employing a common procedure known as Keldysh rotation,

$$\check{D} = \begin{pmatrix} D^R & D^K \\ 0 & D^A \end{pmatrix} = L \sigma_z \underline{D} L^\dagger, \quad (1.44)$$

where L denotes the Hermitian matrix

$$L \equiv \frac{1}{\sqrt{2}} \begin{pmatrix} 1 & -1 \\ 1 & 1 \end{pmatrix}, \quad (1.45)$$

and

$$\sigma_z = \begin{pmatrix} 1 & 0 \\ 0 & -1 \end{pmatrix} \quad (1.46)$$

is the third Pauli matrix. Using this convention, we obtain the Dyson equation

$$\check{D}(t, t') = \check{D}_0(t, t') + \int_{t_0}^{\infty} ds \int_{t_0}^{\infty} ds' \check{D}_0(t, s) \check{\Sigma}(s, s') \check{D}(s', t'). \quad (1.47)$$

Here, the self-energy is given by

$$\check{\Sigma}(s, s') = \begin{pmatrix} \Sigma^R(s, s') & \Sigma^K(s, s') \\ 0 & \Sigma^A(s, s') \end{pmatrix}, \quad (1.48)$$

meaning there are no additional minus signs as in Eq. (1.39). In particular, the triangular shape of all matrices in Eq. (1.47) implies that the coupling corrections to the retarded and advanced Green's function can be calculated using only the corresponding components of G_0 and Σ ,

$$D^{R/A}(t, t') = D_0^{R/A}(t, t') + \int_{t_0}^{\infty} ds \int_{t_0}^{\infty} ds' D_0^{R/A}(t, s) \Sigma^{R/A}(s, s') D^{R/A}(s', t'). \quad (1.49)$$

Let us also give the Dyson equations for the lesser and greater Green's functions,

$$\begin{aligned} D^{\mp\pm}(t, t') &= D_0^{\mp\pm}(t, t') + \int_{t_0}^{\infty} ds \int_{t_0}^{\infty} ds' D_0^R(t, s) \Sigma^R(s, s') D^{\mp\pm}(s', t') \\ &+ \int_{t_0}^{\infty} ds \int_{t_0}^{\infty} ds' D_0^R(t, s) \Sigma^{\mp\pm}(s, s') D^A(s', t') \\ &+ \int_{t_0}^{\infty} ds \int_{t_0}^{\infty} ds' D_0^{\mp\pm}(t, s) \Sigma^A(s, s') D^A(s', t'), \end{aligned} \quad (1.50)$$

which arises in analogous fashion to the kinetic component of Eq. (1.47). Eq. (1.50) is an application of the *Langreth rule* [46, 47], which relates the lesser component

of a convolution to convolutions of the constituents' components: Given the function $C(\tau, \tau') = \int_C d\sigma A(\tau, \sigma) B(\sigma, \tau')$, rewriting the contour integrals as real ones according to Eq. (1.36) results in the identity

$$C^{\pm\mp}(t, t') = \int_{t_0}^{\infty} ds \left[A^R(t, s) B^{\pm\mp}(s, t') + A^{\pm\mp}(t, s) B^A(s, t') \right]. \quad (1.51)$$

A straightforward application of the lesser Green's function lies in computing the particle number

$$N(t) \equiv \langle d(t) d^\dagger(t) \rangle = -i D^{-+}(t, t). \quad (1.52)$$

Often, one is interested in the situation of the *steady state* of the system, where the effects characterizing the regime close to the initial state have died out and the asymptotic behavior has established itself, with $N(t)$ having converged to its steady-state value. In the NEGF formalism for a time-independent Hamiltonian, this is achieved by moving the initial time into the infinite past, $t_0 \rightarrow -\infty$. We furthermore expect that all Green's functions in this situations will only depend on relative times, so we make the ansatz $D^{-+}(t, t') = D^{-+}(t - t')$. Then, the Dyson equation (1.50) for D^{-+} can be written in terms of convolutions,

$$\begin{aligned} D^{-+}(t - t') &= D_0^{-+}(t - t') + \left[D_0^R * \Sigma^R * D^{-+} \right](t - t') \\ &\quad + \left[D_0^R * \Sigma^{-+} * D^A \right](t - t') + \left[D_0^{-+} * \Sigma^A * D^A \right](t - t'), \end{aligned} \quad (1.53)$$

where convolution of two functions A and B is defined as

$$[A * B](t) = \int_{-\infty}^{\infty} ds A(s) B(t - s). \quad (1.54)$$

By considering the Fourier-transformed Green's function,

$$D^{-+}(\omega) = \int_{-\infty}^{\infty} dt e^{i\omega t} D^{-+}(t), \quad (1.55)$$

the convolutions are replaced by products, and iteration of Eq. (1.53) yields

$$D^{-+}(\omega) = (1 + D^R(\omega) \Sigma^R(\omega)) D_0^{-+}(\omega) (1 + D^A(\omega) \Sigma^A(\omega)) + D^R(\omega) \Sigma^{-+}(\omega) D^A(\omega), \quad (1.56)$$

where the Fourier transform of Eq. (1.49) was used,

$$D^{R/A}(\omega) = D_0^{R/A}(\omega) + D_0^{R/A}(\omega) \Sigma^{R/A}(\omega) D^{R/A}(\omega). \quad (1.57)$$

$D^{-+}(\omega)$ simplifies considerably upon introduction of the Fourier transformed initial Green's functions,

$$\begin{aligned} D_0^{-+}(\omega) &= i2\pi\delta(\omega - \epsilon)N_0 \\ D_0^R(\omega) &= \frac{1}{\omega - \epsilon + i\eta}, \end{aligned} \quad (1.58)$$

where N_0 denotes the initial occupation number of the level, and the positive infinitesimal $\eta \rightarrow 0$ encodes the time retardation in frequency space. By applying the Fourier transform of Eq. (1.49) to the first factor of the first term in Eq. (1.56), one obtains

$$D^{-+}(\omega) = \frac{D_0^R(\omega)^{-1}}{D_0^R(\omega)^{-1} - \Sigma^R(\omega)} D_0^{-+}(\omega) (1 + D^A(\omega) \Sigma^A(\omega)) + D^R(\omega) \Sigma^{-+}(\omega) D^A(\omega) \quad (1.59)$$

Since Eq. (1.58) implies $D_0^R(\omega)^{-1} D_0^{-+}(\omega) = 0$, the first term evaluates to zero and we are left with

$$D^{-+}(\omega) = D^R(\omega) \Sigma^{-+}(\omega) D^A(\omega). \quad (1.60)$$

Hence, the occupation of the level in the infinite past has no effect on the steady-state solution for D^{-+} , which can be obtained from the retarded and advanced solutions of Eq. (1.57),

$$D^{R/A}(\omega) = \frac{1}{D_0^{R/A}(\omega)^{-1} - \Sigma^{R/A}(\omega)} = \frac{1}{\omega - \epsilon - \Sigma^{R/A}(\omega)}. \quad (1.61)$$

The retarded and advanced components of the self-energy is given by

$$\begin{aligned} \Sigma^{R/A}(\omega) &= \sum_k \frac{\gamma_k^* \gamma_k}{L} \frac{1}{\omega - \epsilon_k \pm i\eta} = \mathcal{P} \sum_k \frac{\gamma_k^* \gamma_k}{L} \frac{1}{\omega - \epsilon_k} \mp i\pi \sum_k \frac{\gamma_k^* \gamma_k}{L} \delta(\omega - \epsilon_k) \\ &\equiv \Lambda(\omega) \mp i\Gamma(\omega), \end{aligned} \quad (1.62)$$

with the negative and positive signs in the last line applicable for the retarded and advanced components, respectively. The real part, commonly denoted $\Lambda(\omega)$, effects a Lamb shift in the location of the peak of $D^R(\omega)$, and the imaginary part $\Gamma(\omega)$ describes the broadening of the particle linewidth as a result of coupling it to the lead. This imaginary part serves to regularize the denominator in Eq. (1.61), replacing the infinitesimal η . The lesser self-energy is proportional to the linewidth and the distribution function of the lead,

$$\Sigma^{-+}(\omega) = \sum_k \frac{\gamma_k^* \gamma_k}{L} G_{0,k}^{-+}(\omega) = 2\pi i \sum_k \frac{\gamma_k^* \gamma_k}{L} n_F(\epsilon_k) \delta(\omega - \epsilon_k) = i2n_F(\omega) \Gamma(\omega). \quad (1.63)$$

Finally, the pieces can be assembled and the steady state particle number is given by

$$N_{ss} = \int \frac{d\omega}{2\pi} D^{-+}(\omega) = \int \frac{d\omega}{2\pi} \frac{2\Gamma(\omega)}{(\omega - \epsilon - \Lambda(\omega))^2 + \Gamma^2(\omega)} n_F(\omega). \quad (1.64)$$

In summary, the effects of coupling to the particle to the lead and taking the steady-state limit are (i) level broadening leading to a finite linewidth Γ , (ii) energy shift by Λ , and (iii) thermalization according to the lead distribution n_F .

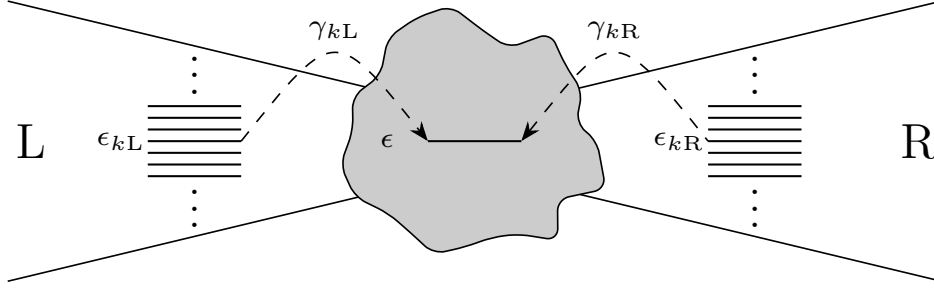


Figure 1.5: Single-level quantum dot of energy ϵ coupled to a pair of leads. The tunnel couplings between dot and leads, $\gamma_{k\alpha}$, $\alpha = L, R$, may differ for varying lead levels.

1.2.3 From Keldysh to current

The use of Green's functions is not limited to determining the dynamics of a system. They are also a valuable tool in the theory of quantum transport. [48, 47] In this section, we will relate the above results on Green's functions to the problem of calculating the charge current flowing through a mesoscopic region between a pair of metallic leads, as sketched in Fig. 1.5. Specifically, the central region may model a molecular quantum dot [19] as discussed in Sec. 1.1. Moreover, we will also introduce the wide-band limit which is assumed in our results presented in Secs. 2.1 to 2.4. The following presentation is based on Ref. [47], where the formalism is laid out in detail.⁵

The Hamiltonian of this setup is given by

$$\begin{aligned}
 H(t) &= H_D + H_L + H_R + H_T, \\
 H_D(t) &= \epsilon d^\dagger d, \\
 H_\alpha &= \sum_k \epsilon_{k\alpha} c_{k\alpha}^\dagger c_{k\alpha}, \quad \alpha \in \{L, R\} \\
 H_T &= \sum_{\alpha=L,R} \sum_k \frac{\gamma_{k\alpha}}{\sqrt{L}} d^\dagger c_{k\alpha} + \text{h. c.},
 \end{aligned} \tag{1.65}$$

where H_D , H_α for $\alpha \in \{L, R\}$, and H_T denote the dot, lead and dot-lead tunneling Hamiltonians, respectively. Compared to the example from the previous section, this model contains a second lead to allow for stationary current flow. The dot energy ϵ and the coupling strengths $\gamma_{k\alpha}$ are assumed to be independent of time. This restriction is removed in Secs. 2.2 to 2.4, where the time-dependence is taken into account, using different formalisms.

The operator for the current flowing through a lead is defined as the rate of change of the corresponding particle number. Focusing on the right lead, this particle number is written as $N_R = \sum_k c_{kR}^\dagger c_{kR}$. Applying the equation of motion yields

⁵Ref. [47] considers a multi-level quantum dot, but this degree of generality is not needed for our work.

the current,

$$I_R(t) \equiv e\partial_t N_R = ie[H, N_R] = ie \sum_k \frac{\gamma_{kR}}{\sqrt{L}} d^\dagger c_{kR} + \text{h. c.} \quad (1.66)$$

In order to calculate the expectation value of this operator, we introduce the mixed Green's functions

$$F_{k\alpha}(\tau, \tau') \equiv -i \langle \mathcal{T}_C c_{k\alpha}(\tau) d^\dagger(\tau') \rangle. \quad (1.67)$$

Taking the lesser component enables us to write

$$\langle I_R(t) \rangle = 2e \text{Re} \sum_k \frac{\gamma_{kR}}{\sqrt{L}} F_{kR}^{-+}(t, t). \quad (1.68)$$

The calculation of the current thus reduces to the calculation of the mixed Green's functions. In order to relate these with the Green's functions introduced previously, we assign to H_T the role of the interaction Hamiltonian and consider the contour S-matrix

$$S_C = \mathcal{T}_C e^{-i \int_C d\tau \hat{H}_T(\tau)}. \quad (1.69)$$

The perturbation expansion of $F_{k\alpha}(\tau, \tau')$ is thus given by

$$\begin{aligned} F_{k\alpha}(\tau, \tau') &= -i \left\langle \mathcal{T}_C e^{-i \int_C d\sigma \hat{H}_T(\sigma)} c_{k\alpha}(\tau) d^\dagger(\tau') \right\rangle_0 \\ &= -i \left\langle \mathcal{T}_C \sum_{j \geq 0} \frac{(-i)^j}{j!} \left[\int_C d\sigma \left(\sum_{k\alpha} \frac{\gamma_{k\alpha}}{\sqrt{L}} d^\dagger(\sigma) c_{k\alpha}(\sigma) + \text{h. c.} \right) \right]^j c_{k\alpha}(\tau) d^\dagger(\tau') \right\rangle_0. \end{aligned} \quad (1.70)$$

Using Wick's theorem, as well as $\langle d^\dagger c_k \rangle_0 = \langle c_k^\dagger d \rangle_0 = \langle c_k c_q \rangle_0 = \langle c_k^\dagger c_q^\dagger \rangle_0 = 0$, we see that the terms of the expansion can be regrouped, leading to

$$F_{k\alpha}(\tau, \tau') = \int_C d\sigma G_{0,k\alpha}(\tau, \sigma) \frac{\gamma_{k\alpha}^*}{\sqrt{L}} D(\sigma, \tau'), \quad (1.71)$$

where the dot and bare lead Green's functions are defined as before,

$$\begin{aligned} D(\tau, \tau') &= -i \langle \mathcal{T}_C d(\tau) d^\dagger(\tau') \rangle, \\ G_{0,k\alpha}(\tau, \tau') &= -i \langle \mathcal{T}_C c_{k\alpha}(\tau) c_{k\alpha}^\dagger(\tau') \rangle_0, \end{aligned} \quad (1.72)$$

respectively. $G_{0,k\alpha}$ denotes the bare lead Green's function for the lead of index α . As in Sec. 1.2.2, we study the steady-state situation by taking the limit of $t_0 \rightarrow -\infty$. Substitution of $D(\tau, \tau')$ into Eq. (1.68) yields for the current through the right lead

$$\langle I_R(t) \rangle = 2e \text{Re} \int_{-\infty}^{\infty} ds \left[\Sigma_R^R(t, s) D^{-+}(s, t) + \Sigma_R^{-+}(t, s) D^A(s, t) \right], \quad (1.73)$$

where the self-energy now also contains a summation over the leads,

$$\Sigma^R(s, s') = \sum_{k\alpha} \frac{\gamma_{k\alpha}^* \gamma_{k\alpha}}{L} G_{0,k\alpha}^R(s, s'). \quad (1.74)$$

The summation over lead modes can be simplified by taking the wide-band limit (WBL), presuming that the coupling γ_α to the leads does not depend on the individual lead mode k , and that the density of states $\bar{\rho}$ in the leads is constant throughout the relevant range of energies.⁶ The latter is equivalent to linearizing the lead spectrum, $\epsilon_{k\alpha} = v_F k$ near the Fermi surface, with the constant Fermi velocity v_F . Using these simplifications, the contribution of lead α to the retarded self-energy evaluates to

$$\begin{aligned} \Sigma_\alpha^R(s, s')^{\text{WBL}} &= i \frac{\gamma_\alpha^* \gamma_\alpha}{L} \theta(s - s') \sum_k e^{-i\epsilon_{k\alpha}(s-s')} \\ &= -i \bar{\rho} \gamma_\alpha^* \gamma_\alpha \theta(s - s') \int d\omega e^{-i\omega(s-s')} \\ &= -i \Gamma_\alpha \delta(s - s'), \end{aligned} \quad (1.75)$$

where we introduced the tunneling rate $\Gamma_\alpha = |\gamma_\alpha|^2 / (2v_F)$. The density of states was used in the form

$$\bar{\rho} = \sum_k \delta(\omega - \epsilon_{k\alpha}) / L = \frac{1}{2\pi v_F} \quad (1.76)$$

to convert the sum over modes \sum_k / L into the frequency integral $\bar{\rho} \int d\omega$. The theta function contributes a factor of $\theta(0) = 1/2$. Comparing to Eq. (1.62), we note that as a result of taking the WBL, Σ^R is purely imaginary and delta-shaped in the time domain. In the same way, the lesser component is obtained,

$$\begin{aligned} \Sigma_\alpha^{<+}(s, s')^{\text{WBL}} &= i \frac{\gamma_\alpha^* \gamma_\alpha}{L} \sum_k e^{-i\epsilon_{k\alpha}(s-s')} n_F(\epsilon_k) \\ &= i \bar{\rho} \gamma_\alpha^* \gamma_\alpha \int d\omega e^{-i\omega(s-s')} n_{F\alpha}(\omega). \end{aligned} \quad (1.77)$$

This frequency integral features an unphysical divergence as a result of the infinite bandwidth in the WBL. It can be cured by introducing a frequency cutoff, but we will in general not make this procedure explicit in the following.

As in Sec. 1.2.2, the steady-state current is obtained by making an ansatz for D^{-+} that only depends on time differences. In the frequency domain, the lesser dot Green's function is then

$$D^{-+}(\omega) = D^R(\omega) [\Sigma_L^{-+}(\omega) + \Sigma_R^{-+}(\omega)] D^A(\omega). \quad (1.78)$$

⁶The WBL is known to be accurate for metallic electrodes, where the temperature is small compared to the Fermi energy. Further remarks on its validity can be found in Ref. [49].

In particular, this implies $D^{-+}(t) = -D^{-+}(-t)^*$, and therefore, in the steady state, after substituting Eqs. (1.75) and (1.77), Eq. (1.73) simplifies to

$$\langle I_R \rangle_{ss} = -i2e\Gamma_R \int \frac{d\omega}{2\pi} \left[D^{-+}(\omega) + n_{FR}(\omega)(D^R(\omega) - D^A(\omega)) \right]. \quad (1.79)$$

In the steady state, one needs to impose $\langle I_R \rangle_{ss} = -\langle I_L \rangle_{ss}$ in order to exclude solutions with infinite charge accumulation on the dot. The current can then be written as $\langle I \rangle_{ss} = (\langle I_R \rangle_{ss} - \langle I_L \rangle_{ss})/2$. In the case of $\Gamma_L = \Gamma_R$, the term proportional to $D^{-+}(\omega)$ in Eq. (1.79) drops out, giving the final result for the WBL steady-state current

$$\langle I \rangle_{ss} = i\frac{e\Gamma}{2} \int \frac{d\omega}{2\pi} [n_{FL}(\omega) - n_{FR}(\omega)] [D^R(\omega) - D^A(\omega)]. \quad (1.80)$$

The most striking feature of this current is that it only depends on the retarded dot Green's function, and its frequency domain is defined by the “window” $n_{FL} - n_{FR}$ in the lead distributions.

1.3 Floquet expansion for driven systems

Driven quantum systems have long been a mainstay of quantum physics in general and transport theory in particular [50, 51, 52]. Accordingly, a wide array of analytical and numerical techniques has been developed for their analysis. Given a system described by a time-dependent Hamiltonian, there is no single, feasible, technique to obtain the system dynamics for a completely general drive. Rather, the choice of method depends strongly on the manner of driving the system, for instance a slow drive may be treated in the adiabatic approximation, or a weak drive may be amenable to perturbation theory. For a periodic drive without restriction on its speed or strength, the Floquet approach has proven successful.

Here, we give an overview of the Floquet technique in preparation for Sec. 2.2, where it is applied to a molecular quantum dot with a periodic driving force. Originating from the theory of differential equations [53, 54], the Floquet technique can be used to treat periodic Hamiltonians,

$$H(t + T) = H(t) \quad \forall t. \quad (1.81)$$

In this case, the Schrödinger equation $i\partial_t\phi(t) = H(t)\phi(t)$ admits a complete set of solutions of the form

$$\phi_\alpha(t) = e^{-iE_\alpha t} u_\alpha(t), \quad (1.82)$$

where u_α inherits the periodicity of the Hamiltonian, and hence admits a decomposition in harmonics of the drive frequency $\Omega = 2\pi/T$,

$$u_\alpha(t + T) = u_\alpha(t) = \sum_{n \in \mathbb{Z}} e^{-in\Omega t} u_{n\alpha}. \quad (1.83)$$

The E_α in Eq. (1.82) are known as quasi-energies. The decomposition in Eq. (1.83) implies that the quasi-energies are only defined up to integer multiples of the drive frequency. Indeed, by shifting the energy one finds

$$e^{-i(E_\alpha + k\Omega)t} u_\alpha(t) = e^{-iE_\alpha t} \sum_{n \in \mathbb{Z}} e^{-i(n-k)\Omega t} u_{n\alpha} = e^{-iE_\alpha t} \sum_{n \in \mathbb{Z}} e^{-in\Omega t} u_{(n+k)\alpha}, \quad (1.84)$$

which is also a solution of the Schrödinger equation. Hence the range of the quasi-energies can be restricted to $0 \leq E_\alpha < \Omega$, analogously to the emergence of the Brillouin zone in systems with spatial periodicity. This leads to the interpretation of the exponential $e^{-iE_\alpha t}$ describing the long-time (low-energy) behavior of the wave function, whereas the periodic factor $u_\alpha(t)$ encodes its evolution on time scales shorter than the drive period. By decomposing the Schrödinger equation into Fourier components, an equation for the mode amplitudes $u_{n\alpha}$ is obtained,

$$\sum_{n \in \mathbb{Z}} H_{mn} u_{n\alpha} = (E_\alpha + m\Omega) u_{m\alpha}, \quad (1.85)$$

meaning that the time-dependent problem can be mapped onto a time-independent one involving an infinite-matrix Hamiltonian with entries

$$H_{mn} = \frac{1}{T} \int_{-T/2}^{T/2} dt e^{i(m-n)\Omega t} H(t). \quad (1.86)$$

This representation of the Schrödinger equation suggests interpreting the role of the drive as a source of “photons” of frequency Ω .

An analogous formalism can also be developed in the language of Green’s functions, as was laid out in Ref. [55]: Consider a general NEGF $\check{G}(t, t')$, where the check mark indicates the 2×2 matrix structure with both times defined on the real line, using the notation from Sec. 1.2. First, time dependence can be expressed in terms of the relative and average times $t_{\text{rel}} = t - t'$, and $t_{\text{av}} = (t + t')/2$, respectively. Then, a Fourier transform is performed in the relative coordinate,

$$\check{D}(t_{\text{av}}, \omega) = \int_{-\infty}^{\infty} dt_{\text{rel}} e^{i\omega t_{\text{rel}}} \check{D}(t_{\text{av}}, t_{\text{rel}}). \quad (1.87)$$

As a consequence of the periodicity of the Hamiltonian, the Green’s function is itself periodic in the average time if initial state effects are disregarded. Hence it can be expanded into Fourier modes,

$$\check{D}(n, \omega) = \frac{1}{T} \int_{-T/2}^{T/2} dt_{\text{av}} e^{in\Omega t_{\text{av}}} \check{D}(t_{\text{av}}, \omega). \quad (1.88)$$

Having performed this expansion, the Green’s function can be written as an infinite-dimensional Floquet matrix in frequency space,

$$\check{D}_{mn}(\omega) = \check{D}\left(m - n, \omega + \frac{m + n}{2}\Omega\right). \quad (1.89)$$

This matrix representation allows to write convolutions in time domain as matrix multiplications in frequency space: For a function

$$C(t, t') = \int_{-\infty}^{\infty} ds A(t, s) B(s, t'), \quad (1.90)$$

the Floquet expansion is given by

$$C_{mn}(\omega) = \sum_{k=-\infty}^{\infty} A_{mk}(\omega) B_{kn}(\omega). \quad (1.91)$$

In order to calculate this matrix product numerically, it is necessary to make an approximation, the most simple one being to only take a finite number N_{Fl} of Floquet modes into account. This corresponds to limiting the dimension of the matrices to $N \equiv 2N_{\text{Fl}} + 1$, with the index k running from $-N_{\text{Fl}}$ to N_{Fl} .

1.4 Open quantum systems and master equations

Only very rarely do quantum systems occur in complete isolation from their surroundings. This is true especially in the context of transport theory, where systems are embedded in environments in order to induce a current flowing through them. More generally, a quantum system will almost invariably interact with its surroundings in some way, leading to various consequences such as hybridization of energy levels, particle loss, or dissipation of energy. Typically, the environment in such a setup contains a macroscopic number of degrees of freedom and allows for less experimental control than the system itself, making it very challenging to describe with an exact quantum model. Moreover, the environment is usually only of interest by virtue of how it affects the system, so the environment dynamics themselves tend to be of lesser relevance.

1.4.1 From von Neumann to Lindblad

The notion of an open system encompasses any quantum system in contact with an environment. In this situation, it has in many cases proven possible to obtain an effective description for the dynamics of the open system in which the environment degrees of freedom no longer occur as variables. Since the resulting model only contains the system degrees of freedom, it can be much easier to treat, while still preserving information about the effects of the environment on the system. Configurations with weak coupling between system and environment are particularly amenable to such an approach. In the following, we will sketch the derivation of an effective model that will prove useful in corroborating our results from the NEGF approach, in Sec. 2.1.

Since the form and eventual tractability of such an effective model for the open system will in any case depend on the configuration in question, we do not aim for generality here, but will instead focus on what is used in Sec. 2.1. The main reference used here is Ch. 6 of Ref. [56], others include the textbooks [57, 58]. A rigorous treatment can be found in Ref. [59].

We consider an arbitrary quantum system in contact with an environment, as illustrated in Fig. 1.6. The composite of system and environment will in the following be referred to as the *super-system*, which includes all system and environment degrees of freedom. Its evolution is governed by the full Hamiltonian

$$H = H_S + H_E + V, \quad (1.92)$$

with the three terms denoting the system, environment, and system-environment interaction Hamiltonians, respectively. In the following we will treat V as an interaction Hamiltonian and make use of the interaction picture as introduced in Sec. 1.2.

As in Sec. 1.2, the starting point of our discussion is the density matrix $\rho(t)$ of the super-system, which in the interaction picture evolves according to the von

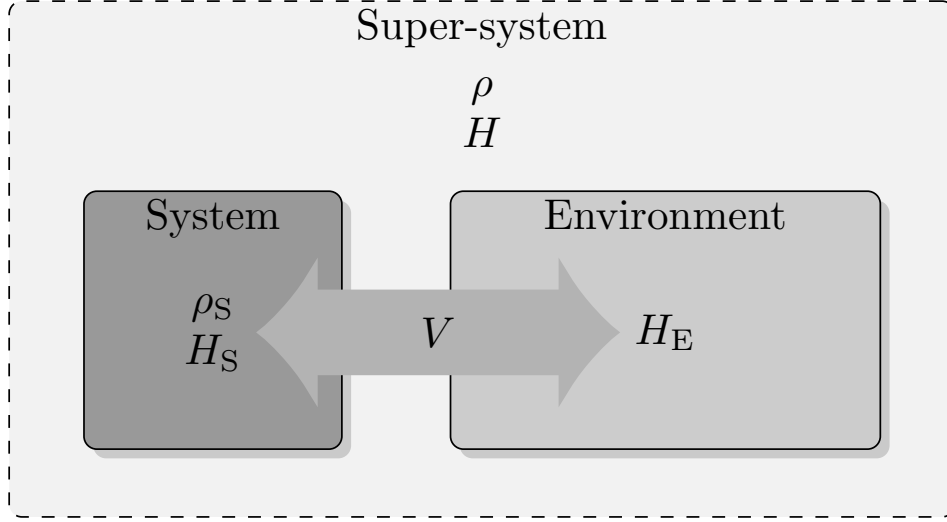


Figure 1.6: Schematic representation of an open system in contact with an environment. The open system dynamics are encoded in the reduced density matrix ρ_S , which exclusively retains the system degrees of freedom. The time evolution of ρ_S is obtained by evolving the density matrix ρ of the super-system with the full Hamiltonian $H = H_S + H_E + V$ and then tracing over the environment degrees of freedom.

Neumann equation

$$\frac{d}{dt}\hat{\rho}(t) = -i[\hat{V}, \hat{\rho}(t)]. \quad (1.93)$$

We aim to find an expression for the *reduced density matrix* $\hat{\rho}_S(t)$, which is obtained from $\hat{\rho}(t)$ by tracing over the environment degrees of freedom,

$$\hat{\rho}_S(t) = \text{tr}_E \hat{\rho}(t). \quad (1.94)$$

A simplified equation of motion for ρ_S (as opposed to ρ) can be obtained from Eq. (1.93), given certain assumptions. First, the super-system is required to be in a factorized state $\rho(t_0) = \rho_S(t_0) \otimes \rho_B$ at the initial time t_0 . Here, ρ_B is a fixed state of the environment, often taken to be a thermal state $\rho_B = e^{-\beta H_E} / \text{tr} e^{-\beta H_E}$ at an inverse temperature β . In this case, the environment is referred to as a *bath*, as indicated by the index B. Second, the coupling between system and environment is assumed to be weak, and that the dynamics of the bath are much faster than those of the system. Under these assumptions, the von Neumann equation can be shown to imply

$$\hat{\rho}_S(t) = \rho_S(t_0) - \int_{t_0}^t ds \int_{t_0}^s du \text{tr}_E [\hat{V}(s), [\hat{V}(s-u), \hat{\rho}_S(s) \otimes \rho_B]] + O(V^3), \quad (1.95)$$

where the interaction picture with respect to $H_S + H_E$ is indicated by hats. By making some further assumptions about the correlators of the environment operators in the interaction Hamiltonian V ,⁷ it is possible to arrive at a linear master equation for ρ_S ,

$$\frac{d\hat{\rho}_S(t)}{dt} = -i[\hat{H}_{LS}, \hat{\rho}_S(t)] + \mathcal{D}[\hat{\rho}_S(t)], \quad (1.96)$$

where \hat{H}_{LS} contributes a shift of the system energy levels due to the coupling to the bath and is hence referred to as the Lamb-shift Hamiltonian. The operator \mathcal{D} is called a dissipator, and its action on the system density matrix is given by

$$\mathcal{D}[\hat{\rho}_S] = \sum_{\mu} \sum_{\omega} \gamma_{\mu}(\omega) \left(C_{\mu}(\omega) \hat{\rho}_S C_{\mu}^{\dagger}(\omega) - \frac{1}{2} \{ C_{\mu}^{\dagger}(\omega) C_{\mu}(\omega), \hat{\rho}_S \} \right), \quad (1.97)$$

where the operators C_{μ} represent various decay channels, and the sum over ω corresponds to adding contributions from the entire spectrum of the system. Eq. (1.96) is known as the *Lindblad equation* [59] for the system density matrix and captures the non-unitary part of the evolution of the system resulting from the contact with the bath.

1.4.2 A note on Markovianity

In the context of open system dynamics, a commonly used notion is that of *Markovian* evolution. Specifically, the Lindblad equation (1.96) is usually taken to indicate that the system evolves in a Markovian manner. The exact meaning of Markovianity is however more complex than this would suggest. A considerable amount of literature is dedicated to the issue, see Refs. [60, 56, 61, 62] among others; here, we borrow from Refs. [57, 56] and establish the main points in as far as will be needed to provide context for our own work.

The origin of the term lies in classical probability theory, where a stochastic process, i.e. a sequence $(X_n)_{n \in \mathbb{N}}$ of random variables is called Markovian, if the distribution of any element in the sequence only depends on its immediate predecessor,

$$P(X_n = x | X_{n-1} = x_{n-1}, \dots, X_0 = x_0) = P(X_n = x | X_{n-1} = x_{n-1}), \quad (1.98)$$

where $P(A|B) \equiv P(A \cap B)/P(B)$ denotes the probability of the event A conditioned on the event B . This property is a manifestation of the process being memoryless, i.e. the transition probabilities between the n th and $(n-1)$ st steps do not depend on the history of the process. This notion is readily generalized to continuous stochastic processes $(X_t)_{t \in I}$. There, denoting by $p(x, t)$ the probability for the process to take the value x at the time t , we have by definition

$$p(x, t) = \int dx' p(x, t | x', t') p(x', t') \quad \forall t' < t, \quad (1.99)$$

⁷These assumptions are related to, but not equivalent to assuming an infinite number of environment degrees of freedom. For details, see Ch. 6 of Ref. [56].

where the conditional probability $p(x, t|x', t')$ acts as a transition kernel for the evolution between t' and t . The Markov condition is formulated in analogy to Eq. (1.98), and imposed for any sequence of times, for example $p(x_3, t_3|x_2, t_2, x_1, t_1) = p(x_3, t_3|x_2, t_2)$. This implies a composition law for the transition kernel,

$$p(x_3, t_3|x_1, t_1) = \int dx_2 p(x_3, t_3|x_2, t_2) p(x_2, t_2|x_1, t_1), \quad (1.100)$$

for all intermediate times $t_1 < t_2 < t_3$, known as the Chapman-Kolmogorov equation.

The quantum version of Markovianity can be introduced by drawing upon Eq. (1.100) and requiring a similar composition rule. More precisely, the role of the probabilities $p(x, t)$ is taken by the system density matrix $\rho_S(t)$. Given a factorized initial state $\rho(t_0) = \rho_S(t_0) \otimes \rho_B$ of the super-system, it is possible to find a family of linear operators $\mathcal{E}(t)$ that encode the evolution of the reduced density matrix $\rho_S(t) = \text{tr}_B \rho(t)$,

$$\rho_S(t_0 + t) = \mathcal{E}(t) [\rho_S(t_0)] \quad (1.101)$$

in such a way it fulfills a composition law analogous to Eq. (1.100). Since the environment degrees have already been traced out, the evolution of $\rho_S(t)$ is not unitary and hence does not inherit the group property of the propagator $U(t, t')$ of the super-system. Nonetheless, by introducing the spectral decomposition $\rho_B = \sum_\beta \lambda_\beta |\phi_\beta\rangle \langle \phi_\beta|$ of the initial bath density matrix, it is possible to write the evolution of ρ_S as

$$\begin{aligned} \rho_S(t_0 + t) &= \text{tr}_B \left[U(t_0 + t, t_0) \rho_S(t_0) \otimes \rho_B U^\dagger(t_0 + t, t_0) \right] \\ &= \sum_\alpha \langle \phi_\alpha | U(t_0 + t, t_0) \rho_S(t_0) \otimes \left(\sum_\beta \lambda_\beta |\phi_\beta\rangle \langle \phi_\beta| \right) U^\dagger(t_0 + t, t_0) | \phi_\beta \rangle \\ &\equiv \sum_{\alpha\beta} W_{\alpha\beta}^\dagger(t) \rho_S(t_0) W_{\alpha\beta}(t), \end{aligned} \quad (1.102)$$

where $W_{\alpha\beta} = \sqrt{\lambda_\beta} \langle \phi_\alpha | U(t_0 + t, t_0) | \phi_\beta \rangle$. This expression is of the form from Eq. (1.101), with

$$\mathcal{E}(t) [\cdot] = \sum_{\alpha\beta} W_{\alpha\beta}^\dagger(t) [\cdot] W_{\alpha\beta}(t) \quad (1.103)$$

denoting the trace-preserving evolution operator for the reduced density matrix. The analogy to Eq. (1.100) is constructed by imposing the semigroup condition

$$\mathcal{E}(t + s) = \mathcal{E}(t) \mathcal{E}(s) \quad \forall t, s \geq 0. \quad (1.104)$$

If this condition is fulfilled and $\mathcal{E}(t)$ is in addition completely positive,⁸ then \mathcal{E} is said to model a Markovian process. It can be shown that the evolution of a density

⁸A map \mathcal{E} mapping operators to operators is called positive if it maps positive operators to positive operators, i.e. operators with only positive eigenvalues. \mathcal{E} is called completely positive if for any positive operator ρ also the operators $\mathbb{1}_d \otimes \mathcal{E}[\rho]$ are positive, for any dimension d .

matrix ρ_S by $\mathcal{E}(t)$ can equivalently be described by the equation

$$\frac{d}{dt}\rho_S = -i[H, \rho_S] + \sum_{\mu=1}^{N^2-1} h_{\mu} \left(C_{\mu} \rho_S C_{\mu}^{\dagger} - \frac{1}{2} \{C_{\mu}^{\dagger} C_{\mu}, \rho_S\} \right), \quad (1.105)$$

with positive coefficients $h_{\mu} \geq 0$. The integer N denotes the dimension of the system Hilbert space, which is assumed to be finite in this context. It should be stressed that the operator H is a function of bath expectation values of the super-system evolution operator $U(t, t_0)$, and does in general not coincide with the system Hamiltonian H_S . Eq. (1.105) is of the same form as Eq. (1.96), showing that the approximations performed in Sec. 1.4.1 do indeed lead to a notion of quantum Markovianity. However, this is far from the only such notion and many alternative definitions exist, an overview of which can be found in Ref. [62].

1.5 Quantum thermodynamics: An overview

Thermodynamics and quantum mechanics are two of the most consequential paradigms in modern science. Their fields of application have historically been separated by massive differences in scale: Classical thermodynamics describes the interplay between macroscopic systems and is used to design macroscopic machines and work cycles. Quantum mechanics, on the other hand, concerns itself with microscopic particles and processes. Even though the laws of thermodynamics can be seen to arise from quantum mechanics, their domain of validity is only reached by taking the *thermodynamic limit* of quasi-infinite particle number N . As a general rule of thumb, particle numbers on the macroscale are on the order of Avogadro's constant, $N_A \approx 6 \times 10^{23}$, and classical thermodynamics is furthermore only of limited use beyond equilibrium. Hence, it took decades after the discovery of quantum mechanics for the question of quantum thermodynamics to attract considerable attention. More recently, fabrication techniques have improved to the point where meso- and nanoscale machines can be reliably realized in experiments, leading to a surge in interest in the topic: On the single-particle scale [63, 64, 65], the thermodynamic limit can evidently not be taken. On the mesoscale, the particle number may still be quite sizable (up to 10^{12} particles), but other assumptions of the classical theory break down nonetheless. In this section, we will outline these fundamental issues of quantum thermodynamics as well as some of the established results, in as far as they are connected to the work in Secs. 2.3 and 2.4.

The central question in quantum thermodynamics can be formulated as *How do the macroscopic laws of classical thermodynamics generalize to hold in quantum systems?* These laws of thermodynamics can be formulated as follows [66]:

1. Infinitesimal changes in the internal energy of a system (dE_S) are the sum of heat flowing into the system (δQ), work performed on it (δW), and changes in chemical energy (δE_C),

$$dE_S = \delta Q + \delta W + \delta E_C, \quad (1.106)$$

where d in contrast to δ indicates a complete differential, meaning that the internal energy of a system is a state function, whereas heat, work, and chemical energy in general are not.

2. A process that adds the heat δQ to a system at temperature T causes the change of entropy

$$dS \geq \frac{\delta Q}{T}. \quad (1.107)$$

3. Entropy changes incurred during isothermal processes vanish in the limit of the temperature tending to zero.

The focus of this work lies on the first two laws. The first law is a statement of energy conservation, which clearly also holds in quantum mechanics. The challenge however consists in finding definitions of system energy, work and heat that

not only fulfill the first law, but also the other two. In order to retain maximum generality, these definitions moreover need to be made with as little reference as possible to a specific model. The second law relates the heat flux δQ during a work cycle with the entropy increase, which is also in need of a definition. Again, the definition should be made in such a manner that the law holds for arbitrary systems and work protocols, in analogy to the vast generality of classical thermodynamics.

Some of the roadblocks on the way to a consistent theory of quantum thermodynamics are readily apparent: Firstly, in classical thermodynamics, the exact nature of the interaction between reservoirs and systems is not taken into account. This simplification results from the fact that at macroscopic scales, the interfaces between systems only occupy negligible space and thus do not significantly modify the energy balance. For quantum systems containing only a few particles, this assumption no longer holds, leading to a conflict between the goal of generality and the need to treat interaction effects explicitly. If these interactions are strong, an even more fundamental concern arises, namely which part of an interface belongs to which system. Considering this issue, it is perhaps not surprising that quantum thermodynamics of weakly coupled system has proved to be the more accessible problem, and a satisfactory theory has emerged decades ago [67, 68, 9, 69]. The formalism of open quantum systems, as described in Sec. 1.4, is instrumental in this endeavor, which we outline below, following Ref. [9].

1.5.1 Open quantum systems and weak-coupling thermodynamics

Consider the reduced density matrix for an open system with a driven Hamiltonian $H_S(t)$ weakly coupled to a bath, which evolves in Markovian fashion,

$$\frac{d}{dt}\rho_S(t) = -i[H_S(t), \rho_S(t)] + \mathcal{D}_t[\rho_S(t)], \quad (1.108)$$

where the time-dependence of $H_S(t)$ is only parametrical, and \mathcal{D}_t is calculated from $H_S(t)$ according to Eq. (1.97), indicating that the Hamiltonian is driven in such a way that the dynamics of the reduced density matrix are still described by a Lindblad equation. In this setting, thermodynamic quantities can be defined that relate to the notions of macroscopic thermodynamics. Specifically,

$$\begin{aligned} E_S(t) &= \text{tr}(\rho_S(t)H_S(t)), \\ \dot{Q}(t) &= \text{tr}\left(\frac{d}{dt}\rho_S(t)H_S(t)\right), \\ \dot{W}(t) &= \text{tr}\left(\rho(t)\frac{d}{dt}H_S(t)\right) \end{aligned} \quad (1.109)$$

are used to denote the internal energy of the system, the rate of heat flowing into it, and the rate of work it performs, respectively. Here, we introduce the convention of indicating time derivatives by using ∂_t , and giving a dot to quantities that describe a rate, but need not actually be time derivatives of a state function. These choices

fulfill $\partial_t E_S(t) = \dot{W} + \dot{Q}$, which generalizes the first law from Eq. (1.106) to the quantum case in a straightforward fashion. Defining the von Neumann entropy with the system density matrix,

$$S_S(t) = -\text{tr} [\rho_S(t) \log \rho_S(t)] \quad (1.110)$$

it can be shown that the rate of change of entropy is given by

$$\partial_t S(t) = \beta \dot{Q}(t) + \dot{S}_i(t), \quad (1.111)$$

where the first term describes the entropy flow into the system, and the second one is the entropy production rate in the system, which is found to be positive,

$$\dot{S}_i(t) \geq 0. \quad (1.112)$$

This result amounts to a quantum version of the second law, Eq. (1.107). It should be stressed that the derivation of Eq. (1.112) hinges on the Markovian evolution on the system density matrix as encoded in the Lindblad equation (1.105), and hence in particular on the weakness of the coupling between system and bath.

In the regime of strong system-bath coupling, no universal formulation of quantum thermodynamics exists. There are however several approaches each capturing some aspects of quantum thermodynamics, of which we want to give an overview now.

1.5.2 Stochastic thermodynamics

Stochastic thermodynamics has its roots in nonequilibrium classical thermodynamics and has proven fruitful with in the study of work in the quantum case. Its starting point is provided by a result of Jarzynski [70] about a classical system initially weakly coupled by a Hamiltonian H_T to a heat bath with Hamiltonian H_B , equilibrated at an inverse temperature β . After this initial time, the bath is decoupled and the system is modeled by a Hamiltonian $H_\lambda(z)$, where $\lambda(t) = t/t_f$ denotes the control parameter used in a switching protocol and $z = (q, p)$ is shorthand for a coordinate in the system phase space. The evolution of the system is then described by the stochastic trajectory $z(t)$ in phase space, where t ranges between initial and final times t_0 and t_f , and the work performed along this trajectory is

$$W = \int_{t_0}^{t_f} dt \dot{\lambda}(t) \partial_\lambda H_\lambda(z(t)). \quad (1.113)$$

The average work $\langle W \rangle$ is obtained by averaging Eq. (1.113) over the initial configurations of the super-system consisting of system and bath. In the case of an initial thermal state at inverse temperature β , it can be shown that the average exponentiated work is equal to the exponentiated free energy difference,

$$\langle e^{-\beta W} \rangle = e^{-\beta \Delta F}, \quad (1.114)$$

with $\Delta F = F(t_f) - F(t_0)$, where the initial equilibrium free energy is defined as

$$F(t_0) = -\frac{1}{\beta} \log Z(t_0), \quad (1.115)$$

with the classical partition function

$$Z(t_0) = \int dz dz' e^{-\beta(H_0(z) + H_B(z') + H_T(z, z'))}. \quad (1.116)$$

where z' denotes the phase space coordinates of the bath. The final equilibrium free energy $F(t_f)$ is defined analogously. The result Eq. (1.114), named *Jarzynski's equality*, establishes an equality between the average of a non-equilibrium quantity and a change of an equilibrium thermodynamic potential. The equilibrium free energy is thus accessible by averaging over nonequilibrium work measurements. Since the inverse exponential function is concave, Jensen's inequality implies

$$\langle W \rangle \geq \Delta F, \quad (1.117)$$

meaning Jarzynski's equality can also be seen as a stronger, nonequilibrium version of Eq. (1.117) which in equilibrium is a consequence of the second law.⁹ By also considering the time-reversed switching protocol Eq. (1.114) was shown to lead to fluctuation theorems [72], by now a central feature of stochastic thermodynamics [73, 74, 75, 76, 77]. These theorems imply that even for classical small systems, the fluctuations of nonequilibrium thermodynamic quantities need to be taken into account, and that they follow laws derived from their equilibrium counterparts.

Driven by this discovery, the first applications to quantum fluctuations followed soon after, prominently Refs. [78, 79]. The classical and quantum cases are by no means equivalent, though. For instance, there is no quantum analogue to Eq. (1.113) that would characterize work as an observable [80, 81, 82]: Measuring work requires taking the difference of two energy measurements and not just a single measurement. However, work in quantum systems is still a random variable in the sense that, the work produced between two measurement times t_0 and t_f is distributed according to a probability density function $p_{t_f, t_0}(w)$, with the mean work production given by the expectation value

$$\langle W \rangle = \int_{-\infty}^{\infty} dw p_{t_f, t_0}(w) w. \quad (1.118)$$

⁹Consider a system in contact with an equilibrium bath at temperature T , separated by a movable wall that permits heat exchange. Assume a process that moves the wall in such a manner that the initial and final states of the system are also of temperature T . The second law for the super-system implies that during this process the total change in entropy is positive, $\Delta S_S + \Delta S_B \geq 0$, where S_S and S_B denote the system and bath entropies, respectively. As the bath is in equilibrium, its entropy change is given by $\Delta S_B = -Q/T$, where Q is the heat flowing into the system. By the first law for the system, $\Delta E_S = Q + W$, and therefore the second law implies $0 = \Delta E_S - W + T \Delta S_B \geq \Delta[E_S - T S_S] - W$, i.e. $W \geq \Delta F$ since $F = E_S - T S_S$. [71]

The system in question is prepared in a thermal state¹⁰ $\rho(t_0) = e^{-\beta H(t_0)} / Z(t_0)$ at t_0 , where the equilibrium partition function of the system in the quantum case is given by

$$Z(t_0) = \text{tr} \left[e^{-\beta H(t_0)} \right]. \quad (1.119)$$

From t_0 to t_f , the system evolves under the influence of the time-dependent Hamiltonian $H(t)$. It is then found that the characteristic function of work can be written as a correlator [80],

$$G_{t_f, t_0}(u) \equiv \int_{-\infty}^{\infty} dw p_{t_f, t_0}(w) e^{i u w} = \left\langle e^{i u H(t_f)} e^{-i u H(t_0)} \right\rangle, \quad (1.120)$$

which in Ref. [84] is used to show the fluctuation relation

$$\frac{p_{t_f, t_0}(w)}{p_{t_0, t_f}(-w)} = \frac{Z(t_f)}{Z(t_0)} e^{\beta w} = e^{-\beta(\Delta F - w)}, \quad (1.121)$$

where p_{t_0, t_f} denotes the probability density function of the work generated under the time-reversed protocol $\tilde{H}(t) = H(t_f - (t - t_0))$. The partition function

$$Z(t_f) = \text{tr} e^{-\beta H(t_f)} \quad (1.122)$$

corresponds to a fictitious thermal equilibrium state $e^{-\beta H(t_f)} / Z(t_f)$ at the final time, even though the system will in general not be in equilibrium at the end of the protocol. The characteristic function G_{t_f, t_0} can also be used to show the quantum version of the Jarzynski equality, $\langle e^{-\beta W} \rangle = e^{-\beta \Delta F}$, where the expectation value is now taken with respect to p_{t_f, t_0} . As in the classical case, this then implies $\langle W \rangle \geq \Delta F$.

In summation, stochastic thermodynamics provides a an approach to quantum thermodynamics that takes into account nonequilibrium effects, and gives a clear picture of how to define work in accordance with the second law, with profound insights into its statistical properties. It does not, however, provide us with a notion of internal system energy, entropy or heat flows in the quantum setting: All time evolution is unitary, which does not apply to the reduced dynamics of a small system in contact with a bath.

1.5.3 Hamiltonians of mean force

The approach outlined above has been adapted to systems evolving while strongly coupled to a bath, in both the classical [85, 86] and quantum cases [87, 88]. Here, we focus on the latter to provide a reference point for our work in Secs. 2.3 and 2.4.

¹⁰The choice of the canonical ensemble is not mandatory. Analogous results have been obtained for a microcanonical setup [83].

The object of study in Ref. [88] is a composite system formed by a smaller system strongly coupled to a bath, modeled by the general Hamiltonian

$$H(t) = H_S(t) + H_B + H_T, \quad (1.123)$$

where the system Hamiltonian H_S is subject to drive. The composite system starts out in a thermal state and evolves unitarily, hence the fluctuation theorem for work production holds,

$$\frac{p_{t_f, t_0}(w)}{p_{t_0, t_f}(-w)} = \frac{Z(t_f)}{Z(t_0)} e^{\beta w}, \quad (1.124)$$

where $Z(t) = \text{tr} e^{-\beta H(t)}$ is the partition function of the composite system in a thermal state. Defining the system free energy

$$F_S(t) = F(t) - F_B \quad (1.125)$$

as the difference of composite and bath free energies, the system equilibrium function is obtained as [88]

$$Z_S(t) = \frac{Z(t)}{Z_B}, \quad (1.126)$$

with the bath partition function given by $Z_B = \text{tr}_B e^{-\beta H_B}$. The work fluctuation relation then reads

$$\frac{p_{t_f, t_0}(w)}{p_{t_0, t_f}(-w)} = \frac{Z_S(t_f)}{Z_S(t_0)} e^{\beta w} = e^{-\beta(\Delta F_S - w)}, \quad (1.127)$$

now involving only the system partition function. The latter can be seen to arise from the Hamiltonian of mean force,

$$H^*(t) = -\frac{1}{\beta} \log \frac{\text{tr}_B e^{-\beta H(t)}}{\text{tr}_B e^{-\beta H_B}}, \quad (1.128)$$

which, even though it only contains system operators, encodes the effect of the coupling to the bath on the system. More precisely, the system state obtained by thermalization with the instantaneous Hamiltonian of mean force coincides with the reduced density matrix obtained by taking a partial trace over the state of the composite system thermalized with $H(t)$,

$$\frac{e^{-\beta H^*(t)}}{Z_S(t)} = \text{tr}_B \frac{e^{-\beta H(t)}}{Z(t)}. \quad (1.129)$$

The Hamiltonian of mean force generalizes the classical potential of mean force as known in reaction rate theory [89] and reduces to the system Hamiltonian in the case of weak system-bath coupling [88].

For classical systems, the potential of mean force has been shown to facilitate definitions that fulfill the first and second law of thermodynamics at strong coupling, including notions of internal energy, heat and entropy [90]. The starting point in that treatment is to define thermodynamic potentials as differences between the total and bath potentials, as in Eq. (1.125). A consistent quantum version, however, is still the object of ongoing research [81, 91].

Chapter 2

Results

2.1 Lifting the Franck-Condon blockade in carbon nanotube quantum dots

*Electron-vibron coupling in quantum dots can lead to a strong suppression of the average current in the sequential tunneling regime. This effect is known as Franck-Condon blockade and can be traced back to an overlap integral between vibron states with different electron numbers which becomes exponentially small for large electron-vibron coupling strength. Here, we investigate the effect of a time-dependent drive on this phenomenon, in particular the effect of an oscillatory gate voltage acting on the electronic dot level. We employ two different approaches: perturbation theory based on nonequilibrium Keldysh Green's functions and a master equation in Born-Markov approximation. In both cases, we find that the drive can lift the blockade by exciting vibrons. As a consequence, the relative change in average current grows exponentially with the drive strength. This section is based on the article Lifting the Franck-Condon blockade in driven quantum dots, written in collaboration with Stefan Walter, Andreas Nunnenkamp, and Thomas L. Schmidt, published in Phys. Rev. B **94**, 205142 (2016).*

2.1.1 Introduction

The field of nanoscale electronics has seen rapid advances in recent years: experimental techniques have improved to the point that the range of realizable electronic components now extends down to the single-molecule scale [92, 93, 94, 95]. Novel fabrication methods afford an increasing amount of precision with regard to the properties of such elements, in particular the conductive behavior. An ultimate goal of this effort is to scale down electronic components such as wires, transistors, and rectifiers to the atomic scale, thus potentially extending the lifetime of Moore's law. Moreover, the physics of nanoscale conductors is not limited to electronic effects. Already at the nanoscale the quantized mechanical degrees of freedom of, e.g., a molecule become important. However, it remains difficult to exploit the me-

chanical properties of such molecules to control transport through the molecule. Interestingly, the situation is different at the mesoscale, where the interplay between the electronic and mechanical degrees of freedom can be engineered in a fashion that allows for the incorporation of mesoscopic constituents into a wide variety of setups [96, 97, 98, 99].

Suspended carbon nanotubes (CNTs) which are free to vibrate comprise exactly such mesoscopic electromechanical systems [97]. CNTs are superb mechanical oscillators due to (i) their high Q-factors and stiffness [100, 101], (ii) high vibrational frequencies in the GHz range [102], and (iii) large electron-phonon coupling [30]. Besides these mechanical properties, the electronic and transport properties of CNTs can also be tuned depending on the setup. For instance, electronic back gates allow for a controlled shaping of the nanotube’s electrostatic potential which can be used to confine single electrons on the CNT, thus creating a quantum dot on the nanotube. Transport through CNT quantum dots has extensively been studied theoretically and experimentally [24, 25]. Nanoelectromechanics is a growing field of research with various experiments investigating the interplay between the mechanical and the quantized electronic degree of freedom in suspended CNTs [103, 104, 105, 30].

A general feature of interacting systems composed of electrons and quantized mechanical vibrations (“vibrons”) is the suppression of conductance, in certain parameter regimes, for strong coupling between the two degrees of freedom. This effect, commonly referred to as Franck-Condon blockade [23], results from the atomic constituents of the system accommodating for the presence of a number of electrons by means of displacement, thus forming composite electron-vibron particles termed polarons. Electronic transport through the system requires the electron number to change and hence the polarons to be broken up, which is energetically disfavored if the electron-vibron coupling that holds them together is strong. This effect has been observed in single-molecule junctions [29] as well as in CNT systems [30], adding to the variety of ways in which material structure can influence conductance. In addition, it has also been shown that the coupling between the mechanical and electronic degrees of freedom can be tailored to some extent [26].

In this paper we examine the effect of time-dependent driving on the Franck-Condon blockade by periodically modulating the electronic level energy using a time-dependent gate voltage. More specifically, we study a system composed of a suspended CNT on which a quantum dot is defined by means of back gates. This quantum dot is considered weakly coupled to a pair of metallic leads in the regime of sequential tunneling. Moreover, electrons on the dot interact strongly with the vibrational degree of freedom of the CNT. Our goal is to investigate the consequences of periodically modulating the electronic level. Most importantly, we find that driving the system results in a strong increase in the time-averaged current in a way which is reminiscent of a transistor.

Our analysis is organized as follows: In Sec. 2.1.2 we present the model used to describe a CNT quantum dot, taking into account a periodic modulation of the electronic level and strong coupling of charge to vibrations. In Sec. 2.1.3 we derive the

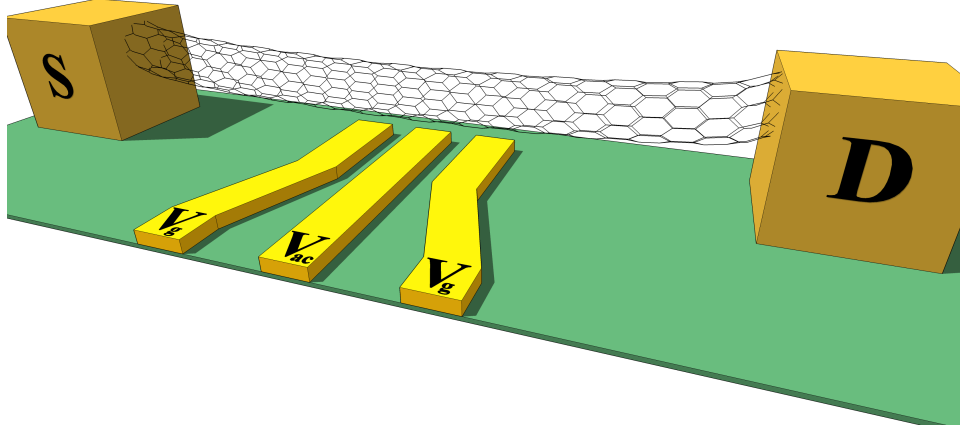


Figure 2.1: Schematics of the setup: Suspended CNT connected to source (S) and drain (D) electrodes, on top of gate electrodes used to create a quantum dot (V_g) and to provide a drive voltage (V_{ac}). Figure by Stefan Walter.

steady-state current through the system using the Keldysh nonequilibrium Green's function formalism. Taking an alternative approach, we set up a master equation for the electronic dynamics in Sec. 2.1.4, leading to a prediction for the current, which we compare to the results presented in Sec. 2.1.3. Finally, we summarize in Sec. 2.1.5 and conclude by discussing possible applications.

2.1.2 Model

We consider a quantum dot consisting of a single electronic level weakly tunnel-coupled to a pair of metallic leads. Such a quantum dot may be realized on a suspended CNT using electronic back gates to confine an electron in a specific section of the nanotube [103, 104, 105, 100, 30, 101, 102, 97, 26]. The vibrations of the CNT can be strongly coupled to the charge degree of freedom of the electron and thus have a great influence on its conductive properties [30, 26, 31]. Additionally, a back gate can be used to apply an AC voltage, thus modulating the dot energy level [106]. We show a schematic representation of the setup in Fig. 2.1.

This setup can be described by the Anderson-Holstein Hamiltonian, $H = H_{\text{dot}} + H_{\text{lead}} + H_{\text{tun}}$, where

$$\begin{aligned}
 H_{\text{dot}} &= \Omega a^\dagger a + \epsilon d^\dagger d + \lambda(a^\dagger + a)d^\dagger d + f(t)d^\dagger d, \\
 H_{\text{lead}} &= \sum_{\alpha=L,R} \sum_k \epsilon_{k\alpha} c_{k\alpha}^\dagger c_{k\alpha}, \\
 H_{\text{tun}} &= g \sum_{\alpha=L,R} \left[d\psi_\alpha^\dagger(x=0) + \text{h.c.} \right],
 \end{aligned} \tag{2.1}$$

denote the dot, lead, and tunneling Hamiltonians, respectively.

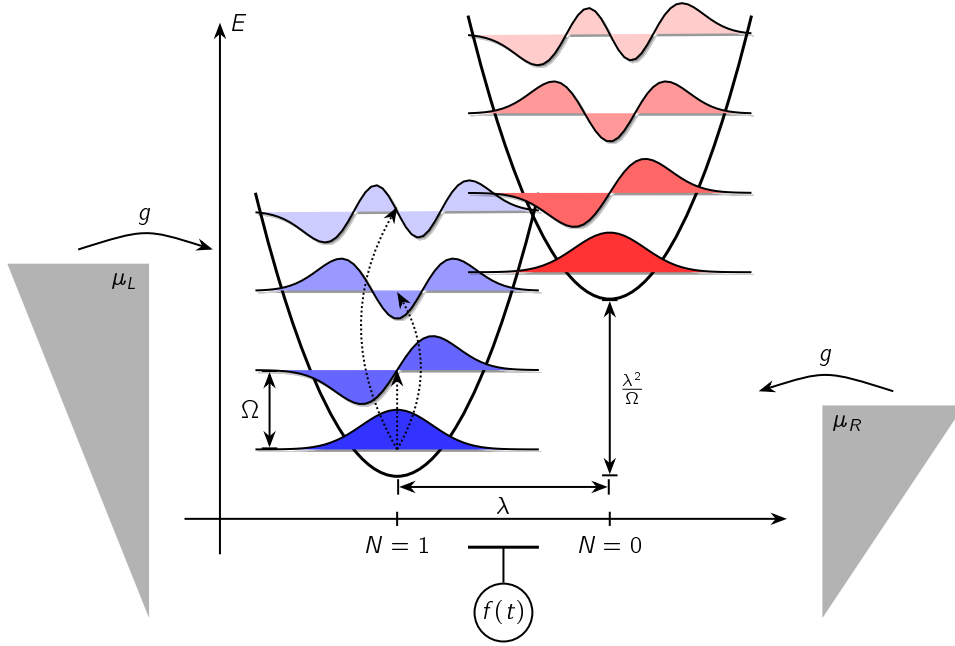


Figure 2.2: Illustration of the Hamiltonian from Eq. (2.1). Electron-vibron coupling corresponds to a shift of the vibron rest position depending on the electron number $N = d^\dagger d$. This shift leads to an exponentially small overlap between the oscillator's ground state wave functions for $N = 0$ and $N = 1$. However, driving $[f(t)]$ causes transitions to excited states (dashed arrows) for which the overlap is significantly larger. Changes in electron number occur by tunneling into either of the leads at chemical potentials μ_L and μ_R , respectively, with tunneling amplitude g . Figure by Thomas L. Schmidt.

While in principle a CNT admits several different types of vibron modes, the coupling to the charge sector is strongest for breathing and longitudinal stretching modes [33]. In our analysis, we restrict the model for the quantum dot to a single electronic level at energy ϵ and a single vibron mode of frequency Ω , setting $\hbar = 1$ throughout. This choice of model captures the Coulomb blocked regime of a multi-electron quantum dot, where a large intra-dot Coulomb interaction restricts the electronic transitions to and from the dot to those between a pair of states with occupation numbers N and $N + 1$ for some N that realizes a degeneracy in charging energy. Moreover, taking the limit of large Coulomb interaction, we also neglect the spin degree of freedom [21], as well as Kondo effects [107]. In addition, we include the gate-induced drive as a time-dependent contribution $f(t)$ to the electronic level energy. The mechanical vibration of the nanotube modulates the dot level energy, which is quantified by the coupling strength λ . The leads $\alpha \in \{L, R\}$ are modeled as fermionic reservoirs with single-particle energies $\epsilon_{k\alpha}$,

described by fermionic operators $c_{k\alpha}$ obeying the canonical anticommutation relations $\{c_{k\alpha}, c_{k'\beta}^\dagger\} = \delta_{kk'}\delta_{\alpha\beta}$. Finally, H_{tun} describes local electron tunneling into and out of the leads using the Fourier transform $\psi_\alpha(x) = L^{-1/2} \sum_k e^{ikx} c_{k,\alpha}$, where L is the length of the lead. An illustration of the Hamiltonian is shown in Fig. 2.2.

In the absence of electron-vibron coupling, the dot features a single resonance at energy ϵ . Electron-vibron coupling leads to the emergence of side-peaks at energies $\epsilon + n\Omega$ with $n \in \mathbb{Z}$. In the following, we focus on the limit of sequential tunneling. This is the dominant transport process for small g and potential differences $eV = \mu_L - \mu_R$, where μ_α is the chemical potential of lead α , such that only a single resonance lies within the bias window.

The electron-vibron coupling term can be removed by applying the polaron transformation [108] given by $\mathcal{U} = \exp[\lambda(a^\dagger - a)d^\dagger/\Omega]$, leading to

$$\begin{aligned} \mathcal{U}H\mathcal{U}^{-1} &= \Omega a^\dagger a + \tilde{\epsilon} d^\dagger d + f(t) d^\dagger d \\ &+ \sum_{\alpha=L,R} \sum_k \epsilon_{k\alpha} c_{k\alpha}^\dagger c_{k\alpha} + g \sum_{\alpha=L,R} [X^\dagger d \psi_\alpha^\dagger(x=0) + \text{h.c.}], \end{aligned} \quad (2.2)$$

where the electron level energy ϵ is renormalized to $\tilde{\epsilon} = \epsilon - \lambda^2/\Omega$ and the electron-vibron coupling is moved to an exponential factor multiplying the tunneling term, $X = e^{-\lambda(a^\dagger - a)/\Omega}$. This leaves us with an expression consisting of a quadratic Hamiltonian H_0 and a weak perturbation H_1 ,

$$\begin{aligned} H_0 &= \Omega a^\dagger a + \tilde{\epsilon} d^\dagger d + f(t) d^\dagger d + \sum_\alpha \sum_k \epsilon_{k\alpha} c_{k\alpha}^\dagger c_{k\alpha} \\ H_1 &= g \sum_\alpha [X^\dagger d \psi_\alpha^\dagger(x=0) + \text{h.c.}], \end{aligned} \quad (2.3)$$

which lends itself to a variety of approaches that are perturbative in the tunneling amplitude g , but still permit potentially large values of the electron-vibron coupling $\lambda \gg \Omega$.

A great deal of insight into similar models has already been obtained. Specifically, the undriven [$f(t) = 0$] variant of the system has been examined with regard to its transport properties [20, 21, 23, 109, 34, 110]. The most striking finding in this context is that of Franck-Condon blockade: strong electron-vibron interaction leads to formation of a composite state, called a polaron, which can be thought of as being made up of an electron and a “cloud” of vibrational excitations surrounding it. If the electron is to tunnel out of the quantum dot, this state has to be broken up, at an energy cost which strongly increases with the coupling, leading to an exponential suppression of tunneling.

In the following, we will investigate in detail the novel effects that arise by periodically modulating the electronic level energy. We will first show that due to the strong electron-vibron coupling, this type of drive can be mapped to a drive of the vibron. Moreover, we will demonstrate that it has a strong influence on electronic transport and that, in particular, the Franck-Condon blockade can be

lifted. It is worth pointing out that a small AC drive voltage applied to the gate can lead to an exponentially strong change of the average current.

The physical interpretation of this process is as follows. Due to the electron-vibron coupling, a time-dependent gate voltage also has the effect of driving the vibron, so the vibron will populate an excited state. Importantly, the overlap integral between excited vibron states for different fermion numbers contains Franck-Condon factors which are exponentially larger than those of the vibron ground states. This makes it possible to lift the Franck-Condon blockade, and hence increases the average current.

Hence, the relative change in average current $I(A)/I(0)$, where A is the amplitude of the AC gate voltage, is close to an exponential function of A . This makes the $I - V$ characteristic reminiscent of that of a transistor, albeit now for AC gate voltages: in our system, a DC bias current can be controlled by a small AC gate voltage. Note that the frequency of the AC gate voltage needs to be close to the vibron frequency, since the effect relies on the excitation of vibrons.

2.1.3 Polaron tunneling approximation

In the following, we use a Keldysh Green's function approach to analyze the influence of the gate voltage on the conductance of the system. The most important measurable quantity in this context is the steady-state current $\langle I \rangle_{ss}$. In the following, we work with the current through the right lead, noting that it is identical to the one through the left lead up to a displacement current introduced by the time dependence of the drive. However, since this current oscillates on a timescale given by the inverse drive frequency, much faster than the tunneling rates to and from the dot, we can safely neglect it on average. Thus $\langle I \rangle_{ss}$ is obtained from expectation value of the operator

$$\begin{aligned} I_R(t) &= e \frac{d}{dt} \sum_k c_{kR}^\dagger c_{kR} = -ie \left[\sum_k c_{kR}^\dagger c_{kR}, H \right] \\ &= ieg \left[d^\dagger(t) X(t) \psi_R(t) - \psi_R^\dagger(t) X^\dagger(t) d(t) \right], \end{aligned} \quad (2.4)$$

where e is the negative electron charge. It will prove expedient to move the time dependence into the perturbative part of the Hamiltonian, which can be accomplished by applying the unitary transformation given by $\mathcal{V}(t) = \exp[i d^\dagger d \int_{t_0}^t ds f(s)]$. This reduces the quadratic Hamiltonian to $\bar{H}_0 = \tilde{\epsilon} d^\dagger d + \Omega a^\dagger a$, and changes the polaron operator to

$$\bar{X}(t) \equiv \mathcal{V}(t) X(t) \mathcal{V}^{-1}(t) = e^{-\frac{\lambda}{\Omega} [a^\dagger e^{i\Omega t} - a e^{-i\Omega t} + iF(t)]}, \quad (2.5)$$

with $F(t) = \frac{\Omega}{\lambda} \int_{t_0}^t ds f(s)$ denoting the integrated drive, where the initial time t_0 always cancels in the following and can hence be chosen arbitrarily. The transformed coupling Hamiltonian then reads

$$\bar{H}_I = g \sum_\alpha \left[\bar{X}^\dagger d \psi_\alpha^\dagger(x=0) + \text{h.c.} \right]. \quad (2.6)$$

It bears pointing out that as a result of the transformation \mathcal{V} the drive has thus been moved onto the vibrational part of the Hamiltonian, lending substance to the intuition that the coupling between electrons and vibrons leads to the possibility of driving the vibrons by driving the electrons.

In the following, we focus on a resonant harmonic drive, $f(t) = A \cos(\Omega t)$. As laid out in Sec. 1.2.3, the Keldysh Green's function formalism together with perturbation theory in the lead coupling g can be employed to calculate the mean steady-state current [48] from the retarded dot Green's function D^R for the undriven case,

$$\langle I \rangle = i \frac{e\Gamma}{2} \int \frac{d\omega}{2\pi} [n_{\text{FL}}(\omega) - n_{\text{FR}}(\omega)] [D^R(\omega) - D^A(\omega)], \quad (2.7)$$

where the coupling g and the lead density of states $\bar{\rho}$ are absorbed into the tunneling rate $\Gamma = 2\pi\bar{\rho}g^2$. We use the wide-band approximation, so the density of states is constant, $\bar{\rho} = 1/(2\pi v_{\text{F}})$ with Fermi velocity v_{F} . In this section, Eq. (2.7) will be used as an approximation to the current in the presence of drive. A more exact treatment using the Floquet formalism is presented in Sec. 2.2. To obtain the average current, we thus need to calculate the nonequilibrium dot Green's function

$$D(\tau, \tau') = -i \left\langle \mathcal{T}_C d^\dagger(\tau) \bar{X}(\tau) \bar{X}^\dagger(\tau') d(\tau') e^{-i \int_C d\sigma \bar{H}_1(\sigma)} \right\rangle_0, \quad (2.8)$$

with components $D^{ij}(t, t')$, where the indices $i, j = +, -$ denote the forward and backward branches of the Keldysh contour C from Fig. 1.3, with the initial time lying in the infinite past. Comparing with the notation of Sec. 2.2, it should be also noted that $D(\tau, \tau')$ as used here contains both electronic and vibrational operators. The expectation value in Eq. (2.8) is taken with respect to the Hamiltonian \bar{H}_0 of the non-interacting system, and the time dependences are understood to be in the interaction picture corresponding to \bar{H}_0 . We note that the presence of the vibrational operators \bar{X} in this expression is a consequence of the polaron transform dressing the electron. As the non-interacting Hamiltonian is not quadratic in \bar{X}, \bar{X}^\dagger , Wick's theorem does not hold for these operators, so the calculation of the terms making up the Green's function in Eq. (2.8) seems rather daunting.

Drawing upon Ref. [35], we hence employ the following approximation: the dwell time of the electron on the quantum dot (which can be estimated as the inverse of the bare tunneling rate Γ) is large compared to the timescale of the polaron which is associated with the inverse of the energy shift $\epsilon - \tilde{\epsilon} = \lambda^2/\Omega$. In this limit, the polaron will relax in the time between two tunneling processes. The diagrammatic form of this polaron-tunneling approximation (PTA) is given in Fig. 2.3, and it has been used before to calculate transport properties of strongly coupled electron-vibron systems. [35, 111, 112] The purpose of this approximation is to avoid having to explicitly expand the exponential from Eq. (2.8) in powers of the tunneling amplitude g . Instead, the $2n$ -th order vibrational correction to the bare dot Green's function $G_{\text{dot}}(\tau - \tau') = -i \langle \mathcal{T}_C d(\tau) d^\dagger(\tau') \rangle$ is seen to be caused by a series of tunneling processes to and from the leads, where the lead Green's function

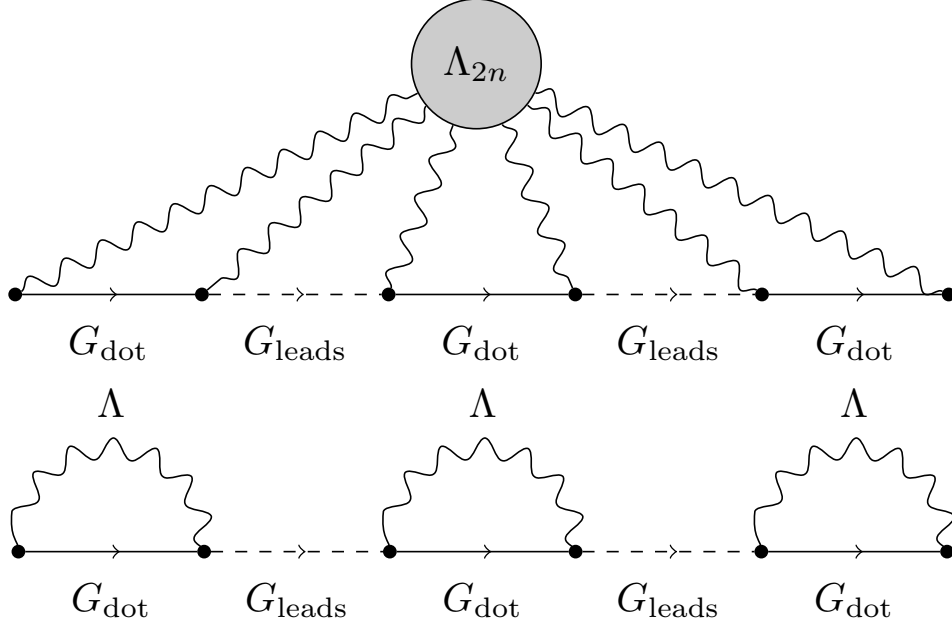


Figure 2.3: *Top*: Generic diagram in the perturbation expansion of the full dot propagator, with Λ_{2n} denoting the $2n$ -correlator of \bar{X} operators, bare dot propagator G_{dot} , and lead propagator G_{leads} . *Bottom*: Polaron tunneling approximation of the same diagram. The vibron cloud is assumed to de-excite between electron tunneling processes, leaving only correlators of second order in the vibron sector, i.e. the top diagram reduces to the bottom one.

is given by

$$G_{0,k\alpha}(\tau, \tau') = -i\langle \mathcal{T}_C c_{k\alpha}(\tau) c_{k\alpha}^\dagger(\tau') \rangle. \quad (2.9)$$

In the following, we use the shorthand $G_{\text{leads}} = g^2 L^{-1/2} \sum_{k\alpha} G_{0,k\alpha}$, which evaluates to the Keldysh matrix

$$\underline{G}_{\text{leads}}(\omega) = i2\pi\bar{\rho} \begin{pmatrix} n_L + n_R - \frac{1}{2} & n_L + n_R \\ n_L + n_R - 1 & n_L + n_R - \frac{1}{2} \end{pmatrix}, \quad (2.10)$$

where $n_L = n_F(\omega - eV/2)$ and $n_R = n_F(\omega + eV/2)$ are the Fermi functions of the left and right lead, respectively. Here, we also made use of the wide band-limit of the lead distributions, as detailed in App. 2.1.6. Each tunneling process involves the mechanical degree of freedom, giving rise to vibron excitations described by the set of correlators

$$\Lambda_{2n}(\tau_1, \tau'_1, \dots, \tau_n, \tau'_n) = \left\langle \mathcal{T}_C \prod_{1 \leq j \leq n} \bar{X}(\tau_j) \bar{X}^\dagger(\tau'_j) \right\rangle. \quad (2.11)$$

The PTA replaces these by products of the quadratic correlators

$$\Lambda(\tau, \tau') = \langle \mathcal{T}_C \bar{X}(\tau) \bar{X}^\dagger(\tau') \rangle \quad (2.12)$$

connecting only two consecutive tunneling events into and out of the quantum dot. These correlators consist of a drive-independent factor and one which explicitly incorporates the drive, i.e., $\Lambda(t, t') = \Lambda_0(t - t') \Lambda_{\text{dr}}(t, t')$, with

$$\Lambda_0(t - t') = -ie^{-\frac{\lambda^2}{\Omega^2}} \begin{pmatrix} e^{\frac{\lambda^2}{\Omega^2} e^{-i\Omega|t-t'|}} & e^{\frac{\lambda^2}{\Omega^2} e^{i\Omega(t-t')}} \\ e^{\frac{\lambda^2}{\Omega^2} e^{-i\Omega(t-t')}} & e^{\frac{\lambda^2}{\Omega^2} e^{i\Omega|t-t'|}} \end{pmatrix} \quad (2.13)$$

and the driven component

$$\Lambda_{\text{dr}}(t, t') = e^{-i \int_{t'}^t ds f(s)}. \quad (2.14)$$

Since the timescale of the vibrons is fast compared to the tunneling, we average the driven part over one drive period, leading to (see App. 2.1.6)

$$\Lambda_{\text{dr}}(t - t') = J_0 \left(\frac{2A \sin \Omega(t - t')/2}{\Omega} \right), \quad (2.15)$$

where J_0 denotes the Bessel function of the first kind. This expression only depends on the relative time coordinate $t - t'$, meaning that the problem becomes readily amenable to Fourier transformation. This leaves us with the leading-order correction in frequency space to the dot propagator,

$$D_0^{ij}(\omega) = \int_{-\infty}^{\infty} dt e^{i\omega t} G_{\text{dot}}^{ij}(t) \Lambda^{ij}(t). \quad (2.16)$$

At this point, the simplified structure of the diagrams in Fig. 2.3 allows us perform a partial resummation and thus retain all orders in the coupling strength g without requiring access to higher-order vibrational correlators. Indeed, incrementing the order in the tunneling is equivalent to appending a single copy each of the polaron-dot and lead propagators to the diagram. In terms of Green's functions, this is equivalent to the frequency-space Dyson equation for the vibron-dressed dot electron propagator,

$$\underline{D}^{-1}(\omega) = \underline{D}_0^{-1}(\omega) - \underline{\Sigma}_{\text{leads}}(\omega). \quad (2.17)$$

with the self-energy $\underline{\Sigma}_{\text{leads}} = g^2 \underline{G}_{\text{leads}}$. This relation gives rise to the full PTA dot Green's function $\underline{D}(\omega)$, as documented in App. 2.1.6. The steady-state current from Eq. (2.7) can now be obtained by integrating over the spectral function $-i[D^{-+}(\omega) - D^{+-}(\omega)]$, which is shown in Fig. 2.4. The plot features tunnel-broadened resonances at all integer multiples of the vibron frequency. The appearance of peak heights being independent of peak order is an artifact caused by the PTA [111]; only the zeroth-order peak is reliable in that regard. Furthermore, the

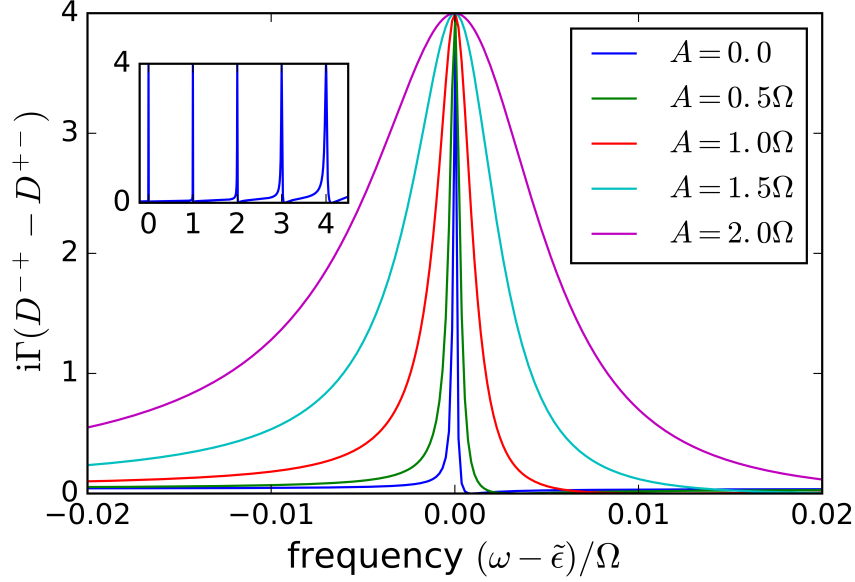


Figure 2.4: Zeroth-order peak (centered around $\omega = \tilde{\epsilon}$) of the PTA spectral function $i\Gamma[D^{+-}(\omega) - D^{++}(\omega)]$ for different values of the drive amplitude A . Stronger drive leads to a significant broadening of the peaks. *Inset*: PTA spectral function, with peaks at every integer multiple of the vibron frequency. Peak width is suppressed by the Franck-Condon factor $e^{-\lambda^2/\Omega^2}$, but increases proportionally to Γ and as a function of frequency. The latter is a result of higher favorability of transitions involving large excitations of the vibron mode.

electron-vibron coupling causes additional broadening of the peaks, which grows larger as a function of peak order. The AC drive causes the peak widths to increase strongly as a function of the drive amplitude, as illustrated in Fig. 2.4.

With the Green's function in Eq. (2.17) we can calculate the steady-state current through the quantum dot

$$\langle I \rangle = -\frac{e}{\pi} \frac{\Gamma}{4} \int_{-eV/2}^{eV/2} d\omega \frac{2\Gamma}{\det \underline{D}^{-1}(\omega)}, \quad (2.18)$$

with V denoting the finite bias voltage between left and right lead, where we take the limit of zero temperature in the leads, $T_{\text{el}} = 0$. The determinant $\det D^{-1}(\omega)$ entails taking the sum over all vibron resonances, modified by the drive. The sequential-tunneling regime is characterized by the fact that only a single such resonance lies within the bias window, i.e., the vibron frequency is larger than the bias eV . Moreover, the width of the resonances is proportional to the square of the tunneling amplitude and suppressed by the Franck-Condon factor, i.e., the resonance width is small compared to the bias window, see Fig. 2.4. Taken together, this allows us to consider only a single resonance as integrand, and to expand the

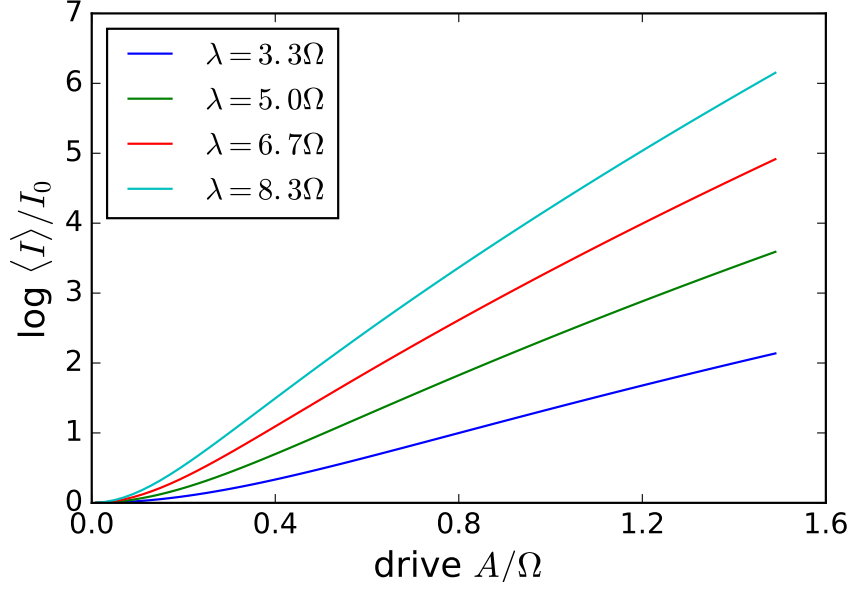


Figure 2.5: Current (logarithmic scale) through the resonantly driven dot, scaled by $I_0 = e^{-\lambda^2/\Omega^2} \Gamma$, as a function of driving amplitude A for different choices of strong electron-vibron coupling λ . Drive lifts the blockade in an almost exponential fashion, with stronger response for larger coupling.

limits of integration in Eq. (2.18) to infinity, resulting in the analytic expression for the current

$$\langle I \rangle = 2e\Gamma e^{-\frac{\lambda^2}{\Omega^2}} \sum_{p \in \mathbb{N}} \Lambda_{\text{dr}}^{(-p)} \frac{1}{p!} \left(\frac{\lambda^2}{\Omega^2} \right)^p, \quad (2.19)$$

where $\Lambda_{\text{dr}}^{(-p)}$ denotes the $(-p)$ th Fourier coefficient of the drive component in Λ ,

$$\Lambda_{\text{dr}}^{(n)} = \sum_{m \geq |n|} \frac{(-1)^{m-n}}{m!m!} \left(\frac{A}{2\Omega} \right)^{2m} \binom{2m}{m+n}. \quad (2.20)$$

For details we refer to App. 2.1.6.

As shown in Fig. 2.5, the current increases almost exponentially as a function of the drive amplitude A , indicating that the Franck-Condon blockade can be lifted through a periodic modulation of the gate voltage. It is to be noted that the deviation from an exponential behavior grows larger as the drive becomes stronger, which might point towards a progressive failure of the PTA. Nonetheless, the above results provide substantial evidence that a CNT quantum dot in the sequential-tunneling regime with strong electron-vibron coupling can be turned into a tunable conductor by means of a time-dependent gate voltage.

2.1.4 Born-Markov analysis

In this section we make use of an alternative approach to the setup under consideration, thus supplementing the result of the Green's function calculation. In particular, we aim to obtain an estimate of the validity the PTA, whose compatibility with a time-dependent drive of the electronic level energy is still untested. For the purposes of the following discussion, it suffices to take into account a single lead, and instead of a steady-state current, study the tunneling rates into this lead, which in the limit of sequential tunneling is proportional to the conductance. [23] The comparability of the latter two quantities is a feature of the sequential-tunneling regime, where the current is made up of consecutive, non-overlapping single-electron tunneling transitions.

The system being weakly coupled to a metallic lead with intractably many degrees of freedom motivates us to perform a partial trace over these lead degrees of freedom. This is the open systems approach outlined in Sec. 1.4: We treat the quantum dot as an open quantum system and the lead as an electron reservoir. [113] The weak coupling Hamiltonian H_I then takes the role of the perturbative system-bath interaction. Under the Born-Markov approximation, the evolution of the system density matrix $\rho_S(t)$ is governed by the quantum master equation [57]

$$\frac{d}{dt}\hat{\rho}_S(t) = - \int_0^\infty ds \operatorname{tr}_B[\hat{H}_I(t), [\hat{H}_I(t-s), \hat{\rho}_S(t) \otimes \rho_B]], \quad (2.21)$$

where the time-dependence in the interaction picture (denoted by a hat) is understood with respect to the quadratic Hamiltonian $\Omega a^\dagger a + [\tilde{\epsilon} + f(t)]d^\dagger d$, and ρ_B denotes the bath density matrix. At this point, an additional simplification presents itself as a consequence of the configuration of our quantum dot: in the Coulomb blockade and sequential tunneling regimes not only the lead excitations, but also the vibrations have fast dynamics compared to the electron on the quantum dot. This means that after the polaron transform the non-perturbative part of the Hamiltonian no longer couples the charge and vibrational degrees of freedom. Hence we can extend the bath to also include the vibron, leaving only the electron in the system. [114, 115] This leads to the bath density matrix composed of the vibrons and the lead $\rho_B = \rho_{\text{vib}} \otimes \rho_{\text{lead}}$. Note that the separation of time scales between electron and vibron relaxation is similar to the reasoning used to motivate the PTA in the previous section. Nevertheless, the two approximations correspond to different partial resummations of a perturbation series and should not be expected to coincide quantitatively.

As outlined in Sec. 1.4, the Born-Markov master equation can be cast in Lindblad form, meaning that a set of coefficients h_μ and system operators C_μ can be found with

$$\frac{d}{dt}\hat{\rho}_S = \sum_\mu h_\mu \left(\hat{C}_\mu \hat{\rho}_S \hat{C}_\mu^\dagger - \frac{1}{2} \{ \hat{\rho}_S, \hat{C}_\mu^\dagger \hat{C}_\mu \} \right). \quad (2.22)$$

Since in our case the vibron degree of freedom is traced over, the Lindblad operators C_μ will be simple functions of the electronic creation and annihilation operators.

However, the presence of the driving term $f(t)d^\dagger d$ casts doubts upon the validity of the approximations leading to this form: in particular, driving the system with a frequency comparable to Ω , as is realistic in the CNT setup, is in conflict with the assumption of separation of time scales, now that the bath includes the vibron. Therefore, we propose the following alternative path to incorporate driving: in a fashion reminiscent of the transformation \mathcal{V} from the previous section, the driving term can be moved onto the vibron sector, where it then can be taken into account by modifying the vibron density matrix in the master equation (2.21). Assuming equilibrium Fermi distributions $n_F(\omega)$ in the lead, the master equation then reads

$$\begin{aligned} \frac{d}{dt}\hat{\rho}_S(t) = & -g^2 \int_0^\infty ds \int d\omega \\ & \left[\langle \tilde{X}(t)\tilde{X}^\dagger(t-s) \rangle n_F(\omega) d d^\dagger e^{i(-\tilde{\epsilon}+\omega)s} \rho_S(t) \right. \\ & + \langle \tilde{X}^\dagger(t)\tilde{X}(t-s) \rangle (1-n_F(\omega)) d^\dagger d e^{-i(-\tilde{\epsilon}+\omega)s} \rho_S(t) \\ & - \langle \tilde{X}^\dagger(t-s)\tilde{X}(t) \rangle d \rho_S(t) d^\dagger (1-n_F(\omega)) e^{i(-\tilde{\epsilon}+\omega)s} \\ & \left. - \langle \tilde{X}(t-s)\tilde{X}^\dagger(t) \rangle d^\dagger \rho_S(t) d n_F(\omega) e^{-i(-\tilde{\epsilon}+\omega)s} \right] + \text{h.c.} \end{aligned} \quad (2.23)$$

where the expectation values are taken with respect to the vibron density matrix ρ_{vib} , which we use below to take into account the drive. Moreover, $\tilde{X}(t) = \exp \left[-\frac{\lambda}{\Omega} (a^\dagger e^{i\Omega t} - a e^{-i\Omega t}) \right]$ denotes the exponential vibron operator. We again assume the lead to be at zero temperature, $T_{\text{el}} = 0$. In the following, we explore different choices for ρ_{vib} , and study the resulting electron tunneling rates.

Vibron in the ground state

To begin with, we assume an unoccupied vibron state and thus $\rho_{\text{vib}}^{(0)} = |0\rangle\langle 0|$, corresponding to the absence of driving and zero temperature. In this case, the traces in Eq. (2.23) are readily performed. Comparing to the master equation in Lindblad form Eq. (2.22) leads to the Lindblad operators $C_{\text{in}}^{(0)} = d^\dagger$ and $C_{\text{out}}^{(0)} = d$ with coefficients

$$\begin{aligned} h_{\text{in}}^{(0)} &= \frac{\Gamma}{2} e^{-\frac{\lambda^2}{\Omega^2}} \sum_{n \geq 0} \frac{(\lambda^2/\Omega^2)^n}{n!} n_F(\tilde{\epsilon} + n\Omega), \\ h_{\text{out}}^{(0)} &= \frac{\Gamma}{2} e^{-\frac{\lambda^2}{\Omega^2}} \sum_{n \geq 0} \frac{(\lambda^2/\Omega^2)^n}{n!} (1 - n_F(\tilde{\epsilon} - n\Omega)), \end{aligned} \quad (2.24)$$

where Γ is defined as before. Due to the specific form of the Lindblad operators, the coefficients $h_{\text{in}}^{(0)}$ and $h_{\text{out}}^{(0)}$ are proportional to the electron tunneling rates. Specifically, the respective appearances of n_F and $1 - n_F$ indicate that $h_{\text{out}}^{(0)}$ governs the case

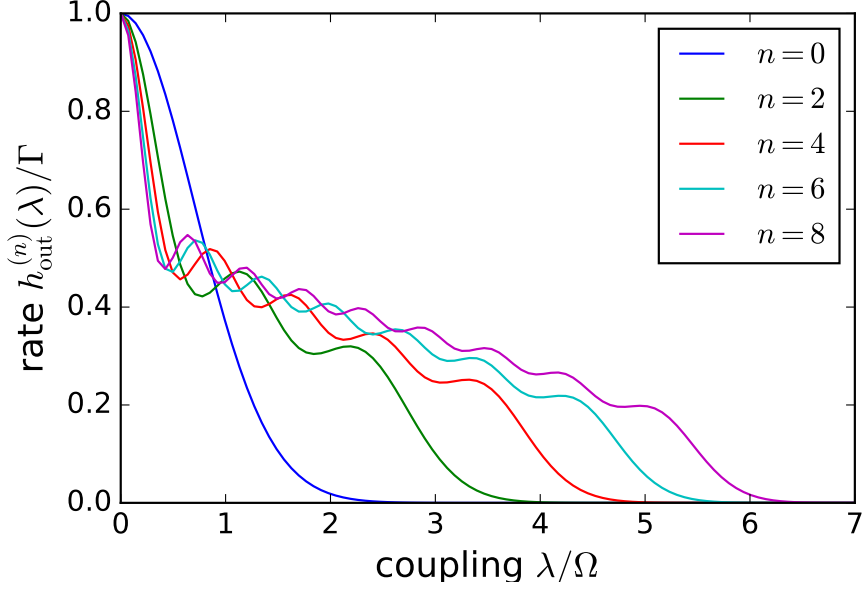


Figure 2.6: Dot electron tunneling rate into the lead, as a function of electron-vibron coupling λ , represented by the Lindblad coefficient $h_{\text{out}}^{(n)}$ for different vibron Fock states n , including the ground state $n = 0$ [Eq. (2.24)]. In the latter case, the rate decreases exponentially for higher electron-vibron coupling, exemplifying Franck-Condon blockade. Higher vibron numbers lead to an intermediate regime of less pronounced decrease. In addition, n manifests itself as the number of local maxima superimposed over the decaying curve.

of tunneling into the lead, whereas $h_{\text{in}}^{(0)}$ describes tunneling in the other direction. The resulting dependence of the decay rates on the coupling strength is shown in Fig. 2.6, illustrating the Franck-Condon blockade in the strong-coupling regime. More quantitatively, we note that the factor $e^{-\lambda^2/\Omega^2}$ matches the Franck-Condon blockade strength obtained from a classical rate equation. [23]

Vibron in a Fock state

Next, we consider the situation where the vibron is prepared in a number state, resulting in the density matrix $\rho_{\text{vib}}^{(n)} = |n\rangle\langle n|$. We can obtain Lindblad coefficients $h_{\text{in}}^{(n)}$ and $h_{\text{out}}^{(n)}$ for any initial occupation number n . The expressions are given in App. 2.1.7 since they are too lengthy to be shown here. In Fig. 2.6 we show the decay rates as functions of the electron-vibron coupling λ/Ω . In contrast to the case of zero initial vibrons, Eq. (2.24), we observe that a number of local maxima is superimposed onto the graphs, implying that the presence of vibrons assists the tunneling of an electron out of the dot. For coupling strengths beyond this non-monotonic region, a more pronounced increase of tunneling as a function of n is

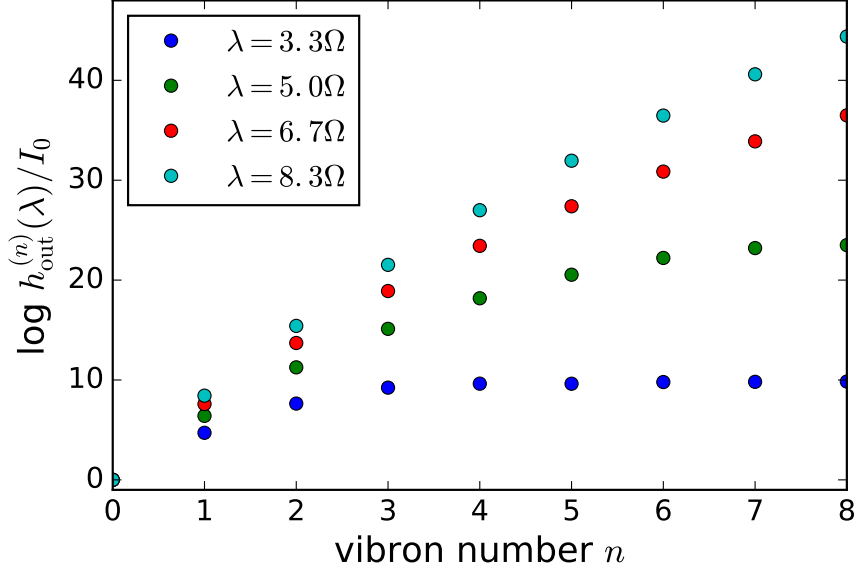


Figure 2.7: Tunneling rate (logarithmic scale) as a function of the vibron number n for different coupling strengths $\lambda > \Omega$. Increasing n leads to faster tunneling, with the growth in tunneling rate highest in the strong-coupling regime, showing near-exponential lifting of Franck-Condon blockade.

observed (see Fig. 2.7), which becomes progressively closer to exponential as the coupling is made larger, implying that the conductive properties of the dot can be exponentially activated by exciting vibrons. Once more, this result is in full agreement with the rate-equation treatment from Ref. [23], where the electron tunneling rates were found to be determined by the matrix elements

$$M_{1 \rightarrow 0}^{q \rightarrow q'} = \left(\frac{\lambda}{\omega}\right)^{q-q'} e^{-\frac{\lambda^2}{2\omega^2}} \sqrt{\frac{q'!}{q!}} L_{q'}^{(q-q')} \left(\frac{\lambda^2}{\omega^2}\right), \quad (2.25)$$

of transitions with initial and final vibron numbers q and $q' \leq q$, respectively. Here $L_n^\alpha(x)$ denote the generalized Laguerre polynomials.¹ Since our approach does not resolve individual vibron transitions, the present results match $\sum_{q'=0}^q |M_{1 \rightarrow 0}^{q \rightarrow q'}|^2$, i.e., the sum of rates for all processes which do not add any vibrons.

Vibron in a coherent state

Finally, we move towards a vibron density matrix that is closer to the driven system we have in mind. A resonant drive of the electron level with amplitude A can be mapped to a vibron drive given by $iA'(a^\dagger e^{-i\Omega_{\text{dr}}t} - a e^{i\Omega_{\text{dr}}t})$, where $A' = A\Omega/(2\lambda)$. If

¹ $L_n^{(\alpha)}(x) = \frac{x^{-\alpha} e^x}{n!} \partial_x^n (e^{-x} x^{n+\alpha})$.

we in addition introduce a vibron damping rate γ to prevent divergences that might arise from driving a part of the bath, this generates the coherent vibron state [116] $|\delta\rangle$ with $\delta \propto iA' / (\Omega_{\text{dr}} - \Omega + i\gamma)$. Therefore, we consider the vibron density matrix $\rho_{\text{vib}}^{(\delta)} = |\delta\rangle \langle \delta|$. For this case, we obtain the Lindblad coefficients

$$\begin{aligned} h_{\text{in}}^{(\delta)} &= \frac{\Gamma}{2} e^{-\frac{\lambda^2}{\Omega^2}} e^{-i2\frac{\lambda}{\Omega}(\sin(\Omega t) \text{Re } \delta - \cos(\Omega t) \text{Im } \delta)} \sum_{m,l \in \mathbb{Z}} e^{i(m+l)\Omega t} \sum_{n \geq 0} \\ &\quad \times \frac{(\lambda^2/\Omega^2)^n}{n!} i^l J_m \left(2\frac{\lambda}{\Omega} \text{Re } \delta \right) J_l \left(-2\frac{\lambda}{\Omega} \text{Im } \delta \right) n_{\text{F}}(\tilde{\epsilon} + (m+l+n)\Omega), \\ h_{\text{out}}^{(\delta)} &= \frac{\Gamma}{2} e^{-\frac{\lambda^2}{\Omega^2}} e^{-i2\frac{\lambda}{\Omega}(\sin(\Omega t) \text{Re } \delta - \cos(\Omega t) \text{Im } \delta)} \sum_{m,l \in \mathbb{Z}} e^{i(m+l)\Omega t} \sum_{n \geq 0} \\ &\quad \times \frac{(\lambda^2/\Omega^2)^n}{n!} i^l J_m \left(2\frac{\lambda}{\Omega} \text{Re } \delta \right) J_l \left(-2\frac{\lambda}{\Omega} \text{Im } \delta \right) (1 - n_{\text{F}}(\tilde{\epsilon} + (m+l-n)\Omega)), \quad (2.26) \end{aligned}$$

where J_n denotes the n th Bessel function of the first kind. Most strikingly, these tunneling rates are time dependent, reflecting the fact that coherent states are not eigenstates of the quadratic Hamiltonian H_0 . The influence of the drive on the decay rates can now be examined by varying the coherent state parameter δ . Specifically, the coherent state displacement δ is proportional to the drive amplitude A' , meaning it can be used as a measure of drive strength. Moreover, the squared absolute value $|\delta|^2$ is proportional to the average number of vibrons in the coherent state, which establishes a link to the Fock state situation discussed previously.

In case of resonant driving, the real part $\text{Re } \delta$ dominates and its magnitude is directly proportional to the drive amplitude. However, the off-resonant situation can be studied in the same fashion by allowing for an imaginary part in δ . There it turns out that detuning between drive and vibron mode reduces the electron tunneling rate, which is in line with the intuition that the conductance is primarily affected by the number of vibrons present on the dot.

In order to make a comparison to the results obtained previously, we proceed to examine the average of $h_{\text{out}}^{(\delta)}$ over one drive period, which can be seen as analogous to the averaging performed to obtain Eq. (2.13) in Sec. 2.1.3. The outcome of this procedure is shown in Fig. 2.8.

Comparing the rates for different values of the drive amplitude uncovers three different regimes: (i) a weak-coupling regime, where increasing the driving strength decreases the tunneling rates, (ii) an intermediate regime showing a moderate increase of the tunneling rates for an increased drive, and (iii) a strong-coupling regime which features an almost exponential rise in tunneling rates as the driving strength is increased. The weak-coupling behavior is mainly an electronic effect: the favored tunneling transition here is the one that does not involve any vibrations. If the drive amplitude is less than the energy gap between dot and lead, there is little effect, but if it is significantly larger, the dot will spend a sizable part of the drive period below the lead; in this position, tunneling is energetically suppressed. For larger drive amplitudes, the portion of a drive period spent below the lead ap-

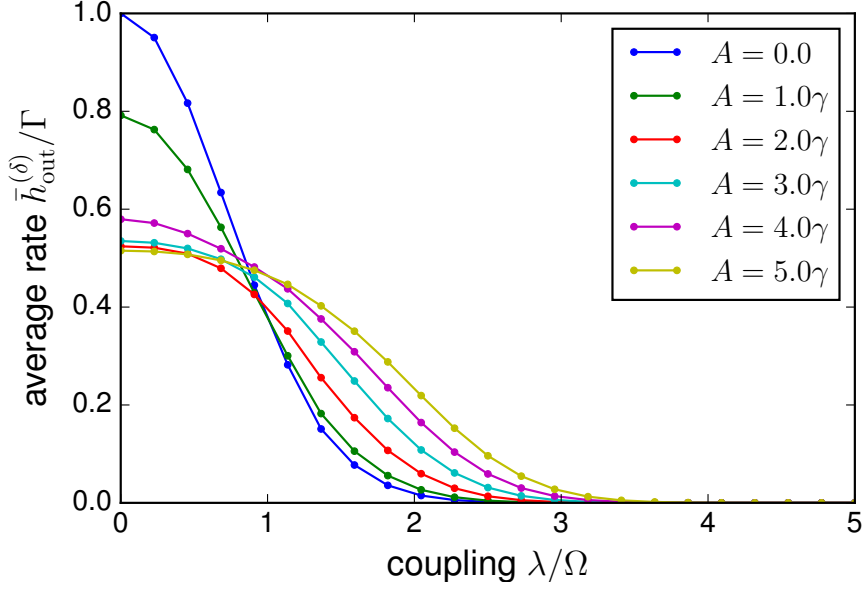


Figure 2.8: Dependence of the electron tunneling rate from the dot (at energy $\tilde{\epsilon} = \Omega/2$) into the lead (at zero energy) on the electron vibron coupling, obtained in the Lindblad formalism with a coherent vibron state. In general, the rate decreases strongly as a function of electron-vibron coupling, exemplifying Franck-Condon blockade. Two different regimes are apparent in the graphs: for weak electron-vibron coupling, the tunneling rate decreases with increasing drive amplitude A as a consequence of the oscillating dot energy dipping below the lead energy for increasing amounts of time. This decrease saturates for large drive, since then the level spends about half of a drive period below the lead energy. For stronger coupling, an increase in tunneling rates with A can be observed, the relative magnitude of which is moderate for $1 \lesssim \lambda/\Omega \lesssim 3$, but becomes more substantial as the coupling is increased beyond that regime, see Fig. 2.9.

proaches $1/2$, just like the resulting tunneling amplitude. For stronger coupling, the converse is true: driving the system makes it more conductive by activating the vibron-assisted tunneling channels. The intermediate regime is less extended here than in the case of vibrons in a Fock state, since $|\delta|^2$, and hence the expected vibron number associated with the coherent state, decreases as λ^{-2} . Lastly, the strong-coupling regime features the weakest currents, but also the strongest relative increase of $h_{out}^{(\delta)}$ as a function of the driving strength, see Fig. 2.9, since conduction there involves the vibrations substantially, similarly to the Fock state case. This results in a current response that is almost perfectly exponential.

The strong-coupling results admit a comparison to the findings of Sec. 2.1.3, where we also derived a relation between the steady-state current and the applied drive strength. In Fig. 2.10 we compare the current obtained by both methods. We

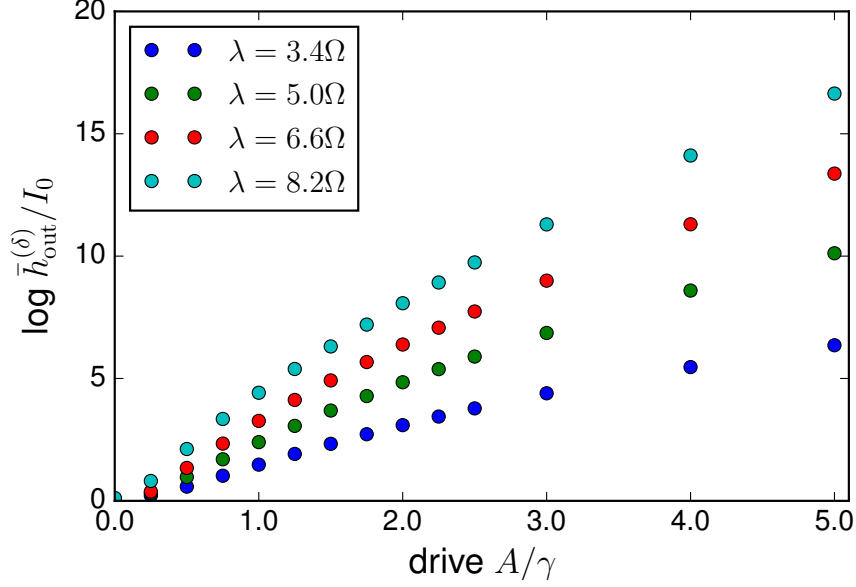


Figure 2.9: Tunneling rate (logarithmic scale) as a function of the drive amplitude A , scaled by the inverse vibron damping γ , for different coupling strengths $\lambda > \Omega$. Increasing A leads to faster tunneling, with the growth in tunneling rate highest in the strong-coupling regime, exhibiting an exponential response over wide ranges of A .

see satisfactory agreement between the two approaches in that, starting from the value of the Franck-Condon factor $e^{-\lambda^2/\Omega^2}$ in the undriven situation, both currents increase roughly exponentially as the drive is turned on. In both cases, further increase of the drive eventually shows a slight attenuation of current growth, resulting in deviations from an exponential characteristic. This leads us to conjecture that these deviations are of a physical nature and not just shortcomings of the specific method used.

2.1.5 Conclusion

We studied the nonequilibrium behavior of a quantum dot with strong interaction between electronic and vibrational degrees of freedom, coupled to a pair of metallic leads in the sequential-tunneling regime. Using Keldysh Green's functions and a partial resummation of diagrams, we obtained the prediction that a periodically modulated gate voltage can be employed to change the transport properties of the system. Specifically, such a form of AC drive gives rise to an increase in steady-state current, lifting the Franck-Condon blockade. This finding turned out to be generally in line with the outcome of a master equation analysis of the electronic dynamics of system: both approaches show a strong current response to

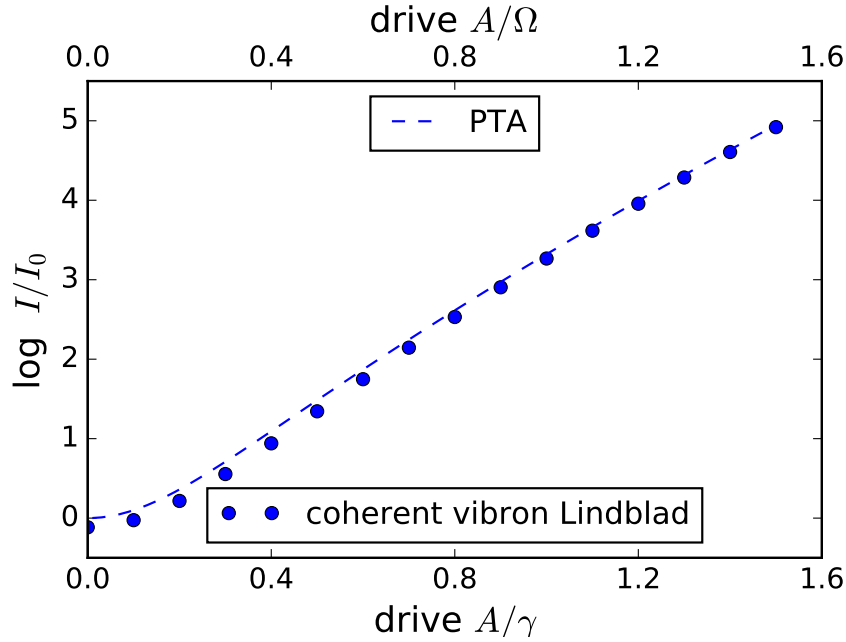


Figure 2.10: Drive dependence of the current (logarithmic scale) through the resonantly driven quantum dot for the case of strong coupling, $\lambda = 6.6\Omega$, as derived in the Green's function and master equation formalisms, respectively. Both cases show a slightly subexponential response to driving, where the deviations from exponential behavior are more pronounced in the Green's function results. There, the drive is parametrized by the amplitude A , and in the master equation approach by the rescaling of A by the vibron damping rate.

the gate voltage, which is close to exponential in the strongly interacting, weakly driven limit. The compatibility of these two results also supports the validity of the polaron-tunneling approximation used in the Green's function treatment in the presence of drive.

The results established here imply a transistor-like behavior of the CNT quantum dot, i.e., a conductance between a pair of leads that can be strongly activated by a gate voltage. The back gates that could be used to supply such a driving gate voltage are already part of some experimentally realized setups, in which they also have been used to modify the electron-vibron interaction and the coupling between quantum dot and leads. Hence, this points towards a variety of arrangements employing CNTs as electronic components of adjustable conductance, since both the coupling strengths and the drive parameters are in the range of experimental feasibility.

Challenges, however, are posed by the fact that the overall currents are still rather small, in spite of the exponential increase. It would therefore be worthwhile to study the intermediate regime where the electron-vibron coupling is not much larger than the frequency of the vibron mode. There, the conductivity is less

strongly suppressed due to the Franck-Condon blockade, albeit at the price of more significant deviations from exponential response.

A further modification could be realized by incorporating the quantum dot into a setup related to circuit quantum electrodynamics (cQED), [117, 118] thus replacing the drive from the gate voltage with one generated by a microwave cavity. Even more, cQED setups would also allow for replacing the classical drive (i.e. a microwave cavity with a large number of photons) by a quantum drive. In such configurations, measurements of the current flowing through the CNT quantum dot could be used to as a detection mechanism for cavity photons. Our finding that the conductance of the electromechanical component is strongly actuated by drive suggests an arrangement of this kind as a possible high-precision measurement device.

2.1.6 Appendix: Details on the NEGF approach

Below, we document the steps leading to the renormalized dot Green's function $D(\omega)$ which is used to obtain the current through the driven quantum dot in the Keldysh formalism. The starting point is the polaron-transformed dot Green's function without renormalization due to tunneling. Using the same notation for the vibrational operator \bar{X} as in the main text, this Green's function reads

$$D_0(\tau, \tau') = \langle d^\dagger(\tau) \bar{X}(\tau) \bar{X}^\dagger(\tau') d(\tau') \rangle_0. \quad (2.27)$$

Since the expectation value is taken with respect to the ground state of the quadratic Hamiltonian $\bar{H}_0 = \Omega a^\dagger a + \tilde{\epsilon} d^\dagger d$, it factors into vibrational and electronic degrees of freedom, where the electronic component can immediately be written as

$$\underline{G}_{\text{dot}}(t - t') = -ie^{-i\tilde{\epsilon}(t-t')} \begin{pmatrix} -N_0 + \Theta(t - t') & -N_0 \\ 1 - N_0 & -N_0 + \Theta(t' - t) \end{pmatrix}, \quad (2.28)$$

with the Heaviside step function Θ , and initial dot occupation N_0 . For the vibron part, we find one of the Keldysh components to be

$$\begin{aligned} \Lambda^{+-}(t, t') &= \langle \bar{X}(t) \bar{X}^\dagger(t') \rangle_0 = \left\langle e^{-\frac{\lambda}{\Omega} [a^\dagger e^{i\Omega t} - a e^{-i\Omega t} + iF(t)]} e^{\frac{\lambda}{\Omega} [a^\dagger e^{i\Omega t'} - a e^{-i\Omega t'} + iF(t')]} \right\rangle_0 \\ &= e^{-\frac{\lambda^2}{\Omega^2}} e^{\frac{\lambda^2}{\Omega^2}} e^{-i\Omega(t-t')} e^{-i \int_{t'}^t ds f(s)}, \end{aligned} \quad (2.29)$$

and analogous results for the others. Here the two exponentials on the left describe the undriven case, in particular the Franck-Condon blockade, and the drive is captured by the remaining factor, which depends on both the initial and final times t and t' . Since we want to capture the steady-state current through the system, we perform an average over one drive period. For the case of resonant driving, this rests upon the vibron timescale being much shorter than the measurement time. Thus we introduce the respective average and relative times $t_{\text{av}} = (t + t')/2$ and

$t_{\text{rel}} = t - t'$, and proceed,

$$\begin{aligned}
& \frac{2\pi}{\Omega} \int_{-\frac{\pi}{\Omega}}^{\frac{\pi}{\Omega}} dt_{\text{av}} \langle \bar{X}(t_{\text{av}} + t_{\text{rel}}/2) \bar{X}^\dagger(t_{\text{av}} - t_{\text{rel}}/2) \rangle_0 \\
&= e^{-\frac{\lambda^2}{\Omega^2}} e^{-\frac{\lambda^2}{\Omega^2}} e^{-i\Omega t_{\text{rel}}} \frac{2\pi}{\Omega} \int_{-\frac{\pi}{\Omega}}^{\frac{\pi}{\Omega}} dt_{\text{av}} e^{-i \int_{t_{\text{av}} - t_{\text{rel}}/2}^{t_{\text{av}} + t_{\text{rel}}/2} ds f(s)} \\
&= e^{-\frac{\lambda^2}{\Omega^2}} e^{\frac{\lambda^2}{\Omega^2}} e^{-i\Omega t_{\text{rel}}} \frac{2\pi}{\Omega} \int_{-\frac{\pi}{\Omega}}^{\frac{\pi}{\Omega}} dt_{\text{av}} e^{-\frac{iA}{\Omega} [\sin \Omega(t_{\text{av}} + t_{\text{rel}}/2) - \sin \Omega(t_{\text{av}} - t_{\text{rel}}/2)]} \\
&= e^{-\frac{\lambda^2}{\Omega^2}} e^{\frac{\lambda^2}{\Omega^2}} e^{-i\Omega t_{\text{rel}}} \frac{2\pi}{\Omega} \int_{-\frac{\pi}{\Omega}}^{\frac{\pi}{\Omega}} dt_{\text{av}} \sum_{n \in \mathbb{Z}} i^n J_n \left(-\frac{2A \sin \Omega t_{\text{rel}}/2}{\Omega} \right) e^{in\Omega t_{\text{av}}} \\
&= e^{-\frac{\lambda^2}{\Omega^2}} (1 - e^{-i\Omega t_{\text{rel}}}) J_0 \left(\frac{2A \sin \Omega t_{\text{rel}}/2}{\Omega} \right), \tag{2.30}
\end{aligned}$$

where $f(t) = A \cos(\Omega t)$ denotes resonant drive.

After this averaging procedure, the bare dot Green's function \underline{D}_0 is connected to the full PTA Green's function \underline{D} via the frequency-space Dyson equation

$$\underline{D}^{-1}(\omega) = \underline{D}_0^{-1}(\omega) - \underline{\Sigma}_{\text{leads}}(\omega), \tag{2.31}$$

which has us perform the Fourier transform of \underline{D}_0 . For the vibron degree of freedom, we note that the undriven part of the result in Eq. (2.30) can be immediately expanded into harmonics of Ω , whereas for the driven part, we can use the series expansion of the zeroth Bessel function, $J_0(x) = \sum_{m \in \mathbb{N}} \frac{(-1)^m}{m!m!} \left(\frac{x}{2}\right)^{2m}$, to calculate the n th Fourier coefficient,

$$\begin{aligned}
\Lambda_{\text{dr}}^{(n)} &= J_0 \left(\frac{2A \sin \Omega t/2}{\Omega} \right)^{(n)} \\
&= \frac{\Omega}{2\pi} \sum_{m \geq 0} \frac{(-1)^m}{m!m!} \frac{A^{2m}}{(i2\Omega)^{2m}} \sum_{k=0}^m \binom{2m}{k} \int_{-\frac{\pi}{\Omega}}^{\frac{\pi}{\Omega}} dt e^{-i(m-k)\Omega t} e^{-in\Omega t} (-1)^{2m-k} \\
&= \sum_{m \geq |n|} \frac{(-1)^{m-n}}{m!m!} \left(\frac{A}{2\Omega} \right)^{2m} \binom{2m}{m+n}. \tag{2.32}
\end{aligned}$$

The dot Green's function is then transformed by convolving the above expres-

sion with the undriven vibron and bare electron parts,

$$\begin{aligned}
\underline{D}_0(\omega) &= \mathcal{F} \left[-i e^{-i\tilde{\epsilon}t} e^{-\frac{\lambda^2}{\Omega^2}} J_0 \left(\frac{2A \sin(\Omega t/2)}{\Omega} \right) \begin{pmatrix} \Theta(t) e^{\frac{\lambda^2}{\Omega^2}} e^{-i\Omega|t|} & 0 \\ 0 & +\Theta(-t) e^{\frac{\lambda^2}{\Omega^2}} e^{-i\Omega|t|} \end{pmatrix} \right] (\omega) \\
&= -i 2\pi e^{-\frac{\lambda^2}{\Omega^2}} \mathcal{F} \left[\sum_{n \in \mathbb{N}} \Lambda_{\text{dr}}^{(n)} e^{in\Omega t} \sum_{k \in \mathbb{N}} \frac{1}{k!} \left(\frac{\lambda^2}{\Omega^2} \right)^k e^{ik\Omega t} \begin{pmatrix} \Theta(t) & 0 \\ 0 & \Theta(-t) \end{pmatrix} \right] (\omega - \tilde{\epsilon}) \\
&= -i 2\pi e^{-\frac{\lambda^2}{\Omega^2}} \sum_{n, k \in \mathbb{N}} \Lambda_{\text{dr}}^{(n)} \frac{1}{k!} \left(\frac{\lambda^2}{\Omega^2} \right)^k \begin{pmatrix} \int_0^\infty dt e^{i(k\Omega + n\Omega + \omega - \tilde{\epsilon})t} & 0 \\ 0 & \int_{-\infty}^0 dt e^{i(k\Omega + n\Omega + \omega - \tilde{\epsilon})t} \end{pmatrix} \\
&= 2\pi e^{-\frac{\lambda^2}{\Omega^2}} \lim_{\eta \rightarrow 0^+} \sum_{n, k \in \mathbb{N}} \Lambda_{\text{dr}}^{(n)} \frac{1}{k!} \left(\frac{\lambda^2}{\Omega^2} \right)^k \begin{pmatrix} \frac{1}{k\Omega + n\Omega + \omega - \tilde{\epsilon} + i\eta} & 0 \\ 0 & -\frac{1}{k\Omega + n\Omega + \omega - \tilde{\epsilon} - i\eta} \end{pmatrix}, \quad (2.33)
\end{aligned}$$

where \mathcal{F} denotes Fourier transform between time and frequency domains, and the cutoff $\eta \rightarrow 0^+$ serves to keep the integrals finite. We dropped the delta functions on the off-diagonal of the Fourier-transformed bare dot electron Green's function because those will not contribute when we invert the matrix in the next step.

Similarly to the bare dot electron Green's function, the sum over the lead Green's functions takes shape as

$$\begin{aligned}
\underline{G}_{\text{leads}}(\omega) &= \frac{1}{L} \sum_k \begin{pmatrix} i 2\pi n_F(\omega_k) \delta(-\omega_k + \omega) + \frac{1}{-\omega_k + \omega + i\eta} & i 2\pi n_F(\omega_k) \delta(-\omega_k + \omega) \\ i 2\pi (n_F(\omega_k) - 1) \delta(-\omega_k + \omega) & i 2\pi n_F(\omega_k) \delta(-\omega_k + \omega) - \frac{1}{-\omega_k + \omega - i\eta} \end{pmatrix}, \quad (2.34)
\end{aligned}$$

for each of the two leads, where n_F again denotes the lead Fermi distribution. Taking the wide-flat-band limit of the lead distribution, we substitute an energy integral for the sum over lead modes, $\frac{1}{L} \sum_k \rightarrow \int dE \rho(E) \approx \bar{\rho} \int dE$, which renders the integration trivial and leaves us with

$$\underline{G}_{\text{leads}}(\omega) = i 2\pi \bar{\rho} \begin{pmatrix} n_L + n_R - \frac{1}{2} & n_L + n_R \\ n_L + n_R - 1 & n_L + n_R - \frac{1}{2} \end{pmatrix}, \quad (2.35)$$

where $n_L = n_F(\omega - eV/2)$ and $n_R = n_F(\omega + eV/2)$. In the polaron tunneling approximation, this Green's function gives rise to the self-energy $\underline{\Sigma}_{\text{leads}} = g^2 \sigma_z \underline{G}_{\text{leads}} \sigma_z$, with the third Pauli matrix²

$$\sigma_z = \begin{pmatrix} 1 & 0 \\ 0 & -1 \end{pmatrix}. \quad (2.36)$$

²This Pauli matrix transformation is required to obtain the sign structure of the self-energy, see Eq. (1.39).

Now we are in position to use Eq. (2.31) to calculate the PTA dot Green's function,

$$\begin{aligned} \underline{D}(\omega) &= (\underline{D}_0(\omega)^{-1} - \Sigma_{\text{leads}}(\omega))^{-1} \\ &= \frac{1}{\det \underline{D}^{-1}(\omega)} \begin{pmatrix} - \left[2\pi e^{-\frac{\lambda^2}{\Omega^2}} \sum_{n \in \mathbb{Z}, k \in \mathbb{N}} \Lambda_{\text{dr}}^{(n)} \frac{1}{k!} \left(\frac{\lambda^2}{\Omega^2} \right)^k \frac{1}{k\Omega + n\Omega + \omega - \tilde{\epsilon}} \right]^{-1} - i\Gamma(n_L + n_R - \frac{1}{2}) & -i\Gamma(n_L + n_R) \\ -i\Gamma(n_L + n_R - 1) & \left[2\pi e^{-\frac{\lambda^2}{\Omega^2}} \sum_{n \in \mathbb{Z}, k \in \mathbb{N}} \Lambda_{\text{dr}}^{(n)} \frac{1}{k!} \left(\frac{\lambda^2}{\Omega^2} \right)^k \frac{1}{k\Omega + n\Omega + \omega - \tilde{\epsilon}} \right]^{-1} - i\Gamma(n_L + n_R - \frac{1}{2}) \end{pmatrix} \end{aligned} \quad (2.37)$$

with the determinant of the inverse Green's function matrix given by

$$\det \underline{D}^{-1}(\omega) = - \left[2\pi e^{-\frac{\lambda^2}{\Omega^2}} \sum_{n \in \mathbb{Z}, k \in \mathbb{N}} \Lambda_{\text{dr}}^{(n)} \frac{1}{k!} \left(\frac{\lambda^2}{\Omega^2} \right)^k \frac{1}{k\Omega + n\Omega + \omega - \tilde{\epsilon}} \right]^{-2} - \frac{\Gamma^2}{4}. \quad (2.38)$$

The sum in this expression runs over all resonances of the vibron mode, where each resonance peak is in turn dressed by drive-induced contributions of the other ones. The resonances are Poisson-weighted in the case of no drive ($A = 0$), and the weakly driven case, where $\Lambda^{(n)}$ is strongly localized around $n = 0$, may be seen as a perturbed version of this.

The analysis in the main text is concerned with the drive dependence of $\underline{D}(\omega)$ around the lowest resonance, which is obtained from the above result by taking $n = -k$.

2.1.7 Appendix: Tunneling rates for Fock vibron state

Here, we provide the Lindblad coefficient for the situation of a vibron prepared in a Fock state, with density matrix $\rho_{\text{vib}}^{(n)} = |n\rangle\langle n|$. In order to cast the master equation Eq. (2.23) into Lindblad form, we calculate the vibron trace

$$\begin{aligned} \langle n| X^\dagger(t) X(t-s) |n\rangle &= e^{-\frac{\lambda^2}{\Omega^2}} \sum_{m \geq 0} \frac{(\lambda^2/\Omega^2)^m}{m!} \sum_{k=0}^n \binom{n}{k} \frac{(-2\lambda^2/\Omega^2)^k}{k!} \\ &\quad \times \sum_{l=0}^k \binom{k}{l} \frac{(-1)^{k-l}}{2^{k-l}} \sum_{p=0}^{k-l} \binom{k-l}{p} e^{i\Omega s(2p-k+l-m)}, \end{aligned} \quad (2.39)$$

which gives rise to the Lindblad coefficients

$$\begin{aligned} h_{\text{in}}^{(n)} &= \frac{\Gamma}{2} e^{-\frac{\lambda^2}{\Omega^2}} \sum_{m \geq 0} \frac{(\lambda^2/\Omega^2)^m}{m!} \sum_{k=0}^n \binom{n}{k} \frac{(-2\lambda^2/\Omega^2)^k}{k!} \\ &\quad \times \sum_{l=0}^k \binom{k}{l} \frac{(-1)^{k-l}}{2^{k-l}} \sum_{p=0}^{k-l} \binom{k-l}{p} n_F(\tilde{\epsilon} - (2p - k + l - m)\Omega), \\ h_{\text{out}}^{(n)} &= \frac{\Gamma}{2} e^{-\frac{\lambda^2}{\Omega^2}} \sum_{m \geq 0} \frac{(\lambda^2/\Omega^2)^m}{m!} \sum_{k=0}^n \binom{n}{k} \frac{(-2\lambda^2/\Omega^2)^k}{k!} \\ &\quad \times \sum_{l=0}^k \binom{k}{l} \frac{(-1)^{k-l}}{2^{k-l}} \sum_{p=0}^{k-l} \binom{k-l}{p} (1 - n_F(\tilde{\epsilon} - (2p - k + l + m)\Omega)). \end{aligned} \quad (2.40)$$

The rates resulting from these coefficients are visualized in Fig. 2.6 of the main text.

2.2 Charge pumping in strongly coupled molecular quantum dots

*The interaction between electrons and the vibrational degrees of freedom of a molecular quantum dot can lead to an exponential suppression of the conductance, an effect which is commonly termed Franck-Condon blockade. Here, we investigate this effect in a quantum dot driven by time-periodic gate voltages and tunneling amplitudes using nonequilibrium Green's functions and a Floquet expansion. Building on previous results showing that driving can lift the Franck-Condon blockade, we investigate driving protocols which can be used to pump charge across the quantum dot. In particular, we show that due to the strongly coupled nature of the system, the pump current at resonance is an exponential function of the drive strength. This section is based on the article Charge pumping in strongly coupled molecular quantum dots, written in collaboration with Han Hoe Yap, Jiangbin Gong, and Thomas L. Schmidt, published in Phys. Rev. B **96**, 195432 (2017).*

2.2.1 Introduction

Recent progress in fabrication and measurement techniques has broken new ground in the field of nanoscale physics: Currently realizable systems allow for the experimental examination and manipulation of single quantum states, putting within reach a wide variety of novel effects [97, 95]. Specifically, the transport properties of such systems are the subject of extensive study, on the quest for pioneering designs of electronic components and circuitry.

One of the core promises of nanoelectronics is to accurately generate and control small amounts of current. In such a context, the paradigm of quantum pumping [119, 120, 121] has received considerable attention. Charge pumping signifies a nonzero time-averaged flow of current through a quantum system as a result of the temporal variation of one [122, 123] or several [124, 125, 126] system parameters, even in the absence of voltage bias. This effect can be achieved, for instance, in a system between two leads at equal chemical potential, where the system parameters are modulated by an external AC signal. Nanoscale charge pumps have potential uses as sources of quantized, tunable currents [127, 128].

The current generated by a quantum pump generally depends in a significant fashion on the drive protocol, which can manifest in various ways: For example, if the drive period is longer than the time scales inherent in the system, an adiabatic time evolution of the system can be used to obtain rather general results for the current [129, 130, 131]. In contrast, for comparatively fast driving, the situation is less straightforward and the resulting pump current tends to depend strongly on the excited state spectrum of the system in question, as well as on the specific driving protocol that is being employed [132, 133].

Charge pumping has been studied frequently in electronic systems. However, nanoscale physics is not limited to electronics alone. In particular, the interactions

between charges and optical or mechanical degrees of freedom open up further avenues for exploration [99, 98, 96]. A prototypical nanoelectromechanical system (NEMS) exists for instance in the form of carbon nanotubes (CNT) [103, 25, 24, 100, 31, 105]. It has recently become possible to use electronic gates to define a quantum dot on a CNT and to tailor the interaction of electrons and quantized vibrational modes (“vibrons”) of the nanotube [134, 26, 30].

In particular, the interplay between electronic and mechanical degrees of freedom in a NEMS can have profound consequences for its conductive properties: The simplest such system – a single vibrational mode interacting with an electronic level – already gives rise to an infinite ladder of composite electromechanical states (“polarons”) that can in principle contribute to conduction. In the limit of strong electron-vibron coupling, the transitions involving low-lying states of this ladder are exponentially suppressed, leading to a drastic reduction in current, a phenomenon called Franck-Condon blockade (FCB) [20, 21, 23]. On the other hand, it was shown recently that an AC gate voltage in resonance with the vibration can be used to actuate conduction channels that are much less strongly suppressed, which lifts the Franck-Condon blockade exponentially in the drive amplitude [135]. In Ref. [135], it was proposed to observe this effect in a CNT quantum dot, since such a system exhibits the required strong coupling, and the AC gate voltage could be supplied by the gates used to define the quantum dot [106]. Here, we extend this setup by using additional gates to also modulate the coupling of the quantum dot to the lead electrodes. The availability of more than one time-dependent parameters then allows us to build a bridge towards charge pumping.

Here, we study the current response of a Franck-Condon-blockaded quantum dot to several periodic drives. We consider a model for a quantum dot with interacting vibrational and electronic sectors, weakly coupled to a pair of metallic leads. A drive protocol is defined which modulates both the coupling to the leads and the energy level of the dot. As a result of this drive, we find that charge pumping through the dot can be achieved. Interestingly, we find that for drive frequencies resonant with the vibron mode, the pump current depends exponentially on the drive amplitude.

Our work is organized as follows: In Sec. 2.2.2, we lay out the model used to describe a doubly-driven electromechanical quantum dot. Sec. 2.2.3 contains the derivation of the current through the system, where we use the Keldysh nonequilibrium Green’s function method in conjunction with the polaron tunneling approximation and a Floquet expansion. We apply this method to a specific driving protocol in Sec. 2.2.5, leading to a description of charge pumping. In Sec. 2.2.6, we summarize our findings and discuss extensions and ideas for application.

2.2.2 Model

In principle, the electronic interactions on a CNT quantum dot can be very complex as different vibron modes may couple to the charges in different electronic orbitals. In the following, we capture the essential physics by using as a min-

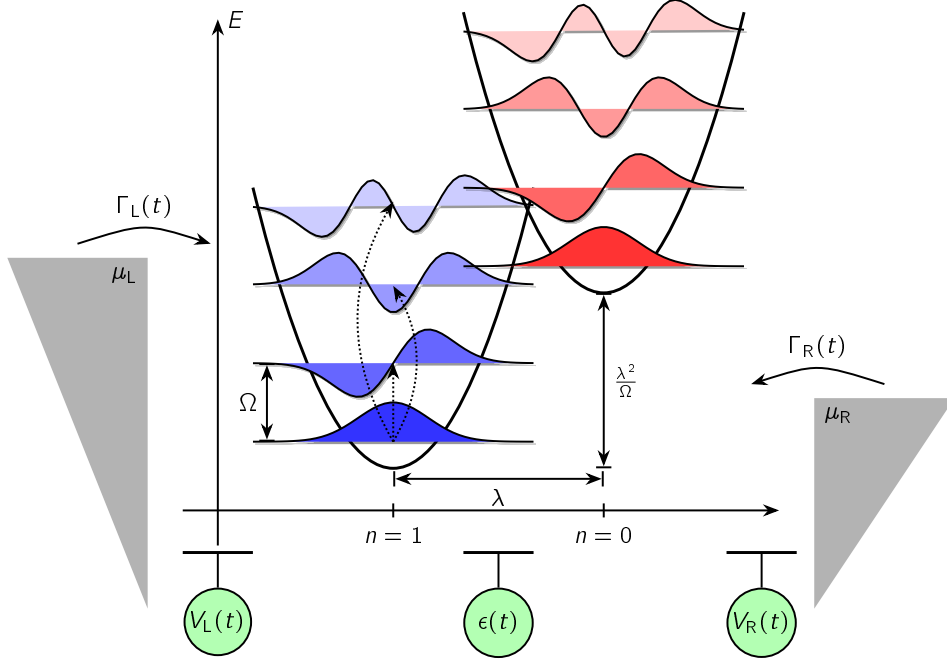


Figure 2.11: Schematics of the Hamiltonian from Eq. (2.41). As a result of electron-vibron coupling, the vibrational spectrum has different ground state energies depending on the electron number $n = \langle d^\dagger d \rangle$, with the unoccupied sector ($n = 0$) having an energy increase of λ^2/Ω . The energy of the dot electron $\epsilon(t)$ and the couplings to the leads $V_{L,R}(t)$ are subject to periodic driving.

imal model for electron-vibron interactions the Anderson-Holstein Hamiltonian $H = H_{\text{dot}} + H_{\text{lead}} + H_{\text{tun}}$, where

$$\begin{aligned}
 H_{\text{dot}} &= \Omega a^\dagger a + \bar{\epsilon}(t) d^\dagger d + \lambda(a^\dagger + a)d^\dagger d, \\
 H_{\text{lead}} &= \sum_{\alpha=L,R} \sum_k \epsilon_{k\alpha} c_{k\alpha}^\dagger c_{k\alpha}, \\
 H_{\text{tun}} &= \sum_{\alpha=L,R} \sum_k [V_{k\alpha}(t) d^\dagger c_{k\alpha} + \text{h.c.}], \tag{2.41}
 \end{aligned}$$

denote the dot, lead and tunneling Hamiltonians, respectively. This is a variant of the Hamiltonian Eq. (2.1) studied in Sec. 2.1, with the only difference being that the dot couples to each mode in the leads via the time-dependent tunneling amplitude $V_{k\alpha}(t)$. A summary of the components of the Hamiltonian is given in Fig. 2.11.

The dot Hamiltonian can be mapped onto a non-interacting model [108] by applying the unitary transformation $\tilde{H} = \mathcal{U} H \mathcal{U}^{-1}$, where $\mathcal{U} = \exp[\lambda(a^\dagger - a)d^\dagger d/\Omega]$. Indeed, this procedure results in a quadratic Hamiltonian $\tilde{H}_0 = \tilde{H}_{\text{dot}} + H_{\text{lead}}$, with $\tilde{H}_{\text{dot}} = \epsilon(t) d^\dagger d + \Omega a^\dagger a$, where the dot electron energy has been renormalized to $\epsilon(t) = \bar{\epsilon}(t) - \lambda^2/\Omega$. While the lead Hamiltonian remains unchanged, the tunneling

amplitudes are dressed by an exponential vibrational factor,

$$\tilde{H}_{\text{tun}} = \sum_{\alpha} \sum_k \left[V_{k\alpha}(t) X^{\dagger} d^{\dagger} c_{k\alpha} + \text{h.c.} \right], \quad (2.42)$$

where $X = e^{-\frac{\lambda^2}{\Omega^2}(a^{\dagger}-a)}$ encodes the modification of the tunneling process due to the polaron.

In the limit of slow tunneling, $V_{k\alpha} \ll \min(\lambda, \Omega)$, insight into the transport properties of the system has been obtained: In the time-independent case, $V_{k\alpha}(t) \equiv V_{k\alpha}$, $\epsilon(t) \equiv \epsilon$, the electron-vibron interaction leads to an exponential suppression of DC current, $\langle I \rangle \propto e^{-\lambda^2/\Omega^2}$. This phenomenon is known as Franck-Condon blockade [20, 21, 23] and can be pictured as follows: As a consequence of electron-vibron interaction, the lattice structure of the dot will be deformed in the presence of an electron, whereby a polaron is formed. If current is to flow through the dot, e.g., if the electron is to tunnel out, this composite state has to be broken up, which is energetically costly for strong electron-vibron interaction. In Sec. 2.1, we showed how application of an AC voltage to the dot can supply the energy required to break up the polaron, facilitating electron tunneling and lifting the current blockade [135]. In the following, we set up a formalism that allows us to treat periodic, resonant drives in both the dot energy $\epsilon(t)$ and the coupling to the leads $V_{k\alpha}(t)$.

2.2.3 Floquet Green's functions

In order to calculate the current through the quantum dot, we make use of the nonequilibrium Green's function technique. The operator describing the charge current flowing through the lead α is given by

$$\begin{aligned} I_{\alpha} &= e \frac{d}{dt} \sum_k c_{k\alpha}^{\dagger} c_{k\alpha} = -ie \left[\sum_k c_{k\alpha}^{\dagger} c_{k\alpha}, \tilde{H} \right] = \\ &= ie \sum_k V_{k\alpha}(t) X^{\dagger}(t) d^{\dagger}(t) c_{k\alpha}(t) + \text{h. c.}, \end{aligned} \quad (2.43)$$

where the time dependence of the operators is understood to arise from evolution with the full Hamiltonian \tilde{H} . Therefore, the current expectation value can be expressed as

$$\langle I_{\alpha}(t) \rangle = e \sum_k V_{k\alpha}(t) F_{k\alpha}^{-+}(t, t) + \text{c.c.}, \quad (2.44)$$

with $F_{k\alpha}(\tau, \tau') = -i \langle T_C c_{k\alpha}(\tau') X^{\dagger}(\tau') d^{\dagger}(\tau') \rangle$ denoting the contour ordered ‘‘mixed’’ dot-lead Keldysh Green's function. Specifically, the times τ and τ' lie on the Keldysh contour C , as depicted in Fig. 1.3.

Polaron tunneling approximation

In principle, the Green's function $F_{k\alpha}(\tau, \tau')$ can be calculated perturbatively in \tilde{H}_{tun} for weak coupling between dot and lead. Unfortunately, a direct resummation of the perturbation series is impossible because \tilde{H}_{tun} contains the vibrational operator X , and thus gives rise to expectation values for which Wick's theorem does not hold. Therefore, we use the same polaron-tunneling approximation as in Sec. 2.1. Within this approximation, the renormalized polaron dot Green's function $D(\tau, \tau') = -i\langle T_C d(\tau) d^\dagger(\tau') X(\tau) X^\dagger(\tau') \rangle$ obeys the Dyson equation

$$D(\tau, \tau') = D_0(\tau, \tau') + \int_C d\sigma_1 \int_C d\sigma_2 D_0(\tau, \sigma_1) \Sigma(\sigma_1, \sigma_2) D(\sigma_2, \tau'), \quad (2.45)$$

where the bare polaron dot Green's function reads

$$D_0(\tau, \tau') = -i \langle T_C d(\tau) d^\dagger(\tau') \rangle_0 \langle T_C X(\tau) X^\dagger(\tau') \rangle_0 \quad (2.46)$$

and the subscript “0” denotes expectation values with respect to \tilde{H}_0 . The self-energy is given by

$$\begin{aligned} \Sigma(\sigma_1, \sigma_2) &= \sum_{k\alpha} V_{k\alpha}(\sigma_1) V_{k\alpha}^*(\sigma_2) G_{0,k\alpha}(\sigma_1, \sigma_2) \\ &\equiv \sum_{\alpha} \Sigma_{\alpha}(\sigma_1, \sigma_2), \end{aligned} \quad (2.47)$$

in terms of the bare lead Green's function

$$G_{0,k\alpha}(\sigma_1, \sigma_2) = -i \langle T_C c_{k\alpha}(\sigma_1) c_{k\alpha}^\dagger(\sigma_2) \rangle_0. \quad (2.48)$$

Having obtained a Dyson equation, the expectation value of the current through either of the leads can now be calculated in the fashion explained in Sec. 1.2.3.

$$\begin{aligned} \langle I_{\alpha}(t) \rangle &= e \sum_k V_{k\alpha}(t) F^{-+}(t, t) + \text{c.c.} \\ &= 2e \text{Re} \int_{-\infty}^{\infty} ds \left[\Sigma_{\alpha}^R(t, s) D^{-+}(s, t) + \Sigma_{\alpha}^{-+}(t, s) D^A(s, t) \right], \end{aligned} \quad (2.49)$$

using the Langreth rule Eq. (1.51) for the lesser component of a convolution.

Floquet expansion

As a result of the time convolution, Dyson equation (2.45) does not admit an analytical solution for arbitrary time dependent drives. For periodic drives, however, we can perform an expansion into Floquet modes to simplify the problem [55], as detailed in Sec. 1.3.

In particular, we write the dot Green's function $\check{D}(t, t')$ as an infinite-dimensional matrix in the fashion of Eq. (1.89),

$$\check{D}_{mn}(\omega) = \check{D}\left(m - n, \omega + \frac{m + n}{2} \Omega_{\text{dr}}\right). \quad (2.50)$$

This representation allows to write convolutions in the time domain as matrix multiplications in frequency space: For a function $C(t, t') = \int_{-\infty}^{\infty} ds A(t, s) B(s, t')$, the Floquet expansion is given by $C_{mn}(\omega) = \sum_{k=-\infty}^{\infty} A_{mk}(\omega) B_{kn}(\omega)$. In order to perform this multiplication, we limit the dimension of the matrices to $N \equiv 2N_{\text{Fl}} + 1$, with the index k running from $-N_{\text{Fl}}$ to N_{Fl} .

In this manner, Eq. (2.49) yields the Floquet components of the current expectation value,

$$\begin{aligned} \langle I_{\alpha}(\omega) \rangle_{mn} = e \sum_{k=-\infty}^{\infty} & \left[(\Sigma_{\alpha}^{\text{R}})_{mk}(\omega) D_{kn}^{-+}(\omega) + (\Sigma_{\alpha}^{-+})_{mk}(\omega) D_{kn}^{\text{A}}(\omega) + \right. \\ & \left. + (\Sigma_{\alpha}^{\text{R}})_{-m-k}(-\omega)^* D_{-k-n}^{-+}(-\omega)^* + (\Sigma_{\alpha}^{-+})_{-m-k}(-\omega)^* D_{-k-n}^{\text{A}}(-\omega)^* \right]. \end{aligned} \quad (2.51)$$

In particular, the total steady-state (DC) current through the quantum dot takes shape as

$$\langle I \rangle^{\text{DC}} = \frac{\Omega_{\text{dr}}}{2\pi} \int_{-\mathcal{T}/2}^{\mathcal{T}/2} dt_{\text{av}} \langle I(t_{\text{av}}) \rangle = \int \frac{d\omega}{2\pi} \langle I(\omega) \rangle_{00}, \quad (2.52)$$

where we defined the current difference $I = I_{\text{L}} - I_{\text{R}}$. It remains to calculate the Floquet expansions of the dot Green's function and of the self-energy, which is readily achieved: Since the Dyson equation, Eq. (2.45), only involves a time convolution, its retarded and advanced components can also be written in terms of a Floquet matrix multiplication,

$$(D^{\text{R,A}})_{mn}(\omega) = (D_0^{\text{R,A}})_{mn}(\omega) + \sum_{k,l=-\infty}^{\infty} (D_0^{\text{R,A}})_{mk}(\omega) \Sigma_{kl}^{\text{R,A}}(\omega) D_{ln}^{\text{R,A}}(\omega). \quad (2.53)$$

This equation can be explicitly solved for $D^{\text{R,A}}$ by inversion, provided we truncate the matrices to a finite dimension N . Once $D^{\text{R,A}}$ are known, the lesser component can also be calculated using the Keldysh integral equation,

$$D^{-+}(t, t') = \int ds ds' D^{\text{R}}(t, s) \Sigma^{-+}(s, s') D^{\text{A}}(s', t'), \quad (2.54)$$

whose Floquet expansion is again given by a matrix multiplication.

Finally, we give the components of the Dyson equation for a general form of the driving protocol used in the following sections,

$$\begin{aligned} \epsilon(t) &= A \cos \Omega_{\epsilon} t, \\ V_{k\alpha}(t) &= v_{k\alpha} [1 + \Delta \cos(\Omega_V t + \phi_{\alpha})], \end{aligned} \quad (2.55)$$

where the formalism admits any kind of commensurate choice for the drive frequencies Ω_{ϵ} and Ω_V . Expanding the bare Green's function, we obtain

$$\begin{aligned} D_0(t_{\text{av}}, t_{\text{rel}}) &= \sum_{n \in \mathbb{Z}} e^{in\Omega_{\epsilon} t_{\text{av}}} \int_{-\infty}^{\infty} \frac{d\omega}{2\pi} e^{-i\omega t_{\text{rel}}} \\ &\times \sum_{m \geq 0} \sum_{k=0}^{2m+n} D_0^{\text{free}} \left(\omega - \left(m + \frac{n}{2} - k \right) \Omega_{\epsilon} \right) \lambda_n^{mk}, \end{aligned} \quad (2.56)$$

where we abbreviated $\lambda_n^{mk} = \frac{(-1)^k}{m!(m+n)!} \left(\frac{A}{2\Omega_\epsilon}\right)^{2m+n} \binom{2m+n}{k}$. The bare dot Green's function in the absence of drive is denoted by $D_0^{\text{free}}(\omega)$, with its retarded component given by

$$\left(D_0^{\text{free}}\right)^R(\omega) = e^{-\lambda^2/\Omega^2} \sum_{k \geq 0} \frac{\lambda^{2k}/\Omega^{2k}}{k!} \frac{1}{\omega - \epsilon - k\Omega + i0^+}. \quad (2.57)$$

Hence, the bare dot Green's function is given by a series of resonances at integer multiples of the vibron frequency, which follow a drive-modified Poisson distribution strongly dependent on the electron-vibron coupling parameter λ/Ω .

Taking the wide-band limit for the leads and their coupling to the dot results in a frequency-independent bare electronic tunneling rate $\Gamma = 2\pi \sum_k |v_{k\alpha}|^2 \delta(\omega - \epsilon_{k\alpha})$, and yields the mode expansion for the retarded self-energy,

$$\Sigma_\alpha^R(n, \omega) = -i \frac{\Gamma_\alpha}{2} \begin{cases} \frac{|\Delta|^2}{4} e^{-i2\phi_\alpha}, & n = -2 \\ \frac{\Delta + \Delta^*}{2} e^{-i\phi_\alpha}, & n = -1 \\ 1 + \frac{|\Delta|^2}{2}, & n = 0 \\ \frac{\Delta + \Delta^*}{2} e^{i\phi_\alpha}, & n = 1 \\ \frac{|\Delta|^2}{4} e^{i2\phi_\alpha}, & n = 2 \end{cases}, \quad (2.58)$$

where the limitation of the Wigner mode indices $n \in \{0, \pm 1, \pm 2\}$ results from the single-mode character of $V_{k\alpha}$. Furthermore, the lesser component reads

$$\begin{aligned} \Sigma_\alpha^{-+}(n, \omega) &= \\ &= i\Gamma_\alpha \begin{cases} \frac{|\Delta|^2}{4} e^{-i2\phi_\alpha} n_{F\alpha}(\omega), & n = -2 \\ \frac{\Delta}{2} e^{-i\phi_\alpha} n_{F\alpha}(\omega - \Omega_V/2) + \frac{\Delta^*}{2} e^{-i\phi_\alpha} n_{F\alpha}(\omega + \Omega_V/2), & n = -1 \\ n_{F\alpha}(\omega) + \frac{|\Delta|^2}{4} n_{F\alpha}(\omega + \Omega_V) + \frac{|\Delta|^2}{4} n_{F\alpha}(\omega - \Omega_V), & n = 0 \\ \frac{\Delta^*}{2} e^{i\phi_\alpha} n_{F\alpha}(\omega - \Omega_V/2) + \frac{\Delta}{2} e^{i\phi_\alpha} n_{F\alpha}(\omega + \Omega_V/2), & n = 1 \\ \frac{|\Delta|^2}{4} e^{i2\phi_\alpha} n_{F\alpha}(\omega). & n = 2 \end{cases} \end{aligned} \quad (2.59)$$

Here, we consider the leads at zero temperature, meaning that the Fermi function of lead α is a step function $n_{F\alpha}(\omega) = \theta(\mu_\alpha - \omega)$, with the chemical potentials μ_α .

After converting these Wigner expansions into Floquet modes via Eq. (2.50), the Dyson equation Eq. (2.53) can be solved to obtain the renormalized dot Green's function and hence the current. A detailed derivation of Eqs. (2.56)–(2.59) can be found in Appendix 2.2.7.

2.2.4 Current under bias

In this section, we use the Floquet-Green's function expression for the calculation of the average current. Specifically, we apply it to a polaron quantum dot subject to a bias $eV \equiv \mu_L - \mu_R$ between left and right leads, with a time-dependent drive

applied to both the dot energy and the coupling to the leads. By comparing to the results from Sec. 2.1 [135], we are also able to estimate the influence of Floquet harmonics beyond the leading order on the lifting of Franck-Condon blockade.

The pumping protocol examined here consists of two single-mode drives,

$$\begin{aligned}\epsilon(t) &= A \cos \Omega t, \\ V_{k\alpha}(t) &= v_{k\alpha} [1 + \Delta \cos (\Omega t/2)].\end{aligned}\tag{2.60}$$

The dot drive $\epsilon(t)$ is chosen to be resonant with the vibron mode so as to maximize the resulting current amplification [135]. Moreover, the coupling is driven at half of this frequency, so that the self-energy, which contains the square of the coupling, is itself in resonance with the dot and the vibron. According to Eq. (2.57), the bare dot Green's function features resonances at all positive integer multiples of Ω . We choose a bias voltage V in such a way as to reach the regime which exhibits the strongest Franck-Condon blockade as well as the most pronounced current response to drive, [135] i.e., $\Gamma \ll eV \ll \Omega$. The integrand $\langle I_{00}(\omega) \rangle$ that gives rise to the DC current flowing through this setup can be seen in Fig. 2.12 for different values of the dot drive amplitude A . All current is due to the single resonance within the bias window, whose width is suppressed by the FCB factor $e^{-\lambda^2/\Omega^2}$, but strongly increases with A . The drive dependence of the integrated DC current $\langle I \rangle^{\text{DC}}$ calculated from Eq. (2.52) is illustrated in Fig. 2.13.

The striking feature here is the degree of difference between the respective current responses to the dot and coupling drives: The dot drive causes exponential lifting of the Franck-Condon blockade as a function of dot drive amplitude A , regardless of the presence of the coupling drive. By contrast, the dependence on the coupling drive amplitude Δ is only quadratic, as is expected from the fact that it directly multiplies the tunneling coefficient $v_{k\alpha}$, the square of which is featured in the bare electronic tunneling rate Γ . Compared to the dependence on the dot drive, the effect of the coupling drive is minuscule: Increasing the amplitude up to the static value $v_{k\alpha}$ of the coupling causes a mere 2% difference in current.

Finally, Fig. 2.13 also shows that the impact of higher Floquet harmonics on the current response is negligible: The Floquet result obtained using a matrix dimension $N_{\text{Fl}} = 5$ in Eq. (2.51) differs little from the outcome of the simplified calculation in Sec. 2.1, where the response to the dot drive was calculated using only time-averaged Green's functions, which is equivalent to truncating the Floquet matrices down to $N_{\text{Fl}} = 1$.

2.2.5 Polaron pumping

In this section we consider the unbiased polaron dot, i.e., we set the chemical potentials of the leads to $\mu_L = \mu_R = 0$. In this case, a DC current can still flow in the presence of a drive protocol which breaks the left-right symmetry. In order to break this symmetry, we add phase differences ϕ_α to the left and right coupling

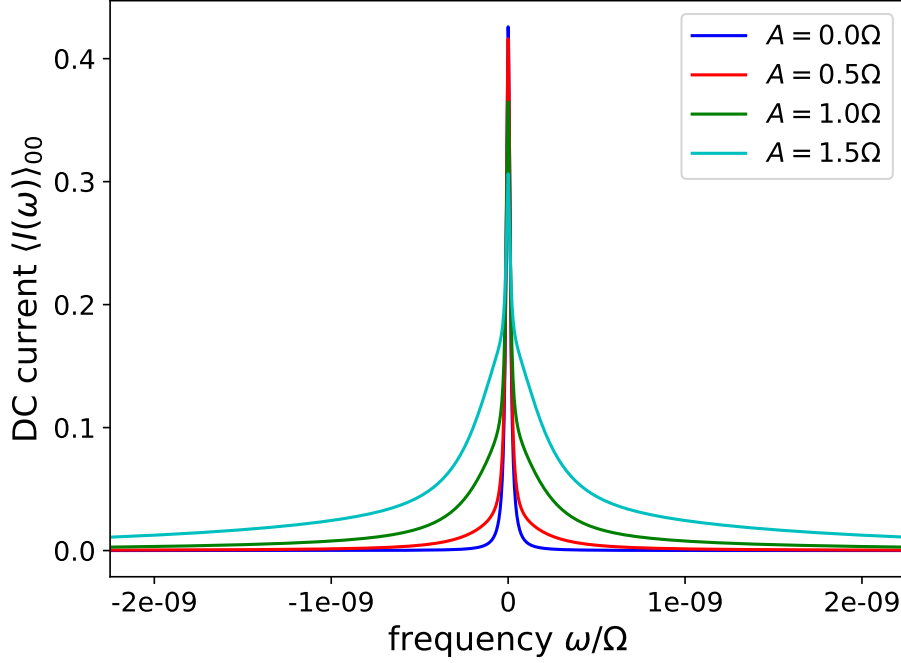


Figure 2.12: Frequency-resolved DC current integrand $\langle I_\alpha(\omega) \rangle_{00}$ through a biased polaron dot ($\mu_L = -\mu_R = \Omega/4$), evaluated near the zeroth-order resonance. We use Eq. 2.51 with Floquet matrix dimension $N_{\text{Fl}} = 5$ for different values of the dot drive amplitude A , and a coupling drive amplitude of $\Delta = 0.6$, as well as a bare electronic tunneling rate $\Gamma = 0.002\Omega$. Increasing A causes substantial widening of the peak, signifying strong current increase.

drives, so that the driving protocol is given by

$$\begin{aligned} \epsilon(t) &= A \cos \Omega t, \\ V_{k\alpha}(t) &= v_{k\alpha} [1 + \Delta \cos(\Omega t/2 + \phi_\alpha)]. \end{aligned} \quad (2.61)$$

For such a setup, various channels contribute to charge transport through the dot, as evidenced by the current integrand depicted in Fig. 2.14, which exhibits several resonances of comparable height. The role of higher Floquet harmonics is evident from the slower convergence of the result as a function of the truncation index N_{Fl} , when compared to the situation with bias. This effect becomes more pronounced as the drive amplitudes are increased.

The interplay between the drive parameters is more complex than in the biased case: Fundamentally, there can be no current without breaking the left-right symmetry, so the phase differences are essential to achieve current flow. In the same vein, the dot drive $\epsilon(t)$ by itself will not produce any current: the coupling drive $V_{k\alpha}(t)$ is also required. This is reflected in Fig. 2.15, where dependencies of the DC

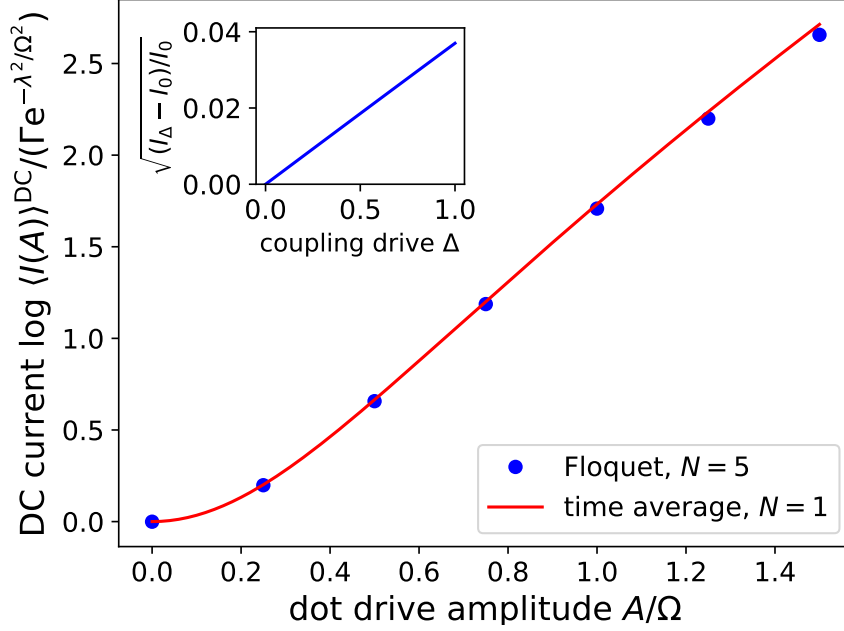


Figure 2.13: Exponential FCB ($\lambda = 4\Omega$) lifting by driving the dot energy in the presence of a bias window $\mu_L = -\mu_R = \Omega/4$. Floquet result (blue) with dimension $N_{\text{Fl}} = 5$ to be compared with the result (red) from Ref. [135], corresponding to $N_{\text{Fl}} = 1$. *Inset*: Increasing the coupling drive for fixed dot drive leads to a small-scale quadratic rise in tunneling current I_Δ .

current $\langle I \rangle^{\text{DC}}$ through the unbiased dot on dot drive and phase shift are on display, with the dependence on the phase difference isolated in the inset: In the absence of dot drive ($A = 0$), no current is measured, independently of coupling drive and phase, and the same is true for the case of zero phase difference ($\phi_L = \phi_R$). Even though the phase difference appears to have little influence on the shape of the resonances, it has a much more significant effect on the integrated current: For a nonvanishing phase difference, a current response to the dot drive is observed, with the current increasing roughly linearly in the regime of $A \ll \Omega$, and in a superlinear fashion for larger values of A . On the other hand, for a fixed value of A , the current depends on the phase difference in a sinusoidal fashion. Taken together, we find that the current response to the driving protocol is given by

$$\langle I(A, \Delta) \rangle^{\text{DC}} \propto \Gamma e^{-\lambda^2/\Omega^2} \frac{A}{\Omega} e^{A/\Omega} \Delta^2 \sin \phi, \quad (2.62)$$

where $\phi = \phi_L - \phi_R$, for $\Delta \lesssim 1$.

Equation (2.62) is the main result of this work. It combines features known from charge pumping through purely electronic quantum dots with the Franck-

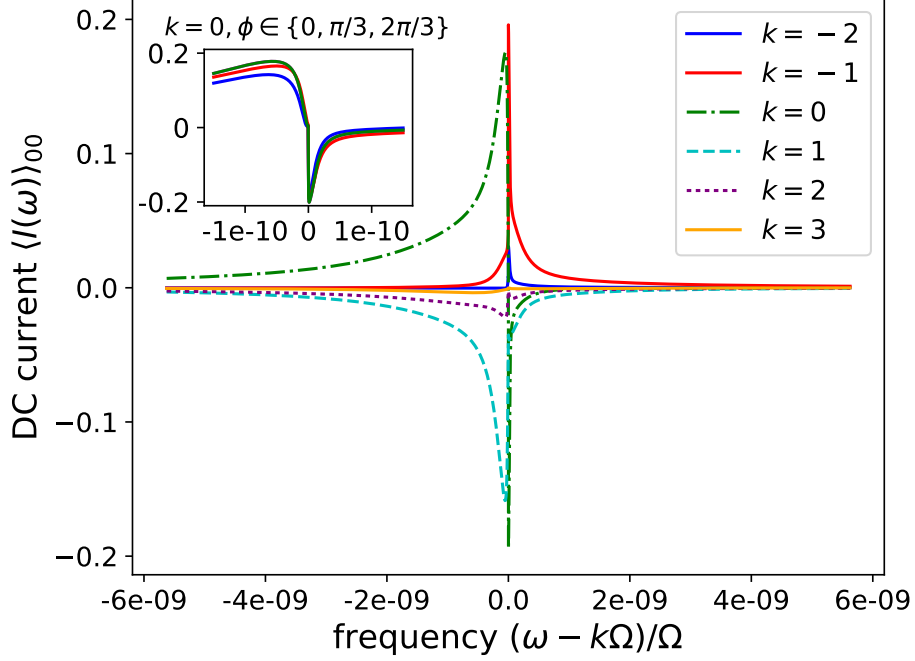


Figure 2.14: Frequency-resolved DC current integrand $\langle I_\alpha(\omega) \rangle_{00}$, through an unbiased polaron dot, evaluated near the peak locations (peak order k), using Eq. (2.51) with Floquet matrix dimension $N_{\text{Fl}} = 21$. The coupling drive amplitude and bare tunneling rate are given by $\Delta = 0.6$ and $\Gamma = 0.002\Omega$, respectively. The side resonances appearing outside the bias window are comparable in size to the central one at $k = 0$, but different sides lead to partial cancellation upon integration. *Inset*: Modification of the shape of the central resonance for different values of phase shift.

Condon physics of strongly coupled electromechanical quantum dots: On the one hand, the factors of the bare tunneling rate, as well as the dot and coupling drive amplitudes, occur in the same fashion as in a quantum dot without mechanical degrees of freedom [126, 136]. Moreover, the dependence on the sine of the phase difference is a feature of adiabatic pumping [137] which persists in the highly non-adiabatic protocol considered here. On the other hand, the frequency dependence of the pumped current is dominated by the condition of resonance with the vibrational frequency and thus the current increase as a function of frequency, which is a feature of the purely electronic case, does not manifest here. Finally, the Franck-Condon blockade factor as well as the exponential increase in current as a function of dot drive are familiar from the lifting of Franck-Condon blockade in the unbiased case of our model [135].

Hence we conclude that the polaron dot exhibits pumping characteristics similar to a non-interacting system, in addition to Franck-Condon blockade and strong

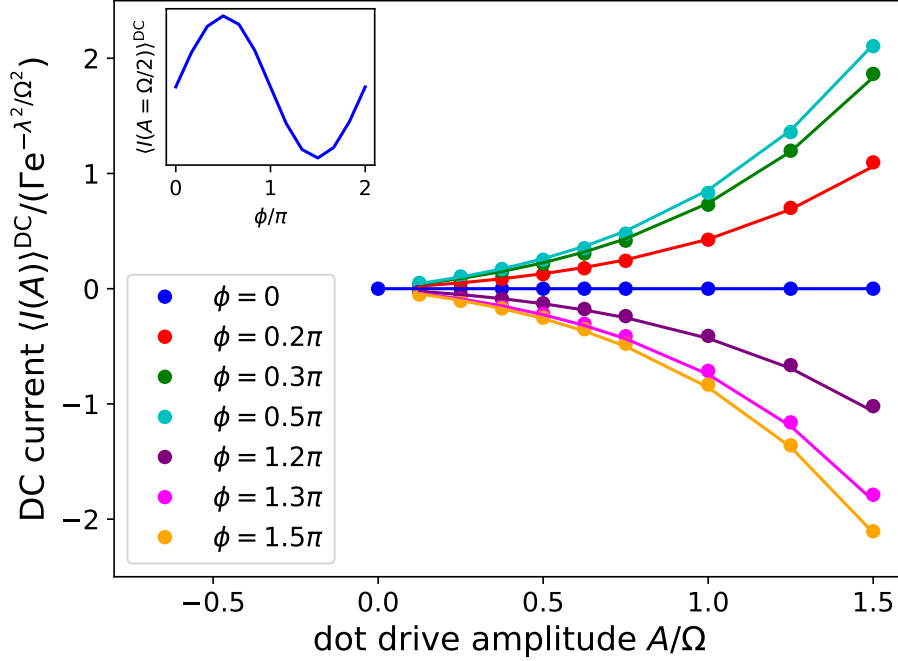


Figure 2.15: DC current $\langle I \rangle^{\text{DC}}$ as a function of the dot drive amplitude A for different values of phase difference $\phi_L = -\phi_R = \phi/2$, and fixed coupling drive amplitude $\Delta = 0.6$. Dots: simulation of Eq. (2.52), lines: numerical fit proportional to $\frac{A}{\Omega} e^{A/\Omega} \sin \phi$. The low-amplitude regime behaves in a way similar to purely electronic pumping, with exponential lifting of FCB ($\lambda = 4\Omega$) evident for larger amplitude. Inset: Sine-shaped phase dependence of $\langle I \rangle^{\text{DC}}$ for a fixed value of A .

amplification of pump current by application of an AC gate voltage.

2.2.6 Conclusion

We have examined the interplay between strong electromechanical coupling and periodic drive protocols in a model of a quantum dot coupled to a pair of metallic leads, subject to AC gate voltages modulating both the dot energy and the coupling to the leads. By combining a perturbative approach in the tunnel coupling with an expansion in Floquet modes, we were able to quantify the effects of multi-parameter drives and of higher drive harmonics on the DC current through the quantum dot.

Our main findings are twofold: Firstly, we studied the case of a biased quantum dot in the limit of bias voltage small compared to the vibron frequency. In this situation, the dominant effect is the lifting of the polaron-induced Franck-Condon blockade as a result of driving the dot energy in resonance with the vibrational mode on the dot. In particular, the coupling drive only has a minimal effect on the

current in this regime, and the current response to the drive is well approximated by the Floquet component which encodes time-averaged contributions. This result also serves to confirm earlier work on drive-induced lifting of Franck-Condon blockade, where only time-averaged correlation functions were considered in the perturbative expansion [135].

Secondly, we applied the same formalism to the unbiased quantum dot. There, the interplay between both dot and coupling drives makes it possible to pump a DC current through the system: Similar to the case of charge pumping in purely electronic systems, we find that in the regime of weak dot drive the DC current flow is approximately proportional to the drive amplitude, as long as a phase difference between the left and right coupling drives is employed to break left-right symmetry. The dependence of the current on this phase is found to always be sinusoidal, irrespective of the dot drive amplitude. In the regime of strong dot drive, in contrast, the current response becomes superlinear and approximates the exponential characteristic found in the biased quantum dot. Thus, the driven unbiased polaron quantum dot combines the exponential lifting of Franck-Condon blockade with features of adiabatic charge pumping through purely electronic systems, even far away from the adiabatic limit.

As recent experiments have used electronic gates to localize quantum dots on carbon nanotubes, we anticipate that these could also be employed to supply the AC voltages we use to predict charge pumping, thus providing an implementation of our model and adding to the versatility of carbon nanotubes as elements of circuitry. Moreover, the Anderson-Holstein Hamiltonian used in this work is a fairly general model and could be realized in multiple ways, as long as there is a way to engineer strong coupling between a fermion and a bosonic mode and subject this system to several resonant drives. In particular, an optomechanical implementation could be envisioned, with cavity modes taking the role of the drive.

The model itself can be extended to include multiple electron levels and oscillator modes by replacing the expression for the dot Green's function by a more complex one; this appears as a promising way to better capture the possible complexities of experiments. Furthermore, the generality of the Floquet formalism also permits the consideration of more complex driving schemes as well as the time-dependent current response. Finally, while the polaron tunneling approximation allows to simplify the diagrammatic expansion substantially and yet capture the effect of electron-phonon interaction in the parameter ranges considered in this work, it would be interesting to explore alternatives such as the Floquet DMFT [55], which would allow to move beyond this approximation, as well as to consider more complex system Hamiltonians.

2.2.7 Appendix: Bare Green's functions

Here, we derive the expressions Eq. (2.56) and Eq. (2.57) for the bare and free dot Green's functions. The free dot Green's function is calculated by evolution with the time independent Hamiltonian $H_0^{\text{free}} = \epsilon d^\dagger d + \Omega a^\dagger a$ and factors into electronic

and vibrational parts,

$$D_0^{\text{free}}(\tau, \tau') = -i \left\langle T_C d(\tau) d^\dagger(\tau') \right\rangle_0^{\text{free}} \left\langle T_C X(\tau) X^\dagger(\tau') \right\rangle_0^{\text{free}}, \quad (2.63)$$

where $X(\tau) = e^{-\frac{\lambda^2}{\Omega^2}(a^\dagger e^{i\Omega\tau} - a e^{-i\Omega\tau})}$. Using Keldysh matrix notation, the electronic Green's function takes shape as

$$\left\langle T_C d(\tau) d^\dagger(\tau') \right\rangle_0^{\text{free}} = e^{-i\epsilon(t-t')} \begin{pmatrix} -N_0 + \theta(t-t') & -N_0 \\ 1 - N_0 & -N_0 + \theta(t'-t) \end{pmatrix}. \quad (2.64)$$

Throughout this work, we focus on times beyond the transient regime, meaning the effect of the initial dot occupation N_0 is negligible and can hence be set to $N_0 = 0$. On the other hand, the vibrational part reads

$$\left\langle T_C X(\tau) X^\dagger(\tau') \right\rangle_0^{\text{free}} = e^{-\lambda^2/\Omega^2} \begin{pmatrix} e^{\frac{\lambda^2}{\Omega^2} e^{-i\Omega|\tau|}} & e^{\frac{\lambda^2}{\Omega^2} e^{i\Omega\tau}} \\ e^{\frac{\lambda^2}{\Omega^2} e^{-i\Omega\tau}} & e^{\frac{\lambda^2}{\Omega^2} e^{i\Omega|\tau|}} \end{pmatrix}. \quad (2.65)$$

The retarded component in Eq. (2.57) is obtained by Fourier transform of Eq. (2.63) and using the definition $(D_0^{\text{free}})_0^{\text{R}} = (D_0^{\text{free}})^{--} - (D_0^{\text{free}})^{-+}$.

The bare dot Green's function differs from the free one by the additional evolution with the drive Hamiltonian $H_{\text{dr}}(t) = A \cos \Omega_\epsilon t$, which implies

$$\begin{aligned} D_0(\tau, \tau') &= D_0^{\text{free}}(\tau, \tau') e^{-i\frac{A}{\Omega_\epsilon}(\sin \Omega_\epsilon \tau - \sin \Omega_\epsilon \tau')} \\ &= \sum_{n \in \mathbb{Z}} e^{in\Omega_\epsilon \tau_{\text{av}}} D_0^{\text{free}}(\tau_{\text{rel}}) i^n J_n \left(-\frac{2A}{\Omega_\epsilon} \sin \frac{\Omega_\epsilon \tau_{\text{rel}}}{2} \right), \end{aligned} \quad (2.66)$$

where J_n denotes the n -th Bessel function of the first kind. By Fourier transforming in the relative time coordinate, we obtain the Wigner expansion,

$$\begin{aligned} &\int_{-\infty}^{\infty} d\tau_{\text{rel}} e^{i\omega\tau_{\text{rel}}} i^n J_n \left(-\frac{2A}{\Omega_\epsilon} \sin \frac{\Omega_\epsilon \tau_{\text{rel}}}{2} \right) \\ &= \int_{-\infty}^{\infty} d\tau_{\text{rel}} e^{i\omega\tau_{\text{rel}}} i^n \sum_{m \geq 0} \frac{(-1)^m}{m!(m+n)!} \left(-\frac{A}{\Omega_\epsilon} \sin \frac{\Omega_\epsilon \tau_{\text{rel}}}{2} \right)^{2m+n} \\ &= \int_{-\infty}^{\infty} d\tau_{\text{rel}} e^{i\omega\tau_{\text{rel}}} i^n \sum_{m \geq 0} \frac{(-1)^m}{m!(m+n)!} \left(-\frac{A}{i2\Omega_\epsilon} \right)^{2m+n} \left(e^{i\frac{\Omega_\epsilon \tau_{\text{rel}}}{2}} - e^{-i\frac{\Omega_\epsilon \tau_{\text{rel}}}{2}} \right)^{2m+n} \\ &= \int_{-\infty}^{\infty} d\tau_{\text{rel}} \sum_{m \geq 0} \sum_{k=0}^{2m+n} e^{i(\omega + k\Omega_\epsilon - m\Omega_\epsilon - \frac{n}{2}\Omega_\epsilon)\tau_{\text{rel}}} \frac{(-1)^k}{m!(m+n)!} \left(\frac{A}{2\Omega_\epsilon} \right)^{2m+n} \binom{2m+n}{k} \\ &= 2\pi \sum_{m \geq 0} \sum_{k=0}^{2m+n} \delta \left(\omega - \left(m + \frac{n}{2} - k \right) \Omega_\epsilon \right) \frac{(-1)^k}{m!(m+n)!} \left(\frac{A}{2\Omega_\epsilon} \right)^{2m+n} \binom{2m+n}{k}. \end{aligned} \quad (2.67)$$

This expression is then convolved with $D_0^{\text{free}}(\omega)$:

$$D_0(t_{\text{av}}, t_{\text{rel}}) = \sum_{n \in \mathbb{Z}} e^{in\Omega_\epsilon t_{\text{av}}} \int_{-\infty}^{\infty} \frac{d\omega}{2\pi} e^{-i\omega t_{\text{rel}}} \sum_{m \geq 0} \sum_{k=0}^{2m+n} D_0^{\text{free}} \left(\omega - \left(m + \frac{n}{2} - k \right) \Omega_\epsilon \right) \lambda_n^{mk}, \quad (2.68)$$

with

$$\lambda_n^{mk} = \frac{(-1)^k}{m!(m+n)!} \left(\frac{A}{2\Omega_\epsilon} \right)^{2m+n} \binom{2m+n}{k}. \quad (2.69)$$

2.2.8 Appendix: Self-energy

In the following, we give the derivations of the mode expansions Eq. (2.58) and Eq. (2.59) for the retarded and lesser component of the lead self-energy, respectively. Resummation of the perturbation series for $D(\tau, \tau')$ produces the Dyson equation (2.45), with a self-energy Σ which contains the time dependence of the coupling $V_{k\alpha}(t) = v_{k\alpha} [1 + \Delta \cos(\Omega_V t + \phi_\alpha)]$,

$$\Sigma(\tau_1, \tau_2) = \sum_{k\alpha} V_{k\alpha}(\tau_1) V_{k\alpha}^*(\tau_2) G_{k\alpha}(\tau_1, \tau_2). \quad (2.70)$$

Introducing Wigner coordinates and Fourier transforming, we obtain

$$\begin{aligned} \Sigma(t_{\text{av}}, \omega)_\alpha &= \sum_k |v_{k\alpha}|^2 \int_{-\infty}^{\infty} dt_{\text{rel}} e^{i\omega t_{\text{rel}}} V_{k\alpha}(t_{\text{av}} + t_{\text{rel}}/2) V_{k\alpha}^*(t_{\text{av}} - t_{\text{rel}}/2) G_{k\alpha}(t_{\text{rel}}) \\ &= \sum_k |v_{k\alpha}|^2 \int_{-\infty}^{\infty} dt_{\text{rel}} e^{i\omega t_{\text{rel}}} \left[\frac{|\Delta|^2}{4} e^{-i2\phi_\alpha} G_{k\alpha}(t_{\text{rel}}) e^{-i2\Omega_V t_{\text{av}}} + \frac{|\Delta|^2}{4} e^{i2\phi_\alpha} G_{k\alpha}(t_{\text{rel}}) e^{i2\Omega_V t_{\text{av}}} \right. \\ &\quad + \left(1 + \frac{|\Delta|^2}{4} e^{i\Omega_V t_{\text{rel}}} + \frac{|\Delta|^2}{4} e^{-i\Omega_V t_{\text{rel}}} \right) G_{k\alpha}(t_{\text{rel}}) \\ &\quad + \left(\frac{\Delta}{2} e^{i(\Omega_V t_{\text{rel}}/2 + \phi_\alpha)} + \frac{\Delta^*}{2} e^{i(-\Omega_V t_{\text{rel}}/2 + \phi_\alpha)} \right) G_{k\alpha}(t_{\text{rel}}) e^{i\Omega_V t_{\text{av}}} \\ &\quad \left. + \left(\frac{\Delta}{2} e^{-i(\Omega_V t_{\text{rel}}/2 + \phi_\alpha)} + \frac{\Delta^*}{2} e^{-i(-\Omega_V t_{\text{rel}}/2 + \phi_\alpha)} \right) G_{k\alpha}(t_{\text{rel}}) e^{-i\Omega_V t_{\text{av}}} \right]. \quad (2.71) \end{aligned}$$

In order to obtain the retarded and lesser components of the self energy, we substitute the free lead Green's functions

$$\begin{aligned} G_{k\alpha}^{\text{R}}(t_{\text{rel}}) &= -i\theta(t_{\text{rel}}) e^{-i\epsilon_{k\alpha} t_{\text{rel}}}, \\ G_{k\alpha}^{-+}(t_{\text{rel}}) &= i n_{\text{F}}(\epsilon_{k\alpha}) e^{-i\epsilon_{k\alpha} t_{\text{rel}}}, \end{aligned} \quad (2.72)$$

respectively. Using the identity $\lim_{\eta \rightarrow 0^+} (\omega - \epsilon_{k\alpha} + i\eta)^{-1} = \mathcal{P}(\omega - \epsilon_{k\alpha})^{-1} - i\pi\delta(\omega - \epsilon_{k\alpha})$, with the notation \mathcal{P} for the principal value, the integral is readily performed. In the wide-band limit, the bare electronic tunneling rate $\Gamma = 2\pi \sum_k |v_{k\alpha}|^2 \delta(\omega - \epsilon_{k\alpha})$ is set to be independent of frequency, which yields Eqs. (2.58) and (2.59).

2.3 Quantum thermodynamics of the resonant-level model with driven system-bath coupling

*We study nonequilibrium thermodynamics in a fermionic resonant-level model with arbitrary coupling strength to a fermionic bath, taking the wide-band limit. In contrast to previous theories, we consider a system where both the level energy and the coupling strength depend explicitly on time. We find that, even in this generalized model, consistent thermodynamic laws can be obtained, up to the second order in the drive speed, by splitting the coupling energy symmetrically between system and bath. We define observables for the system energy, work, heat, and entropy, and calculate them using nonequilibrium Green's functions. We find that the observables fulfill the laws of thermodynamics, and connect smoothly to the known equilibrium results. This section is based on the article Quantum thermodynamics of the resonant-level model with driven system-bath coupling, written in collaboration with Massimiliano Esposito and Thomas L. Schmidt, published in Phys. Rev. B **97**, 085435 (2018).*

2.3.1 Introduction

Thermodynamics has long been central to the understanding and optimization of the performance of work cycles and machines. As a result of recent advances in fabrication technology and measurement techniques, the range of realizable machines now extends down to the size of a single molecule [97, 138, 139, 140]. At this length scale, many of the assumptions underlying the edifice of thermodynamics are no longer valid. Specifically, the paradigm of a nanoscale system coupled to a bath features a variety of subtleties that are not present in macroscopic setups. First, the extent of the contact area between system and bath may be similar to that of the system itself, meaning the details of the coupling become relevant and can no longer be treated in the same general fashion as in the macroscopic case. Second, if the coupling is of sufficient strength, even the distinction between system and bath may itself become blurred [141]. Finally, the task of taking into account nonequilibrium effects is much more intricate at the nanoscale and has received a great deal of recent attention. These difficulties are compounded by quantum effects that play no role macroscopically but rise to prominence in small systems. However, even the problem of formulating a microscopic theory of nonequilibrium thermodynamics for a classical system is daunting in itself [90, 142, 86, 143].

The key to establishing a framework of nonequilibrium quantum thermodynamics is to define quantities that transfer the concepts of system energy, entropy, heat, and work to the nanoscale regime in the context of a given system, while preserving as much generality as possible. To this end, a wide variety of approaches has been pursued, studying setups which roughly fall into the two categories of weak [67, 57, 73, 69, 144] and general couplings [70, 85, 80, 73, 145, 146, 74, 147, 148, 149, 150] between system and bath, respectively. For the case of weak coupling, consistent thermodynamics has been established [57, 73, 69, 151], as

outlined in Sec. 1.5.1, but beyond weak coupling, the situation is much less clear: There, the meaning of work and work fluctuations has been understood, but the quest for definitions of system energy and heat remains open [70, 80, 74].

Recently, the formalism of nonequilibrium Green’s functions has been applied to the question of statistical physics and thermodynamics in paradigmatic quantum systems [152]. The advantage of this approach lies in its inherent ability to treat both nonequilibrium and strong-coupling situations, meaning that Green’s functions can readily provide a wide range of candidates for thermodynamic definitions. The subjects of these studies are variants of the resonant-level model, consisting of an electronic level coupled to metallic leads, under the influence of a drive protocol. This constitutes a minimal description of a quantum dot coupled to source and drain electrodes and driven by means of AC gate voltages. Electronic transport in the time-dependent resonant-level model and its extensions has been studied for several years [153, 154, 34, 135, 155], but more recently its thermodynamic properties have come into the spotlight. Several sets of thermodynamic definitions have been proposed in this way, with varying ranges of validity [156, 157, 158, 159, 160, 161, 162, 163, 164]. In particular, it has proved challenging to find appropriate generalizations of corresponding equilibrium quantities [158], and to incorporate drive protocols and coupling structures of general form [160, 161].

Our work considers a resonant-level model in the spirit of Ref. [160], where the electron level is subjected to a time-dependent drive and coupled to a single lead, which we consider in the wide-band limit. To arrive at a more realistic model for experiments [165], we extend the existing models by in addition allowing for a time-dependent coupling between system and bath, and show that it admits an analytical solution in terms of Green’s functions. These solutions give rise to nonequilibrium thermodynamic quantities, which connect smoothly to their equilibrium counterparts, and obey the laws of thermodynamics in the quasi-adiabatic limit. In doing so, we give a definition of the heat current which differs from those considered in Ref. [157] and thus resolve the apparent inconsistency caused by time-dependent coupling.

The paper is structured as follows: In Sec. 2.3.2, we introduce the resonant-level model and its solution in the presence of time-dependent parameters. Next, we use this solution to define thermodynamic quantities in Sec. 2.3.3, and demonstrate the first law of thermodynamics in our model. We proceed in Sec. 2.3.4 by confirming that the adiabatic limit of our definitions matches established equilibrium results. In Sec. 2.3.5 we perform an expansion in derivatives of the drive protocol, from which we conclude that our definitions are compatible with the second law of thermodynamics up to second order in drive velocities. We compare this expansion with exact numerical results in Sec. 2.3.6. Finally, we summarize our findings and compare to related results in the literature, in Sec. 2.3.7.

2.3.2 Resonant-level model

We study a model Hamiltonian for a single electronic level coupled to a fermionic lead of length L ,

$$\begin{aligned} H(t) &= H_D(t) + H_B + H_T(t), \\ H_D(t) &= \epsilon(t)d^\dagger d, \\ H_B &= \sum_k \epsilon_k c_k^\dagger c_k, \\ H_T(t) &= \sum_k \frac{\gamma(t)}{\sqrt{L}} d^\dagger c_k + \text{h. c.}, \end{aligned} \quad (2.73)$$

where $H_D(t)$, H_B , and $H_T(t)$ are the dot, lead, and tunneling Hamiltonians, respectively. Here, d^\dagger and d denote the creation and annihilation operators for the dot electron and fulfill the fermionic commutation relation $\{d, d^\dagger\} = 1$. Analogously, the operators c_k^\dagger and c_k are associated with the lead electrons, with the index k enumerating the lead modes. In the absence of the tunneling term, we assume thermal equilibrium in the lead, thus imposing $\langle c_k^\dagger c_q \rangle_0 = \delta_{kq} n_F(\epsilon_k)$, where $n_F(\epsilon_k) = [1 + e^{\beta(\epsilon_k - \mu)}]^{-1}$ denotes the Fermi-Dirac distribution at inverse temperature β with chemical potential μ , and the subscript 0 denotes expectation values taken with respect to the quadratic Hamiltonian $H_D(t) + H_B$. Both the dot energy $\epsilon(t)$ and the dot-lead coupling strength $\gamma(t)$ are subject to time-dependent drive, and no assumption is made regarding the magnitude of $\gamma(t)$. In this way, the Hamiltonian in Eq. (2.73) combines nonequilibrium physics and potentially strong coupling between system and bath, and hence features several of the challenges inherent in the attempt to formulate quantum thermodynamics. The schematics of the model are visualized in Fig. 2.16.

In the following, we describe the dynamics of the resonant-level model of Eq. (2.73) in terms of nonequilibrium Green's functions [47], which can be calculated analytically, as laid out in Sec. 1.2. Specifically, we consider the tunneling Hamiltonian H_T in the role of the interaction, and use a perturbation series to capture the renormalization of dot properties as a consequence of this interaction.

Resumming the perturbation series leads to a Dyson equation for the full dot Green's function as in Eq. (1.34),

$$D(\tau, \tau') = D_0(\tau, \tau') + \int_C d\sigma d\sigma' D_0(\tau, \sigma) \Sigma(\sigma, \sigma') D(\sigma', \tau'), \quad (2.74)$$

as a function of the bare dot Green's function $D_0(\tau, \tau') = -i\langle d(\tau)d^\dagger(\tau') \rangle_0$. Thus, the consequences of coupling to the leads are fully quantified by the self-energy, which is given by

$$\Sigma(\sigma, \sigma') = \frac{\gamma(\sigma)\gamma^*(\sigma')}{L} \sum_k G_{0,k}(\sigma, \sigma'), \quad (2.75)$$

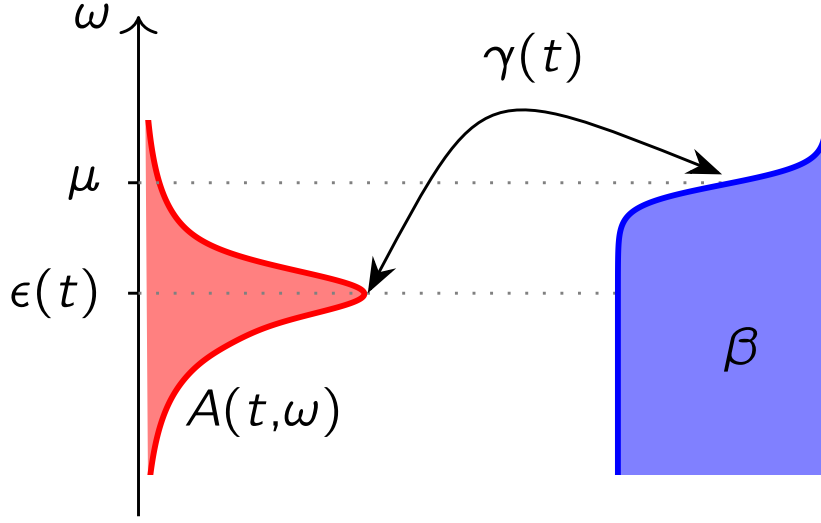


Figure 2.16: Resonant-level model of a driven single-electron quantum dot at energy $\epsilon(t)$, with time-dependent tunnel coupling $\gamma(t)$ to a single metallic lead at inverse temperature β , with chemical potential μ . The coupling results in broadening of the dot electron level with profile $A(t, \omega)$, see Eq. (2.82).

where $G_{0,k}(\sigma, \sigma') = -i\langle \mathcal{T} c_k(\sigma) c_k^\dagger(\sigma') \rangle_0$ denotes the bare lead Green's function. To calculate this function analytically, we assume the wide-band limit, i.e., a linear spectrum $\epsilon_k = v_F k$ with infinite bandwidth. The wide-band limit constitutes an excellent approximation at temperatures less than the Fermi energy of the bath, and leads to a constant density of states $\bar{\rho} = 1/(2\pi v_F)$. The retarded self energy is then given by

$$\Sigma^R(s, s') = -i\Gamma(s)\delta(s - s'), \quad (2.76)$$

where we introduced the tunneling linewidth³ $\Gamma(s) = \pi\bar{\rho}|\gamma(s)|^2$, which we assume to be strictly positive. Importantly, the wide-band limit produces a delta-shaped $\Sigma^R(s, s')$. Similarly, we evaluate the lesser component,

$$\Sigma^{<+}(s, s') = 2\pi i \bar{\rho} \gamma(s) \gamma^*(s') \int \frac{d\omega}{2\pi} e^{-i\omega(s-s')} n_F(\omega), \quad (2.77)$$

which depends on the lead distribution $n_F(\omega)$.

Eq. (2.74) admits an analytical solution: First, we note that we can solve it for the retarded and advanced Green's functions by taking the retarded component of each factor. Then, we proceed by iteratively replacing instances of the exact Green's function D^R in Eq. (2.74) by the entire right hand side of Eq. (2.74). This

³This definition differs by a factor of 2 from the more conventional one used in the previous section. The choice here serves the purpose of keeping expressions as compact as possible.

leads to an expansion in powers of the self-energy, which sums to

$$D^R(t, t') = -i\theta(t - t')e^{-i\int_{t'}^t ds\epsilon(s)}e^{-\int_{t'}^t ds\Gamma(s)}. \quad (2.78)$$

The advanced component is then given by $D^A(t, t') = D^R(t', t)^*$. Together with the lesser self-energy, they give rise to the D^{-+} via the Langreth rule, Eq. (1.51),

$$D^{-+}(t, t') = \int_{-\infty}^{\infty} ds ds' D^R(t, s)\Sigma^{-+}(s, s')D^A(s', t'), \quad (2.79)$$

which we simplified by noting that an additional term [47], which is proportional to the dot occupation at the initial time t_0 , drops out since $t_0 \rightarrow -\infty$. Using Eqs. (2.77) and (2.78), we thus evaluate the lesser dot Green's function as

$$D^{-+}(t, t') = 2i \int \frac{d\omega}{2\pi} n_F(\omega) e^{-i\omega(t-t')} V(t, \omega) V^*(t', \omega), \quad (2.80)$$

where we defined the function

$$V(t, \omega) = \int_{-\infty}^t ds \sqrt{\Gamma(s)} \exp \left\{ \int_s^t dy [i\omega - i\epsilon(y) - \Gamma(y)] \right\} \quad (2.81)$$

which encodes the history of the driving protocol $[\epsilon(t), \Gamma(t)]$. This result is in agreement with the findings of an equation-of-motion approach [153]. By choosing $t = t'$, this Green's function provides us with the expectation value of the dot particle number, $N(t) = -iD^{-+}(t, t)$,

$$N(t) = \int \frac{d\omega}{2\pi} n_F(\omega) A(t, \omega), \quad (2.82)$$

where we wrote

$$A(t, \omega) = 2|V(t, \omega)|^2. \quad (2.83)$$

Note that Eq. (2.82) appears as a straightforward generalization of the dot particle number in a stationary system, where $A(t, \omega)$ would be replaced by the Lorentzian spectral function

$$A_0(\omega) = \frac{2\Gamma}{(\omega - \epsilon)^2 + \Gamma^2}. \quad (2.84)$$

Since it can be shown that in the stationary case A and A_0 coincide (see App. 2.3.8), the expression $A(t, \omega)$ can be viewed as a drive-induced modification of the dot spectral function. However, it bears pointing out that in general A does not match the definition of the non-stationary spectral function: $A(t, \omega) \neq -2 \text{Im} D^R(t, \omega)$, where $D^R(t, \omega)$ stands for the Wigner transform of the retarded dot Green's function.

We have thus arrived at a fully analytical solution of the resonant-level model in the presence of two drives, after taking the wide-band limit. In a way similar to the particle number, expectation values of any other operator on the dot and lead Hilbert spaces can be calculated from the Green's function matrix $\check{D}(t, t')$.

2.3.3 Thermodynamic definitions and first law

In the following, we define thermodynamic quantities for our system in terms of quantum mechanical expectation values and use the Green's functions obtained in the previous section to calculate them. Herein, we require these definitions to be compatible with the laws of thermodynamics, in the presence of dot and coupling drives as well as arbitrary dot-lead coupling strength.

It has been shown previously [156, 160] that for the case of time-independent coupling, such a set of definitions may be obtained by defining a system energy that consists of the expectation value of the dot Hamiltonian with half the coupling Hamiltonian added,

$$E_S(t) = \left\langle H_D(t) + \frac{1}{2}H_T(t) \right\rangle. \quad (2.85)$$

This kind of splitting is indicative of the fact that in the presence of strong coupling, one cannot simply identify the dot with the “system”, and the lead with the “bath”, in the thermodynamic sense of these terms. Moreover, energy added to the total ensemble by the coupling drive must be partitioned between system and bath. The choice of a partition factor of 1/2 has the added feature that the system energy can then be written as an expectation value of dot operators only, $E_S = -i\langle\partial_t d^\dagger d - d^\dagger \partial_t d\rangle/2$. In the following, we show that, even in the case of driven coupling, this choice of system energy conforms to the first and second laws of thermodynamics.

The expectation values in Eq. (2.85) are readily expressed in terms of Green's functions, leading to the exact result

$$E_S(t) = \int \frac{d\omega}{2\pi} \omega n_F(\omega) A(t, \omega) - 2 \int \frac{d\omega}{2\pi} n_F(\omega) \text{Im} [\partial_t V(t, \omega) V^*(t, \omega)], \quad (2.86)$$

with $V(t, \omega)$ and $A(t, \omega)$ as in Eqs. (2.81) and (2.83). We define the rate of change in work performed on the system as split into three parts,

$$\dot{W}(t) \equiv \dot{W}_{SB}(t) + \dot{W}_C(t) + \dot{W}_B(t), \quad (2.87)$$

where $\dot{W}_{SB}(t) = \langle\partial_t H(t)\rangle$ and $\dot{W}_C(t) = \mu\partial_t N(t)$ denote the power supplied by the drive to system and bath, and the chemical work rate associated with particle flow into the dot, respectively. Below, we will always use the dot symbol to denote a rate, as opposed to ∂_t which stands for a time derivative. $\dot{W}_{SB}(t)$ is found to be

$$\begin{aligned} \dot{W}_{SB}(t) &= \partial_t \epsilon(t) N(t) + \langle\partial_t H_T(t)\rangle \\ &= \partial_t \epsilon(t) \int \frac{d\omega}{2\pi} n_F(\omega) A(t, \omega) + \frac{2\partial_t \Gamma(t)}{\sqrt{\Gamma(t)}} \int \frac{d\omega}{2\pi} n_F(\omega) \text{Im} V(t, \omega), \end{aligned} \quad (2.88)$$

whereas the chemical chemical work rate equals

$$\dot{W}_C(t) = 4\mu \sqrt{\Gamma(t)} \int \frac{d\omega}{2\pi} n_F(\omega) \text{Re} V(t, \omega) - 2\mu\Gamma(t) \int \frac{d\omega}{2\pi} n_F(\omega) A(t, \omega). \quad (2.89)$$

The third term in Eq. (2.87) is a work done by the system-bath coupling to change the particle numbers in the bath. It is reminiscent of the work that the coupling needs to do to create a volume in the bath recently identified in Ref. [86], but in the grand canonical ensemble. In order to obtain the rate of work performed on the system only, this contribution therefore needs to be subtracted. It is given by

$$\dot{W}_B(t) \equiv \frac{1}{\pi} \partial_t \Gamma(t) = 2 \partial_t \Gamma(t) \partial_\mu N_B^{\text{eq}} / \bar{\rho}, \quad (2.90)$$

where $\bar{\rho}$ is the lead density of states as in Sec. 2.3.2 and $N_B^{\text{eq}} = \bar{\rho} \int \frac{d\omega}{2\pi} n_F(\omega)$ denotes the (infinite) equilibrium particle number in the lead. Its change with respect to the chemical potential, $\partial_\mu N_B^{\text{eq}}$, is finite and can be seen as the grand canonical analogue of a compressibility. One sees therefore that \dot{W}_B arises from changes in the tunneling linewidth $\Gamma(t)$ which modify the level repulsion among the levels in the lead, in turn causing a change in the lead particle number.

Among the results of Sec. 2.3.5, we will find that this definition of \dot{W}_B is compatible with the second law of thermodynamics. Lastly, we define the heat current flowing into the system as

$$\dot{Q}(t) = -\partial_t \left\langle H_B + \frac{1}{2} H_T(t) \right\rangle - \dot{W}_C(t) - \dot{W}_B(t). \quad (2.91)$$

Mirroring Eq. (2.85), this definition associates half of the coupling energy with the bath, and explicitly features the reversed work flows due to particle transfer and work performed on the bath. Our notion of heat flow presents a generalization of the one used in Ref. [156] for time-dependent coupling, which differs from the one considered in Ref. [157].

If we sum up the definitions from Eqs. (2.85), (2.87), and (2.91), we obtain the energy balance

$$\partial_t E_S = \dot{Q} + \dot{W}, \quad (2.92)$$

which makes manifest the first law of thermodynamics in our system, with E taking on the role of the internal energy.

2.3.4 Link to equilibrium

In this section, we show that the definitions made in Sec. 2.3.3 are compatible with the concept of the Hamiltonian of mean force as discussed in Sec. 1.5.3. We start by defining a potential of mean force for the adiabatic limit of our model. Then we take the limit of infinitely slow drive, $\partial_t \epsilon \rightarrow 0$ and $\partial_t \Gamma \rightarrow 0$ of the definitions made in Sec. 2.3.3 and find that the two approaches coincide, thus ensuring that our quantities reduce to the correct adiabatic limit.

We can view Eq. (1.125) as the starting point for the mean-force approach: There, a thermodynamic potential for the system (dot) is defined by as the difference of the corresponding potential for the “super-system” comprising both dot and

lead, and that of the lead itself. Here, we choose to work in the grand canonical ensemble that is characterized by a fixed inverse temperature β and chemical potential μ , in analogy to our Green's function approach. The grand canonical ensemble of the super-system is realized by weak coupling to a “super-bath”, thus fixing β and μ for the ensemble. This setup has been employed for a classical model [142], as well as for the resonant-level model with a single drive parameter [160].

In the absence of drive, and assuming that the super-system is coupled to the super-bath in a fashion permitting energy and particle exchange, we can obtain the weak coupling thermodynamics of the super-system from the equilibrium grand canonical potential

$$\begin{aligned}\Omega^{\text{eq}} &\equiv -\frac{1}{\beta} \log \text{tr} e^{-\beta(H-\mu N)} \\ &= -\frac{1}{\beta} \int \frac{d\omega}{2\pi} \rho(\omega) \log(1 + e^{-\beta(\omega-\mu)})\end{aligned}\quad (2.93)$$

where N is the particle number operator of the super-system. Here, $\rho(\omega)$ denotes the stationary density of states of the super-system. It is defined as the sum of dot and lead contributions, which in terms of Green's functions is given by

$$\rho(\omega) = -2 \text{Im} D^{\text{R}}(\omega) - 2 \sum_k \text{Im} G_k^{\text{R}}(\omega). \quad (2.94)$$

Following Ref. [160], we note that the sum over the exact lead Green's functions obeys the Dyson equation

$$\sum_k G_k^{\text{R}}(\omega) = \sum_k G_{0,k}^{\text{R}}(\omega) + |\gamma|^2 D^{\text{R}}(\omega) \sum_k [G_{0,k}^{\text{R}}(\omega)]^2. \quad (2.95)$$

Writing the unperturbed lead Green's function in the frequency domain, $G_{0,k}^{\text{R}}(\omega) = (\omega - \epsilon_k + i0^+)^{-1}$, we see that the correction becomes

$$\begin{aligned}& |\gamma|^2 D^{\text{R}}(\omega) \sum_k [G_{0,k}^{\text{R}}(\omega)]^2 \\ &= -D^{\text{R}}(\omega) \partial_\omega \left[|\gamma|^2 \sum_k G_{0,k}^{\text{R}}(\omega) \right] = -D^{\text{R}}(\omega) \partial_\omega \Sigma^{\text{R}}(\omega)\end{aligned}\quad (2.96)$$

According to Eq. (2.76), this correction vanishes in the wide-band limit. Therefore the lead component of $\rho(\omega)$ is not renormalized by the coupling, facilitating its interpretation as a “pure bath” term which does not contribute to the system thermodynamics and is subtracted from Eq. (2.93) in the sense of Eq. (1.125). We thus define the (system) grand canonical potential of mean force,

$$\Omega_{\text{S}}^{\text{eq}} \equiv -\frac{1}{\beta} \int \frac{d\omega}{2\pi} A_0(\omega) \log(1 + e^{-\beta(\omega-\mu)}), \quad (2.97)$$

where $A_0(\omega)$ is the stationary spectral function defined in Eq. (2.84). Changes in Ω_S^{eq} resulting from modification of the system parameters are equal to the corresponding changes in Ω^{eq} . With this choice of Ω_S^{eq} , we can use equilibrium thermodynamics to obtain expressions for the equilibrium values of particle number, system entropy and energy,

$$N^{\text{eq}} = -\partial_\mu \Omega_S^{\text{eq}} = \int \frac{d\omega}{2\pi} A_0(\omega) n_F(\omega) \quad (2.98)$$

$$S^{\text{eq}} = -\partial_T \Omega_S^{\text{eq}} = \int \frac{d\omega}{2\pi} A_0(\omega) \sigma_F(\omega) \quad (2.99)$$

$$E_S^{\text{eq}} = \Omega_S^{\text{eq}} + \mu N^{\text{eq}} + \frac{1}{\beta} S^{\text{eq}} = \int \frac{d\omega}{2\pi} A_0(\omega) \omega n_F(\omega). \quad (2.100)$$

where in Eq. (2.99) we defined the frequency-resolved entropy factor

$$\sigma_F(\omega) = -n_F(\omega) \log n_F(\omega) - [1 - n_F(\omega)] \log [1 - n_F(\omega)]. \quad (2.101)$$

These quantities can be related to the adiabatic limit of the definitions in Sec. 2.3.3 by introducing a parametric time dependence in A_0 via $\epsilon(t)$ and $\Gamma(t)$. The expressions obtained by substituting this time-dependent Lorentzian $A_0(t, \omega)$ into Eqs. (2.98), (2.99), and (2.100) can then be used to calculate the adiabatic particle and energy currents,

$$\begin{aligned} \partial_t N^{\text{eq}}(t) &= \int \frac{d\omega}{2\pi} n_F (\partial_\Gamma A_0 \partial_t \Gamma + \partial_\epsilon A_0 \partial_t \epsilon) = [\partial_t N]^{(1)} \\ \partial_t E_S^{\text{eq}}(t) &= \int \frac{d\omega}{2\pi} \omega f (\partial_\Gamma A_0 \partial_t \Gamma + \partial_\epsilon A_0 \partial_t \epsilon) = [\partial_t E]^{(1)}, \end{aligned} \quad (2.102)$$

where the right hand sides refer to the adiabatic expansions of the time derivatives of Eqs. (2.82) and (2.86), respectively, which are detailed in App. 2.3.9. Similarly, we can interpret the time derivative of the grand canonical potential as the rate of mechanical work performed on the system,

$$\begin{aligned} \partial_t \Omega_S^{\text{eq}}(t) &= -\frac{1}{\beta} \int \frac{d\omega}{2\pi} (\partial_\Gamma A_0 \partial_t \Gamma + \partial_\epsilon A_0 \partial_t \epsilon) [\sigma_F(\omega) - \beta(\omega - \mu) n_F(\omega)] \\ &= \dot{W}_{\text{SB}}^{(1)} + \dot{W}_{\text{B}}, \end{aligned} \quad (2.103)$$

as can be gleaned from Eq. (2.127). Hence we conclude that the adiabatic limit of the system quantities defined in Sec. 2.3.3 matches the result of adiabatic weak coupling thermodynamics as encoded in the grand canonical potential of mean force from Eq. (2.97).

2.3.5 Second law

Having obtained a definition for the heat flowing into the system, we now address the question of how to define the system entropy. To this end, we generalize the

adiabatic expression given in Eq. (2.99) and show the compatibility of this choice with the previous definitions by exhibiting the second law.

In analogy to the non-adiabatic result for the particle number on the dot, Eq. (2.82), we define the system entropy beyond the adiabatic limit by replacing the Lorentzian spectral function A_0 in Eq. (2.99) with the function A as in Sec. 2.3.2,

$$S(t) \equiv \int \frac{d\omega}{2\pi} A(t, \omega) \sigma_F(\omega). \quad (2.104)$$

Next, we show the second law in the sense that the entropy production rate is non-negative up to second order in the quasi-adiabatic expansion:

$$\partial_t S - \beta \dot{Q} \geq 0, \quad (2.105)$$

with equality up to first order. Details of the expansion can be found in App. 2.3.9.

Starting with the first order, we note that on the one hand, the derivative of Eq. (2.104) is approximated by

$$[\partial_t S]^{(1)} = \int \frac{d\omega}{2\pi} \sigma_F(\omega) (\partial_\Gamma A_0 \partial_t \Gamma + \partial_\epsilon A_0 \partial_t \epsilon), \quad (2.106)$$

whereas on the other hand, we obtain the corresponding terms for the heat flow from Eq. (2.127),

$$\begin{aligned} \dot{Q}^{(1)} &= \frac{1}{\beta} \int \frac{d\omega}{2\pi} \sigma_F (\partial_\Gamma A_0 \partial_t \Gamma + \partial_\epsilon A_0 \partial_t \epsilon) \\ &\quad - \frac{1}{\beta} \int \frac{d\omega}{2\pi} \log(1 + e^{-\beta\omega}) \partial_\omega \left(-\frac{\omega - \epsilon}{\Gamma} A_0 \partial_t \Gamma - A_0 \partial_t \epsilon \right) \\ &\quad - \int \frac{d\omega}{2\pi} n_F A_0 \left(\frac{\omega - \epsilon}{\Gamma} \partial_t \Gamma + \partial_t \epsilon \right) - \dot{W}_B. \end{aligned} \quad (2.107)$$

An integration by parts in the second integral yields a term that cancels the third integral, as well as a boundary contribution equal to $\partial_t \Gamma / \pi$, thus canceling $-\dot{W}_B$. The first integral coincides with $[\partial_t S]^{(1)}$, which implies that to first order in adiabatic expansion, the change in system entropy is entirely due to heat flow,

$$[\partial_t S]^{(1)} = \beta \dot{Q}^{(1)}. \quad (2.108)$$

Moreover, the quasi-adiabatic expansion shows that our definitions give rise to exact differentials for the system energy as well as reversible work and heat flows to first order in time derivatives,

$$\begin{aligned} \partial_\Gamma \partial_\epsilon \dot{Q}^{(1)} &= \partial_\epsilon \partial_\Gamma \dot{Q}^{(1)}, \\ \partial_\Gamma \partial_\epsilon \dot{W}^{(1)} &= \partial_\epsilon \partial_\Gamma \dot{W}^{(1)}. \end{aligned} \quad (2.109)$$

In particular, the reversible heat therefore fulfills the requirement of being a state function. This should be contrasted with the observation made in Ref. [157], that a

certain class of heat definitions, arising from a splitting of the coupling energy as in Eq. (2.85), fails to exhibit this property as soon as driven coupling is introduced. As our choice of \dot{Q} from Eq. (2.91) differs from the class of heat definitions considered in Ref. [157], this problem does not arise here.

Moving to the second order in time derivatives, we note that the relevant part of $\dot{Q}^{(2)}$ are given by the last two integrals in Eq. (2.126),

$$\begin{aligned}\delta\dot{Q}^{(2)} &\equiv \dot{Q}^{(2)} - \dot{Q}^{(1)} \\ &= \frac{\Gamma^2}{2} \int \frac{d\omega}{2\pi} \partial_\omega n_F A_0^2 \left(\partial_t \frac{\omega - \epsilon}{\Gamma} \right)^2 \\ &\quad + \int \frac{d\omega}{2\pi} (\omega - \mu) \partial_\omega n_F \partial_t \left(\frac{A_0^2 \Gamma}{2} \partial_t \frac{\omega - \epsilon}{\Gamma} \right).\end{aligned}\quad (2.110)$$

On the other hand, the expansion of $\partial_t S$ is immediate from Eq. (2.121),

$$\begin{aligned}\delta\dot{S}^{(2)} &\equiv [\partial_t S]^{(2)} - [\partial_t S]^{(1)} \\ &= \int \frac{d\omega}{2\pi} \partial_\omega \sigma_F \partial_t \left(\frac{A_0^2 \Gamma}{2} \partial_t \frac{\omega - \epsilon}{\Gamma} \right).\end{aligned}\quad (2.111)$$

Using $\partial_\omega \sigma_F(\omega) = \beta(\omega - \mu) \partial_\omega f$, we see that this matches the second term in Eq. (2.110), and therefore we obtain

$$\delta\dot{S}^{(2)} - \beta \delta\dot{Q}^{(2)} = -\frac{\Gamma^2}{2} \int \frac{d\omega}{2\pi} (\partial_\omega f) A_0^2 \left(\partial_t \frac{\omega - \epsilon}{\Gamma} \right)^2 \geq 0, \quad (2.112)$$

which proves the second law of thermodynamics (2.105) to second order. We remark that the integral occurring in Eq. (2.112) equals the negative of the second-order term in the work performed on the super-system, Eq. (2.124). Hence the excess entropy production beyond the adiabatic limit can be interpreted as a consequence of mechanical friction causing heat to leave the system.

2.3.6 Comparison with exact numerical results

In this section, we compare the analytical results which were derived up to the second order in the drive speed with exact numerical results. For this purpose, we study a protocol where both dot and coupling drives are cosine-shaped,

$$\begin{aligned}\epsilon(t) &= \epsilon_0 + \Delta_\epsilon \cos \omega_\epsilon t \\ \Gamma(t) &= \Gamma_0 + \Delta_\Gamma \cos \omega_\Gamma t,\end{aligned}\quad (2.113)$$

and we set $\mu = 0$. By tuning the parameters, this protocol can be made to include the regimes of strong dot-lead coupling and non-adiabatic drive.

The dot particle number $N(t)$ as calculated from Eq. (2.82) is displayed in Fig. 2.17, and contrasted with the adiabatic result for $N(t)$ that is obtained by using the Lorentzian spectral function $A_0(t, \omega)$, with time-dependence parameters $\epsilon(t)$

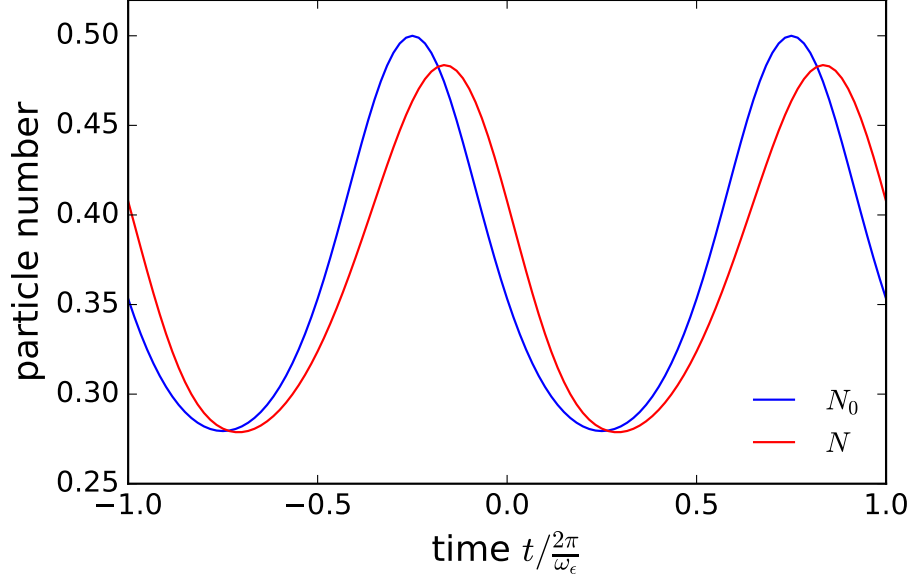


Figure 2.17: Dot particle number as a function of time, for $\epsilon_0 = 0.5$, $\Delta_\epsilon = 0.5$, $\omega_\epsilon = 0.5$, $\Gamma_0 = 1$, $\Delta_\Gamma = 0.2$, $\omega_\Gamma = 0.5$. *Blue*: adiabatic $N_0(t)$ obtained using the Lorentzian spectral density $A_0(t, \omega)$. *Red*: Exact $N(t)$ from Eq. (2.82).

and $\Gamma(t)$. We observe that non-adiabaticity causes the exact result to lag behind the adiabatic one, in line with the retarded character of the time integrals in the definition of $A(t, \omega)$.

Moreover, in Fig. 2.18 we compare the exact entropy production $\partial_t S - \beta \dot{Q}$, calculated numerically based on Eqs. (2.104) and (2.91) with the corresponding result (2.112) in the quasi-adiabatic limit. While the exact result indeed converges to the quasi-adiabatic case for slow driving, significant deviations from the quasi-adiabatic result occur already for parameters where $N(t)$ is still very close to the adiabatic result. In particular, whereas the time integral of the entropy production rate over a drive cycle is positive, the rate itself features negative transients, which can be interpreted as a sign of non-Markovianity in our model for strong dot-lead coupling. This is in marked contrast to the weak-coupling case [57].

2.3.7 Conclusions

We have presented an analytical solution of the resonant-level model in the wide-band limit, in the presence of both time-dependent dot energy and tunnel coupling. We defined thermodynamic quantities, which we calculated using this solution, and found them to be in accordance with the first law of thermodynamics. We found that the adiabatic limit of our definitions matches the results known from stationary thermodynamics. Finally, a quasi-adiabatic expansion allowed us to verify the

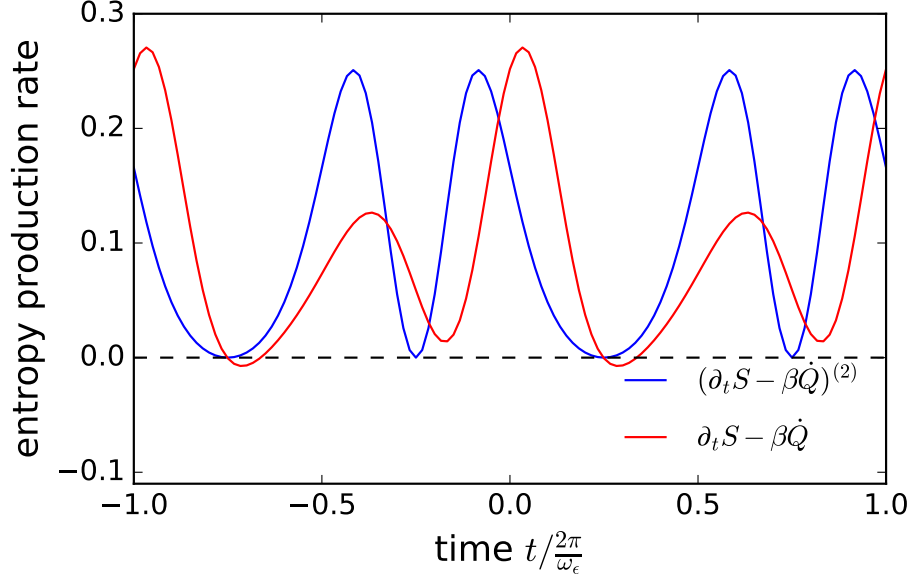


Figure 2.18: Difference of entropy production rate $\partial_t S(t)$ and inverse temperature multiplied by heat, for $\epsilon_0 = 0.5$, $\Delta_\epsilon = 0.5$, $\omega_\epsilon = 0.5$, $\Gamma_0 = 1$, $\Delta_\Gamma = 0.2$, $\omega_\Gamma = 0.5$. *Blue*: Second-order quasi-adiabatic entropy production rate $(\partial_t S - \beta\dot{Q})^{(2)}$. This rate is positive for all times, in accordance with the second law as in Eq. (2.112). *Red*: $\partial_t S - \beta\dot{Q}$ as calculated from Eqs. (2.91) and (2.104). This rate can become negative beyond the adiabatic limit, reflecting the influence of higher orders in the quasi-adiabatic expansion. Moreover, the non-Markovianity of the system itself may lead to negative transients.

second law of thermodynamics to second order in time derivatives of the drive protocol.

It is worthwhile to compare the definitions made here with other recent research on the subject. The choice of a system energy that includes half of the coupling contribution has previously been studied in the case of constant tunnel coupling [156, 160, 161]. Our work generalizes these results to driven coupling, whereby we find that the terms $\pm\dot{W}_B$ need to be added to the definitions (2.87) and (2.91) of the rate of work performed by the system and the heat current flowing through it, respectively. Specifically, the quasi-adiabatic expansion of our exact results matches the findings of Ref. [160] if we take the limit of time-independent Γ . Our definitions also give rise to a state function for the reversible heat, which resolves the issue pointed out in Ref. [157] for time-dependent Γ .

Compared to the case of constant tunneling, time-dependent tunnel amplitudes also give rise to a nontrivial gauge invariance. A time-dependent dot level energy $\epsilon(t)$ can easily be mapped onto a time-dependent tunnel amplitude, $\gamma(t) \propto \gamma_0(t) \exp[-i \int^t ds \epsilon(s)]$. Our results all have this gauge invariance. In contrast,

several works have suggested that system quantities can be defined by isolating $\epsilon(t)$ dependent quantities in the “super-system” observables [160, 161]. However, this procedure is not gauge-invariant and thus cannot be used in the case of time-dependent tunnel amplitudes.

Several challenges remain to be overcome on the way to a full understanding of nonequilibrium quantum thermodynamics in the resonant-level model: Beyond the wide-band approximation, the precise correspondence between the Green’s function approach and the results obtained for the grand canonical ensemble in the adiabatic limit as in Sec. 2.3.4 is still unclear. Similar problems arise if one considers higher moments of the Hamiltonian instead of expectation values only [161]. Finally, it is an appealing prospect to find a version of the second law that holds for all orders in drive speed as opposed to just second order.

2.3.8 Appendix: Adiabatic limit

In the following, we derive approximations for the quantities defined in Sec. 2.3.3 for the case of slow driving. First, we establish the adiabatic limit of infinitely slow drive. Then, we move to the quasi-adiabatic case by expanding the exact expressions in terms of time derivatives of the drive protocol $[\epsilon(t), \Gamma(t)]$.

The function

$$V(t, \omega) = \int_{-\infty}^t ds \sqrt{\Gamma(s)} e^{\int_s^t dy [i\omega - i\epsilon(y) - \Gamma(y)]} \quad (2.114)$$

from Eq. (2.81) is the central subject of the calculations in this section. Its static limit is obtained by assuming constant $\epsilon \equiv \epsilon_0$ and $\Gamma \equiv \Gamma_0$,

$$V^{(0)}(\omega) = \frac{\sqrt{\Gamma_0}}{i(\epsilon_0 - \omega) + \Gamma_0}. \quad (2.115)$$

Using this to calculate $A^{(0)} = 2|V^{(0)}(\omega)|^2$, we obtain

$$A^{(0)}(\omega) = \frac{2\Gamma_0}{(\omega - \epsilon_0)^2 + \Gamma_0^2}, \quad (2.116)$$

which coincides with the spectral function $A_0(\omega)$. From Eq. (2.82), we immediately obtain the particle number,

$$N^{(0)} = \int \frac{d\omega}{2\pi} A_0(\omega) n_F(\omega) = \int \frac{d\omega}{2\pi} \frac{2\Gamma_0}{(\omega - \epsilon_0)^2 + \Gamma_0^2} n_F(\omega). \quad (2.117)$$

Similarly, we obtain for the system energy,

$$E_S^{(0)} = \int \frac{d\omega}{2\pi} \omega n_F(\omega) A_0(\omega), \quad (2.118)$$

since the second term in Eq. (2.86) is approximated by zero.

2.3.9 Appendix: Quasi-adiabatic expansion

In this section, we move beyond the adiabatic limit in approximating the particle number, system energy, as well as heat and work rates. To this end we reinstate the time dependence of Γ and ϵ in $V(t, \omega)$ which occurs in all the quantities considered here. We then expand both drives up to second order in time derivatives resulting in the expansion⁴

$$\begin{aligned} V^{(2)}(t, \omega) = & \frac{\sqrt{\Gamma}}{i(\epsilon - \omega) + \Gamma} - \frac{\partial_t \Gamma}{2\sqrt{\Gamma}} \frac{1}{[i(\epsilon - \omega) + \Gamma]^2} + \frac{3\sqrt{\Gamma}(i\partial_t \epsilon + \partial_t \Gamma)^2}{[i(\epsilon - \omega) + \Gamma]^5} \\ & + \left[-\frac{\partial_t \Gamma(i\partial_t \epsilon + \partial_t \Gamma)}{4\sqrt{\Gamma}} - \frac{1}{6}\sqrt{\Gamma}(i\partial_t^2 \epsilon + \partial_t^2 \Gamma) \right] \frac{6}{[i(\epsilon - \omega) + \Gamma]^4} \\ & + \left[\frac{\partial_t^2 \Gamma}{4\sqrt{\Gamma}} - \frac{(\partial_t \Gamma)^2}{8\sqrt{\Gamma}^3} + \frac{\sqrt{\Gamma}}{2}(i\partial_t \epsilon + \partial_t \Gamma) \right] \frac{2}{[i(\epsilon - \omega) + \Gamma]^3}, \end{aligned} \quad (2.119)$$

where all drives are evaluated at time t . By substituting this expression, we readily obtain second-order results for the currents $\partial_t N$, \dot{W} , $\partial_t E_S$, and \dot{Q} . Since the second-order contributions to these quantities go beyond the adiabatic results in the sense of Sec. 2.3.4, we refer to them as quasi-adiabatic expansion.

The particle current is given by the time derivative of Eq. (2.82).

$$\partial_t N(t) = \int \frac{d\omega}{2\pi} n_F(\omega) \partial_t A(t, \omega), \quad (2.120)$$

where by substituting Eq. (2.119), we find the second-order expansion of $\partial_t A(t, \omega) = 2\partial_t |V(t, \omega)|^2$ to be given by

$$\begin{aligned} [\partial_t A(t, \omega)]^{(2)} = & (\partial_\Gamma A_0 \partial_t \Gamma + \partial_\epsilon A_0 \partial_t \epsilon) \\ & - \partial_t \partial_\omega \left(\frac{A_0^2 \Gamma}{2} \partial_t \frac{\omega - \epsilon}{\Gamma} \right), \end{aligned} \quad (2.121)$$

where we suppress the arguments t and ω from here onward. Therefore, the second-order quasi-adiabatic expansion of the particle current reads

$$\begin{aligned} [\partial_t N(t)]^{(2)} = & \int \frac{d\omega}{2\pi} n_F (\partial_\Gamma A_0 \partial_t \Gamma + \partial_\epsilon A_0 \partial_t \epsilon) \\ & + \int \frac{d\omega}{2\pi} \partial_\omega n_F \partial_t \left(\frac{A_0^2 \Gamma}{2} \partial_t \frac{\omega - \epsilon}{\Gamma} \right). \end{aligned} \quad (2.122)$$

Analogously, by starting from Eq. (2.86), we find the second-order expression for the system energy current,

$$\begin{aligned} [\partial_t E_S]^{(2)} = & \int \frac{d\omega}{2\pi} \omega n_F (\partial_\Gamma A_0 \partial_t \Gamma + \partial_\epsilon A_0 \partial_t \epsilon) \\ & + \int \frac{d\omega}{2\pi} \omega \partial_\omega n_F \partial_t \left(\frac{A_0^2 \Gamma}{2} \partial_t \frac{\omega - \epsilon}{\Gamma} \right). \end{aligned} \quad (2.123)$$

⁴The expansion of $V(t, \omega)$ was performed by Thomas L. Schmidt.

The work flow into the system consists of three distinct contributions, $\dot{W} = \dot{W}_{\text{SB}} + \dot{W}_{\text{C}} + \dot{W}_{\text{B}}$, the first two of which require expansion: The power applied to the super-system is approximated by expanding Eq. (2.88),

$$\begin{aligned}\dot{W}_{\text{SB}}^{(2)} &= \int \frac{d\omega}{2\pi} n_{\text{F}} A_0 \left(\partial_t \epsilon + \frac{\omega - \epsilon}{\Gamma} \partial_t \Gamma \right) \\ &\quad - \frac{\Gamma^2}{2} \int \frac{d\omega}{2\pi} \partial_{\omega} n_{\text{F}} A_0^2 \left(\partial_t \frac{\omega - \epsilon}{\Gamma} \right)^2,\end{aligned}\quad (2.124)$$

and the chemical work flow is given by $\dot{W}_{\text{C}}^{(2)} = \mu[\partial_t N]^{(2)}$, which is immediate from Eq. (2.122). Finally, we consider the heat current, $\dot{Q} = -\partial_t \langle H_{\text{B}} + H_{\text{T}}/2 \rangle - \dot{W}_{\text{C}} - \dot{W}_{\text{B}}$. The last term is the reverse of the first-order expression quantifying mechanical work performed on the bath, whereas the first two terms can be expressed as

$$-\partial_t \langle H_{\text{B}} + H_{\text{T}}/2 \rangle - \mu \partial_t N = -\dot{W}_{\text{SB}} + \partial_t E_{\text{S}} - \mu \partial_t N, \quad (2.125)$$

which leads to the approximation

$$\begin{aligned}\dot{Q}^{(2)} &= -\dot{W}_{\text{SB}}^{(2)} + (\partial_t E_{\text{S}})^{(2)} - \mu \partial_t N^{(2)} - \dot{W}_{\text{B}} \\ &= - \int \frac{d\omega}{2\pi} n_{\text{F}} A_0 \left(\partial_t \epsilon + \frac{\omega - \epsilon}{\Gamma} \partial_t \Gamma \right) \\ &\quad + \int \frac{d\omega}{2\pi} (\omega - \mu) n_{\text{F}} (\partial_{\Gamma} A_0 \partial_t \Gamma + \partial_{\epsilon} A_0 \partial_t \epsilon) \\ &\quad + \frac{\Gamma^2}{2} \int \frac{d\omega}{2\pi} \partial_{\omega} n_{\text{F}} A_0^2 \left(\partial_t \frac{\omega - \epsilon}{\Gamma} \right)^2 \\ &\quad + \int \frac{d\omega}{2\pi} (\omega - \mu) \partial_{\omega} n_{\text{F}} \partial_t \left(\frac{A_0^2 \Gamma}{2} \partial_t \frac{\omega - \epsilon}{\Gamma} \right) - \dot{W}_{\text{B}}.\end{aligned}\quad (2.126)$$

Making use of the relations $\beta(\omega - \mu) n_{\text{F}}(\omega) = \sigma_{\text{F}}(\omega) - \log(1 + e^{-\beta\omega})$ and $\partial_{\Gamma} A_0(\omega) = -\partial_{\omega}[(\omega - \epsilon)A_0/\Gamma]$, we can rewrite the first-order terms as

$$\begin{aligned}\dot{Q}^{(1)} &= \frac{1}{\beta} \int \frac{d\omega}{2\pi} \sigma_{\text{F}} (\partial_{\Gamma} A_0 \partial_t \Gamma + \partial_{\epsilon} A_0 \partial_t \epsilon) \\ &\quad - \frac{1}{\beta} \int \frac{d\omega}{2\pi} \log(1 + e^{-\beta\omega}) \partial_{\omega} \left(-\frac{\omega - \epsilon}{\Gamma} A_0 \partial_t \Gamma - A_0 \partial_t \epsilon \right) \\ &\quad - \int \frac{d\omega}{2\pi} n_{\text{F}} A_0 \left(\frac{\omega - \epsilon}{\Gamma} \partial_t \Gamma + \partial_t \epsilon \right) - \dot{W}_{\text{B}},\end{aligned}\quad (2.127)$$

where after integrating by parts, the second line cancels the third. Furthermore, by comparing Eq. (2.127) to the time derivative of the equilibrium grand canonical potential of Eq. (2.97) and the work rate in Eq. (2.124) we obtain the relation (2.103).

2.4 Initial states in quantum thermodynamics

We examine the role of initial-state contributions to the quantum thermodynamics of the driven resonant-level model. By solving the equations of motion, we obtain an analytical expression for the work performed on the system given a general drive protocol and arbitrary coupling to a bath. We establish that our definition of work coincides with the one introduced in stochastic thermodynamics. This connection is shown to imply that in the long-time limit, the work performed as a result of a periodic drive is positive also for a non-thermal initial state, in accordance with the second law of thermodynamics. This section was written in collaboration with Edwin G. Idrisov, Massimiliano Esposito, and Thomas L. Schmidt. It represents work in progress and will be submitted for publication in the near future.

2.4.1 Introduction

Quantum mechanics and thermodynamics are often thought of as operating on vastly different length scales. While the former is the foundation of our understanding of physics at the nanoscale, the latter is rooted in the macroscopic world, where it is instrumental in the design of work cycles and machines. It is only in recent years that fabrication and measurement methods have improved to the point that machines on the quantum scale can be reliably implemented and analyzed [97, 138, 139, 140, 37]. A theory of quantum thermodynamics – or even just classical microscopic thermodynamics – has thus become highly desirable, as it would facilitate goals such as the design of novel electronic components as well the understanding of chemical reactions, among others [166, 138, 167, 168].

The central goal of quantum thermodynamics is to adapt the laws of thermodynamics in order to capture the behavior of quantum systems, while preserving as much as possible of the generality that constitutes the power of classical thermodynamics. On the path to this goal, obstacles are manifold. Many of the underlying premises of classical thermodynamics do not carry over to the quantum regime. First, the thermodynamic limit of large particle numbers is clearly not given in quantum systems. Second, the smaller the systems in question are, the more attention has to be paid to the precise manner of how they are coupled to each other. In particular, the thermodynamics of strongly coupled quantum systems still lacks a unifying framework, in spite of considerable recent attention [141, 90, 81, 91]. Third, the roles of fluctuations and non-equilibrium, already nontrivial in classical systems [86, 143], are even more prominent in quantum settings.

A great variety of techniques have been employed to establish quantum thermodynamics: The case of a system weakly coupled to a bath was resolved using open systems [67, 9, 69]. The strong-coupling situation has proved to be more complex. One promising approach is given by stochastic thermodynamics [70, 78, 80, 84, 83, 81], which has been used to give a consistent definition of work for non-equilibrium quantum systems as well as to establish general fluctuation theorems [72, 73, 74, 77]. However, the notions of system energy and

heat flows, and thus the first law of thermodynamics, are less straightforward in this approach [81]. On the other hand, recent work has examined the possibility of using exactly solvable model systems to define thermodynamic quantities [160, 169]. There, several sets of definitions exist that fulfill a quantum version of the first law, but a general formulation of the second law remains elusive [156, 170, 157, 158, 159, 160, 161, 162, 163, 171, 169].

In this work, we examine the role of the initial state in the quantum thermodynamics of the strongly coupled resonant-level model coupled to a metallic lead. Considering the work performed by a periodic driving protocol, we establish a link to stochastic thermodynamics. There, it is known that the work production over a drive period is positive provided that the composite system of dot and lead is initially in a thermal state, which can be seen as a signature of the second law of thermodynamics for quantum systems. We show that, for an initially uncoupled setup of dot and lead, the work production in the long-time limit is also positive, even though the composite system is never in a thermal state. Furthermore, we exhibit the non-equivalence of the two configurations in the long-time limit by considering nonlocal correlations in the lead.

Our analysis is structured as follows: In Sec. 2.4.2, we lay out the resonant-level model and give its solution in the presence of arbitrary coupling strength and drive protocol, taking into account initial state effects. In Sec. 2.4.3, we discuss the work production as a result of a periodic driving protocol, and see that it is closely related to the work production discussed in stochastic thermodynamics. Moreover, we introduce the factorized and thermal initial states whose thermodynamics aim to compare. Next, we use Sec. 2.4.4 to analyze the limit of long evolution times and quantify the asymptotic effect of the initial configuration of the system. In particular, we find that the asymptotic work production per period is positive even in situations without thermalization at any point in time. We furthermore use the evolution of correlations in the lead to point out that initial-state dependence still occurs in non-local correlators. A summary of our results is given in Sec. 2.4.5.

2.4.2 Model

The resonant-level model for a quantum dot has previously been solved with the non-equilibrium Green's function formalism [160, 169]. Here we take a different approach, using equations of motion [153]. The system consists of a single electron level coupled to metallic lead of size L , which acts as a bath. Its Hamiltonian is given by

$$\begin{aligned} H(t) &= H_D(t) + H_B + H_T(t), \\ H_D(t) &= \epsilon(t)d^\dagger d, \\ H_B &= -i v_F \int_{-\infty}^{\infty} dx \psi^\dagger(x) \partial_x \psi(x), \\ H_T(t) &= \gamma(t)d^\dagger \psi(x=0) + \text{h. c.}, \end{aligned} \tag{2.128}$$

where $H_D(t)$, H_B , and $H_T(t)$ are the dot, lead, and coupling Hamiltonians, respectively. We assume a linear energy spectrum in the lead, with Fermi velocity v_F . The continuum limit $L \rightarrow \infty$ is implicit here, and is in agreement with the infinite integration domain in H_B . The operators d and d^\dagger respectively annihilate or create an electron on the dot, and similarly $\psi(x)$ and $\psi^\dagger(x)$ are the annihilation and creation operators of a lead particle at position x . They fulfill fermionic commutation relations, $\{d, d^\dagger\} = 1$, and $\{\psi(x), \psi^\dagger(y)\} = \delta(x - y)$. We allow for a general drive protocol, with both the dot energy ϵ and the tunnel coupling amplitude $\gamma \in \mathbb{R}$ depending on time. No restrictions are placed on the strength of the coupling or on the speed of the drive. The only further approximation we use consists of taking the wide-band limit of the dot-lead coupling, meaning a constant density of states in the leads, $\bar{\rho} = 1/(2\pi v_F)$. Lastly, the spin degree of freedom is not relevant to our analysis, so we do not consider it here.

The resulting equations of motion in the Heisenberg picture read

$$\begin{aligned}\partial_t d(t) &= -i\epsilon(t)d(t) - i\gamma(t)\psi(x=0, t) \\ \partial_t \psi(x, t) &= -v_F \partial_x \psi(x, t) - i\gamma(t)d(t)\delta(x).\end{aligned}\tag{2.129}$$

As shown in Ref. [153], these admit the solution

$$\begin{aligned}d(t) &= e^{\int_{t_0}^t ds(-i\epsilon(s)-\Gamma(s))} d(t_0) \\ &\quad - i \int_{t_0}^t ds \gamma(s) e^{\int_s^t dy(-i\epsilon(y)-\Gamma(y))} \psi_0(-v_F(s-t_0)), \\ \psi(x, t) &= \psi_0(x - v_F(t-t_0)) - \frac{i\gamma(\tilde{t})}{v_F} \theta(x) d(\tilde{t}_x),\end{aligned}\tag{2.130}$$

using the shorthand $\tilde{t}_x = t - x/v_F$, and introducing the initial values $d(t_0)$ and $\psi_0(x)$ for the dot and lead operators, respectively.

This solution allows us to calculate the time evolution of any observable of the system. For instance, the particle number on the dot is given by

$$N(t) \equiv \langle d^\dagger(t)d(t) \rangle = \text{tr} \left[\rho(t_0) d^\dagger(t)d(t) \right],\tag{2.131}$$

where in the second equality we introduced the initial density matrix $\rho(t_0)$ of the composite system of dot and lead. Moreover, we define the mechanical work rate as

$$\dot{W}(t) \equiv \langle \partial_t H(t) \rangle,\tag{2.132}$$

in agreement with Refs. [74, 156, 160]. Here and in the following we use a dot superscript to indicate that a quantity is interpreted as a rate, not necessarily that it is a time derivative [169]. Explicit expressions for $N(t)$ and $\dot{W}(t)$ are given in App. 2.4.6.

2.4.3 Work production

The definition of work is a subtle matter in quantum thermodynamics: Work cannot be defined as an observable since it is related to an energy difference and hence requires more than one measurement [80, 88, 74]. Below, we show the equivalence of our definition in Eq. (2.132) and the work rate as introduced in stochastic thermodynamics.

The latter approach [80] defines the mechanical work performed on a system between the time of initialization t_0 and a final time t as the difference between two measurements of the total system energy, one at t_0 and the other at t . In this way, work is represented as a random variable with probability density function $p(w, t)$. Its expectation value is given by

$$\langle w(t) \rangle = \text{tr} \left[U^\dagger(t, t_0) H(t) U(t, t_0) \rho(t_0) \right] - \text{tr} [H(t_0) \rho(t_0)], \quad (2.133)$$

where $\rho(t_0) = e^{-\beta H(t_0)} / \text{tr} e^{-\beta H(t_0)}$ denotes the density matrix of a thermal initial state of the composite system, and $U(t, t_0)$ is the propagator in the Schrödinger picture, fulfilling

$$i\partial_t U(t, t_0) = H(t) U(t, t_0). \quad (2.134)$$

$\langle w(t) \rangle$ can be shown to be bounded from below by the difference of the equilibrium free energies calculated with the initial and final Hamiltonians [78, 84],

$$\langle w(t) \rangle \geq F(t) - F(t_0), \quad (2.135)$$

where the free energy $F(t)$ of a hypothetical equilibrium state at time t is given by

$$F(t) = -\frac{1}{\beta} \log \text{tr} e^{-\beta H(t)}. \quad (2.136)$$

In particular, Eq. (2.135) implies positive work production,

$$\langle w(t) \rangle \geq 0, \quad (2.137)$$

for a periodic drive protocol that ensures $F(t) = F(t_0)$.

On the other hand, Eq. (2.132) implies

$$\dot{W}(t) = \text{tr} \left[U^\dagger(t, t_0) \partial_t H(t) U(t, t_0) \rho(t_0) \right]. \quad (2.138)$$

By taking the time derivative of Eq. (2.133), we see that the work rates in both approaches are the same,

$$\partial_t \langle w(t) \rangle = \dot{W}(t). \quad (2.139)$$

This implies that the positivity relation Eq. (2.137) also holds for the integrated work produced according to Eq. (2.138), if the composite system is prepared in a thermal initial state.

The prerequisite of an initially thermal state is rather restrictive: Consider a dot prepared in isolation from a thermalized lead, the coupling to which is then switched on afterwards, together with the drive protocol. In this case, the composite system will never fully thermalize. Hence, the commonly required initial thermalization may be hard to achieve in practice. In the following, we use the work production to examine how the thermodynamics of a system prepared like this differs from that of an initially thermalized system.

Specifically, we compare two initial state configurations: First, a factorized state (*i*) of the composite system, $\rho^{(i)}(t_0) = \rho_D(t_0) \otimes \rho_B(t_0)$, where the bath is in a thermal state at an inverse temperature β ,

$$\rho_B(t_0) = \frac{e^{-\beta H_B(t_0)}}{\text{tr } e^{-\beta H_B(t_0)}}. \quad (2.140)$$

We specify the initial state of the system by supplying its initial occupation $N(t_0)$. Setup (*i*) is analogous to the choice in Ref. [169], but with a finite initial time t_0 . Second, we consider a state (*ii*), where the composite system is thermalized as a whole,

$$\rho^{(ii)}(t_0) = \frac{e^{-\beta H(t_0)}}{\text{tr } e^{-\beta H(t_0)}}, \quad (2.141)$$

which is the usual assumption in stochastic thermodynamics.

As a first part of the comparison, we illustrate the evolution during the first few drive cycles. To this end, we let each of these states evolve subject to the example drive protocol

$$\begin{aligned} \epsilon(t) &= \delta_1 + \delta_2 \cos \Omega t \\ \Gamma(t) &= \Gamma_0, \end{aligned} \quad (2.142)$$

choosing a sinusoidal drive of the dot energy and a constant dot-lead tunneling rate $\Gamma_0 = \gamma_0^2/(2\nu_F)$. The work rates corresponding to either of the setups can be explicitly calculated using the results in App. 2.4.6. The evolution of the work rates starting from the initial time are visualized in Fig. 2.19, with the asymptotic work rate \dot{W}_∞ obtained for an initial state in the infinite past, $t_0 = -\infty$ added for comparison. It is evident that close to t_0 the effects of the initial state are significant, resulting in positive work production for the thermalized setup (*ii*) over the course of a drive period $T = 2\pi/\Omega$,

$$\Delta W^{(ii)} \equiv \int_{t_0}^{t_0+T} dt \dot{W}_t^{(ii)} \geq 0, \quad (2.143)$$

in agreement with Eq. (2.137). For the factorized setup (*i*) on the other hand, the integrated work production during the first drive cycle is negative. Moving away from the initial time, the dependence of the work rate on the initial state exponentially, and in both setups the work rate approaches the asymptotic, \dot{W}_∞ ,

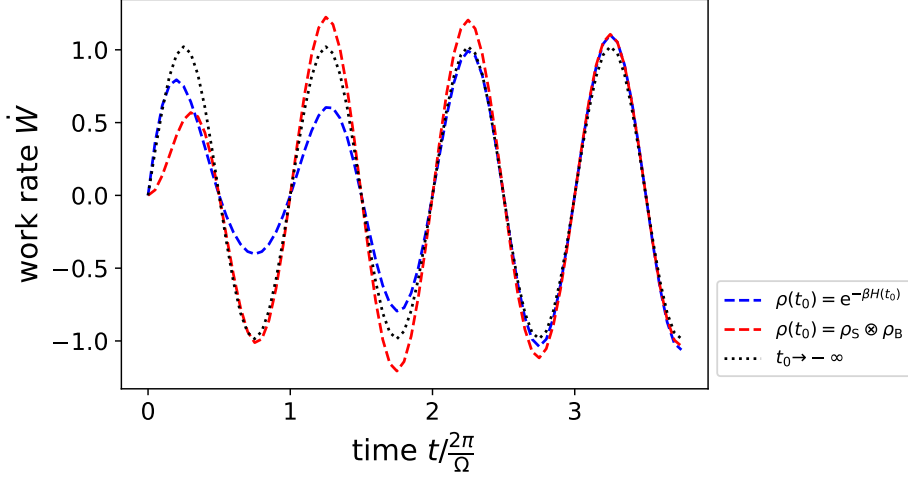


Figure 2.19: Mechanical work rate $\dot{W}(t) = \partial_t \epsilon(t) N(t)$ resulting from the drive protocol (2.142), for different initial conditions. *Red*: Factorized initial state $\rho(t_0)$ at t_0 . Work production integrated over multiples of the drive period starting at t_0 is negative. *Parameters*: $\delta_1 = 1$, $\delta_2 = -0.4$, $\Omega = 10$, $\Gamma_0 = 1$. *Blue*: Thermal initial state $\rho(t_0)$. Work production integrated over multiples of the drive period starting at t_0 is positive. *Black*: Limit of $t_0 \rightarrow -\infty$. Periodic asymptotic work rate, integrated work production is zero. For $t \gg t_0$ the initial state effects decay and for both initial states the work rate converges to the asymptotic one.

which has the same periodicity as the drive protocol. This example thus shows that the effect of the initial configuration on thermodynamics is substantial for short evolution times, but the long-time behavior suggests that the initial-state effects decay over time.

2.4.4 Long-time limit

Let us consider evolution times much larger than the inverse tunneling rate Γ^{-1} . As found in App. 2.4.6 and exemplified in Fig. 2.19, the initial state contributions to correlators involving the dot operators decay to zero in the long-time limit. This can be seen as the closest analogue to equilibration that is possible for the case of arbitrary coupling and a time-dependent Hamiltonian: For local properties of the dot, the initial state contributions vanish asymptotically. Next, we investigate the work production after this pseudo-equilibration process has occurred, i.e. we take the limit of an initial state in the infinite past. In this case, the asymptotic work rate W_∞ is given by taking $t_0 = -\infty$ in either Eq. (2.150) or Eq. (2.157).

In the following, we show that the work production obtained by integrating W_∞

over a drive period is positive far away from the initial time,

$$\Delta W_\infty = \int_0^T dt \dot{W}_\infty(t) \geq 0, \quad (2.144)$$

which establishes an asymptotic version of Eq. (2.143). Indeed, the exponential decay of the initial state contributions to the work rate $\dot{W}^{(ii)}$ calculated with the thermalized initial state implies

$$\Delta W_m^{(ii)} \equiv \int_{t_0+mT}^{t_0+(m+1)T} dt \dot{W}^{(ii)}(t) \xrightarrow{m \rightarrow \infty} \Delta W_\infty, \quad (2.145)$$

where the periodicity $\dot{W}_\infty(t) = \dot{W}_\infty(t+T)$ is used to fix the integration interval on the right hand side to $[0, T]$. If now ΔW_∞ were strictly negative, Eq. (2.145) would imply that for sufficiently large m , all the increments $\Delta W_m^{(ii)}$ are bounded from above by a strictly negative number. On the other hand, since $\dot{W}^{(ii)}$ is based on a thermalized initial state, Eq. (2.137) implies

$$\sum_{m=0}^n \Delta W_m^{(ii)} = \int_{t_0}^{t_0+(n+1)T} dt \dot{W}^{(ii)}(t) \geq 0 \quad (2.146)$$

for any integer n , which leads to a contradiction. Hence we proved $\Delta W_\infty \geq 0$. The expression for $\dot{W}^{(i)}$ in Eq. (2.150) shows that the integrated work production per drive cycle converges to ΔW_∞ in the same manner as for $\dot{W}^{(ii)}$. Therefore, the asymptotic work production per cycle is positive, even for a factorized initial state with negative work production during the early drive cycles. We conclude that in the long-time limit, the work production in our model is positive even though the conditions imposed by stochastic thermodynamics are not met.

This result does however not imply that the two initial setups (i) and (ii) lead to asymptotically equivalent evolution for all observables: The bath correlators $\langle \psi^\dagger(x, t) \psi(y, t) \rangle$ do not converge in the same manner as the local quantities $N(t)$ and \dot{W} in the long-time limit. As detailed in App. 2.4.6, for any evolution time t , non-decaying initial-state signatures remain in correlators of some bath sites that are sufficiently far away from the dot. This makes manifest the difference between a thermal state of the composite system and an initially factorized state that is then coupled and left to evolve.

2.4.5 Conclusion

We connected stochastic thermodynamics to a set of definitions in terms of the expectation values in the resonant-level model for a driven quantum dot at arbitrary coupling to a bath. In particular, the definitions of the work rate known from the literature in both contexts are shown to coincide. This implies a positive work production during a drive cycle, if the system starts out in thermal equilibrium. By explicitly calculating the work rate in the resonant-level model for a thermal

initial state as well as for a factorized initial state of dot and leads, we see that the one-period work production is the same for both initial setups if the initial time lies in the infinite past. This is then used to show that the work production per period in the resonant-level model in the long-time limit is also positive, even though the system may not have been in a thermal state at any point, as is the case for the factorized setup. Our results indicate that the validity of the laws of quantum thermodynamics does not rely on an initially thermalized state.

2.4.6 Appendix: Expectation values

Here, we use the solution of the Heisenberg equations,

$$\begin{aligned} d(t) &= e^{\int_{t_0}^t ds(-i\epsilon(s)-\Gamma(s))} d(t_0) - i \int_{t_0}^t ds \gamma(s) e^{\int_s^t dy(-i\epsilon(y)-\Gamma(y))} \psi_0(-v_F(s-t_0)), \\ \psi(x, t) &= \psi_0(x - v_F(t-t_0)) - \frac{i\gamma(\tilde{t})}{v_F} \theta(x) d(\tilde{t}), \end{aligned} \quad (2.147)$$

to calculate observables for the two different initial setups (i) and (ii). Our focus lies on the dot particle number $N(t) = \langle d^\dagger(t) d(t) \rangle$, the rate of mechanical work $\dot{W} = \langle \partial_t H(t) \rangle$, as well as on the equal-time bath correlator $C_{xy}(t) = \langle \psi^\dagger(x, t) \psi(y, t) \rangle$.

For setup (i), we use the factorized initial state

$$\rho^{(i)}(t_0) = \rho_D(t_0) \otimes [e^{-\beta H_B(t_0)} / \text{tr } e^{-\beta H_B(t_0)}]. \quad (2.148)$$

This leads to the initial correlators

$$\begin{aligned} \langle d^\dagger(t_0) d(t_0) \rangle &= \text{tr}_D [\rho_D(t_0) d^\dagger(t_0) d(t_0)] \equiv N(t_0), \\ \langle d^\dagger(t_0) \psi(x, t_0) \rangle &= 0, \\ \langle \psi^\dagger(x, t_0) \psi(y, t_0) \rangle &= \frac{1}{v_F} \int \frac{d\omega}{2\pi} e^{i\omega \frac{y-x}{v_F}} n_F(\omega) \end{aligned} \quad (2.149)$$

where we denoted the initial dot occupation by $N(t_0)$ and used the wide-band limit, as well as the thermal initial occupation of the bath modes, to calculate the bath correlator. In order to calculate the lead correlator, we considered the momentum space representation $\psi(x, t_0) = \sum_k e^{ikx} c_k / \sqrt{L}$, with the thermal expectation value for the lead mode given by $\langle c_k^\dagger c_q \rangle = \delta_{kq} n_F(\epsilon_k)$. Moreover, we took the wide-band limit of the momentum summation, which leads to the frequency integral $\sum_k / L \rightarrow \bar{\rho} \int d\omega$, with the density of states $\bar{\rho} = 1/(2\pi v_F)$. The divergence of the bath correlator is due to linearizing the spectrum of the lead, $\epsilon_k = v_F k$, and can be cured by imposing a cutoff. We will not explicitly perform this procedure in the following. Substituting Eq. (2.147) into the desired expectation values, we can use

the initial correlators from Eq. (2.149) to obtain

$$\begin{aligned}
N^{(i)}(t) &= N(t_0)e^{-2\int_{t_0}^t dy\Gamma(y)} + \int \frac{d\omega}{2\pi} n_F(\omega) A(t, \omega) \\
\dot{W}^{(i)}(t) &= \partial_t \epsilon(t) N(t) + 4\partial_t \sqrt{\Gamma(t)} \int \frac{d\omega}{2\pi} n_F(\omega) \text{Im } V(t, \omega) \\
C_{xy}^{(i)}(t) &= \frac{1}{v_F} \int \frac{d\omega}{2\pi} e^{i\omega \frac{y-x}{v_F}} n_F(\omega) \\
&\quad + \frac{\gamma(\tilde{t}_x)\gamma(\tilde{t}_y)}{v_F^2} \theta(x)\theta(y) N(t_0) e^{\int_{t_0}^{\tilde{t}_x} ds [i\epsilon(s) - \Gamma(s)]} e^{\int_{t_0}^{\tilde{t}_y} ds [-i\epsilon(s) - \Gamma(s)]} \\
&\quad + 2 \frac{\gamma(\tilde{t}_x)\gamma(\tilde{t}_y)}{v_F^2} \theta(x)\theta(y) \int \frac{d\omega}{2\pi} e^{i\omega \frac{y-x}{v_F}} V(\tilde{t}_y, \omega) V^*(\tilde{t}_x, \omega) n_F(\omega) \\
&\quad - \frac{\gamma(\tilde{t}_y) \sqrt{2v_F}}{v_F^2} \theta(y) \int \frac{d\omega}{2\pi} e^{i\omega \frac{y-x}{v_F}} V(\tilde{t}_y, \omega) n_F(\omega) \\
&\quad - \frac{\gamma(\tilde{t}_x) \sqrt{2v_F}}{v_F^2} \theta(x) \int \frac{d\omega}{2\pi} e^{i\omega \frac{y-x}{v_F}} V^*(\tilde{t}_x, \omega) n_F(\omega), \tag{2.150}
\end{aligned}$$

where, using the notation from Ref. [169], we introduced the generalized spectral function $A(t, \omega) = 2|V(t, \omega)|^2$, with

$$V(t, \omega) = \int_{t_0}^t ds \sqrt{\Gamma(s)} e^{\int_s^t dy [i\omega - i\epsilon(y) - \Gamma(y)]}. \tag{2.151}$$

Regarding the dot quantities $N^{(i)}$ and $\dot{W}^{(i)}$, we conclude that the initial condition $N(t_0)$ only features in the first terms of $N^{(i)}$ and $\dot{W}^{(i)}$, which are exponentially suppressed for large evolution times $t - t_0$. Such a term will be referred to as *transient* in the following. As for the bath correlators $C_{xy}^{(i)}$, we note that the first term results from the initial thermalization of the isolated bath, whereas all the others arise during the evolution in contact with the dot. These terms are hence to be understood using the convention $\gamma(t) = 0$ for $t \leq t_0$.

Given setup (ii) with $\rho^{(ii)}(t_0) = \frac{e^{-\beta H(t_0)}}{\text{Tr } e^{-\beta H(t_0)}}$ on the other hand, the initial thermalization of the composite system needs to be taken into account. More precisely, we assume the system to be in a thermal state up to the initial time t_0 . For all times $s \leq t_0$ we thus have the dot particle number

$$\langle d^\dagger(s) d(s) \rangle = \int \frac{d\omega}{2\pi} n_F(\omega) A_0(\omega), \tag{2.152}$$

the dot-lead correlator

$$\langle d^\dagger(s) \psi(x, s) \rangle = \frac{\gamma_0}{v_F} \int \frac{d\omega}{2\pi} e^{i\omega x/v_F} n_F(\omega) \left[\frac{\theta(x/v_F)}{\omega - \epsilon_0 + i\Gamma_0} + \frac{\theta(-x/v_F)}{\omega - \epsilon_0 - i\Gamma_0} \right], \tag{2.153}$$

as well as the lead correlator

$$\begin{aligned} \langle \psi^\dagger(x, s) \psi(y, s) \rangle &= \frac{1}{v_F} \int \frac{d\omega}{2\pi} e^{i\omega \frac{y-x}{v_F}} n_F(\omega) \\ &\quad - i \frac{\gamma_0^2}{v_F^2} \int \frac{d\omega}{2\pi} e^{i\omega \frac{y-x}{v_F}} n_F(\omega) \left[\frac{\theta(y/v_F) \theta(-x/v_F)}{\omega - \epsilon_0 + i\Gamma_0} - \frac{\theta(-y/v_F) \theta(x/v_F)}{\omega - \epsilon_0 - i\Gamma_0} \right], \end{aligned} \quad (2.154)$$

making explicit the coupling-induced corrections to the correlators compared to the factorized setup (i). Specifically, the diagonal dot-lead correlators $\langle d^\dagger \psi_0 \rangle$ do not vanish any longer, and $\langle \psi_0^\dagger \psi_0 \rangle$ acquires a correction term proportional to γ_0^2 . As a result of the initial thermalization, the initial dot occupation depends on the spectral function $A_0(\omega) = 2\Gamma_0/[(\omega - \epsilon_0)^2 + \Gamma_0^2]$, where ϵ_0 and $\Gamma_0 = \gamma_0^2/(2v_F)$ denote the initial dot energy and tunneling rate into the lead, respectively. The initial conditions involving the undetermined function ψ_0 can be shown to follow from Eqs. (2.152), (2.153), and (2.154):

$$\langle d^\dagger(t_0) \psi_0(x) \rangle = \frac{\gamma_0}{v_F} \int \frac{d\omega}{2\pi} n_F(\omega) \frac{e^{i\omega x/v_F}}{\omega - \epsilon_0 - i\Gamma_0}, \quad (2.155)$$

as well as

$$\langle \psi_0^\dagger(x) \psi_0(y) \rangle = \frac{1}{v_F} \int \frac{d\omega}{2\pi} e^{i\omega \frac{y-x}{v_F}} n_F(\omega). \quad (2.156)$$

Thermalization thus manifests in the dot particle number and work rate as follows,

$$\begin{aligned} N^{(ii)}(t) &= e^{-2 \int_{t_0}^t dy \Gamma(y)} \int \frac{d\omega}{2\pi} A_0(\omega) n_F(\omega) \\ &\quad - i \frac{\gamma_0}{v_F} \sqrt{2v_F} e^{\int_{t_0}^t dy (i\epsilon(y) - \Gamma(y))} \int \frac{d\omega}{2\pi} \frac{e^{-i\omega(t-t_0)} V(t, \omega)}{\omega - \epsilon_0 - i\Gamma_0} n_F(\omega) \\ &\quad + i \frac{\gamma_0}{v_F} \sqrt{2v_F} e^{\int_{t_0}^t dy (-i\epsilon(y) - \Gamma(y))} \int \frac{d\omega}{2\pi} \frac{e^{i\omega(t-t_0)} V^*(t, \omega)}{\omega - \epsilon_0 + i\Gamma_0} n_F(\omega) \\ &\quad + \int \frac{d\omega}{2\pi} A(t, \omega) n_F(\omega), \\ \dot{W}^{(ii)}(t) &= \partial_t \epsilon(t) N(t) + 4\partial_t \sqrt{\Gamma(t)} \int \frac{d\omega}{2\pi} n_F(\omega) \text{Im} V(t, \omega) \\ &\quad + 2\partial_t \gamma(t) \frac{\gamma_0}{v_F} \text{Re} \left[e^{\int_{t_0}^t dy [i\epsilon(y) - \Gamma(y)]} \int \frac{d\omega}{2\pi} n_F(\omega) \frac{e^{-i\omega(t-t_0)}}{\omega - \epsilon_0 - i\Gamma_0} \right]. \end{aligned} \quad (2.157)$$

As in the findings (2.150) for setup (i), we see that the effect of the initial thermalization of the composite system on the local quantities $N^{(ii)}$ and $\dot{W}^{(ii)}$ consists of transient contributions only: In the limit of $t_0 = -\infty$, the signatures of the respective initial states vanish. The situation is different for the lead correlator, which fulfills

$$\begin{aligned} C_{xy}(t) &= \langle \psi_0^\dagger(x - v_F(t - t_0)) \psi_0(y - v_F(t - t_0)) \rangle \\ &\quad + \frac{i\gamma(\tilde{t}_x)}{v_F} \theta(x) \langle d^\dagger(\tilde{t}_x) \psi(y - x, \tilde{t}_x) \rangle - \frac{i\gamma(\tilde{t}_y)}{v_F} \theta(y) \langle \psi^\dagger(x - y, \tilde{t}_y) d(\tilde{t}_y) \rangle \end{aligned} \quad (2.158)$$

at all times t . In particular, for any $t > t_0$, we can consider sites $x, y > v_F(t - t_0)$, recalling that we took the limit of infinite lead length. For this choice, the retarded times \tilde{t}_x and \tilde{t}_y lie further in the past than t_0 . Hence $C_{xy}^{(ii)}(t)$ is given by the thermal correlator defined by the initial conditions in Eqs. (2.153) and (2.154): The sites x and y lie outside of the light cone defined by the Fermi velocity of the lead and no information about the drive protocol has yet reached them at time t . This implies that for any time t , the thermal correlations of the initial state are manifest in a non-transient manner in the lead. Inside this light cone, the lead correlator is influenced by the drive, as described by

$$\begin{aligned}
C_{xy}^{(ii)}(t) = & \int \frac{d\omega}{2\pi} n_F(\omega) \left\{ \frac{1}{v_F} e^{i\omega \frac{y-x}{v_F}} \right. \\
& + i \frac{\gamma_0}{v_F} \frac{\gamma(\tilde{t}_x)}{v_F} \theta(x) e^{\int_0^{\tilde{t}_x} dz (i\epsilon(z) - \Gamma(z))} \frac{e^{i\omega(y/v_F - (t-t_0))}}{\omega - \epsilon_0 - i\Gamma_0} \\
& - \sqrt{\frac{2}{v_F}} \frac{\gamma(\tilde{t}_x)}{v_F} \theta(x) V^*(\tilde{t}_x, \omega) e^{i\omega \frac{y-x}{v_F}} \\
& - i \frac{\gamma_0}{v_F} \frac{\gamma(\tilde{t}_y)}{v_F} \theta(y) e^{\int_0^{\tilde{t}_y} dz (-i\epsilon(z) - \Gamma(z))} \frac{e^{-i\omega(y/v_F - (t-t_0))}}{\omega - \epsilon_0 + i\Gamma_0} \\
& - \sqrt{\frac{2}{v_F}} \frac{\gamma(\tilde{t}_y)}{v_F} \theta(y) V(\tilde{t}_y, \omega) e^{i\omega \frac{y-x}{v_F}} \\
& + \frac{\gamma(\tilde{t}_x)\gamma(\tilde{t}_y)}{v_F^2} \theta(x)\theta(y) e^{\int_0^{\tilde{t}_x} dz (i\epsilon(z) - \Gamma(z))} e^{\int_0^{\tilde{t}_y} dz (-i\epsilon(z) - \Gamma(z))} A_0(\omega) \\
& - i \sqrt{\frac{2}{v_F}} \frac{\gamma_0}{v_F} \frac{\gamma(\tilde{t}_x)\gamma(\tilde{t}_y)}{v_F^2} \theta(x)\theta(y) e^{\int_0^{\tilde{t}_x} dz (i\epsilon(z) - \Gamma(z))} V(\tilde{t}_y, \omega) \frac{e^{i\omega(y/v_F - (t-t_0))}}{\omega - \epsilon_0 - i\Gamma_0} \\
& + i \sqrt{\frac{2}{v_F}} \frac{\gamma_0}{v_F} \frac{\gamma(\tilde{t}_x)\gamma(\tilde{t}_y)}{v_F^2} \theta(x)\theta(y) e^{\int_0^{\tilde{t}_y} dz (-i\epsilon(z) - \Gamma(z))} V^*(\tilde{t}_x, \omega) \frac{e^{-i\omega(x/v_F - (t-t_0))}}{\omega - \epsilon_0 + i\Gamma_0} \\
& \left. + 2 \frac{\gamma(\tilde{t}_x)\gamma(\tilde{t}_y)}{v_F^2} \theta(x)\theta(y) V^*(\tilde{t}_x, \omega) V(\tilde{t}_y, \omega) e^{i\omega \frac{y-x}{v_F}} \right\}. \tag{2.159}
\end{aligned}$$

Chapter 3

Summary

Nonequilibrium quantum transport is a vast and rapidly evolving field. The work presented in this thesis has approached the topic from multiple directions, studying electromechanical interaction, quantum pumping and quantum thermodynamics. These approaches, connected by the quest to understand the effects of periodic driving on transport, have uncovered several new results:

First, in Sec. 2.1, a model for a quantum dot with strong electromechanical interaction was examined, coupled to a pair of leads and with a time-dependent drive controlling the dot energy. Without the drive, such a system is characterized by an exponential suppression of conductance due to electron-vibron interaction. By applying the nonequilibrium Green's function (NEGF) formalism in conjunction with the polaron tunneling approximation, it was shown that this suppression of transport can be exponentially lifted by applying a resonant drive to the dot energy. Thus, a DC current amplification may be achieved by applying an AC signal to the quantum dot. These results are in agreement with the outcome a Born-Markov analysis of the system.

Second, in Sec. 2.2, the same system was studied under the influence of a multi-drive protocol, introducing a time dependence in both the dot energy and in the coupling to the leads. The NEGF approach was combined with a Floquet expansion to study charge transport through the dot under the influence of a general drive in the absence of bias, leading to the discovery of a protocol that can pump a charge current in either direction, which also enjoys the exponential lifting effect documented in Sec. 2.1.

Third, in Sec. 2.3, a proposal for quantum thermodynamics was given for the resonant-level model of a quantum dot, allowing for strong system-bath coupling and driven system energy as well as driven coupling. The NEGF formalism is used to obtain an analytical solution of the system dynamics for arbitrary driving speeds, which is then used to define the notions of system energy, heat, work and entropy. In doing so, the quantities are split into system and bath components in such a way that they agree with the outcome of an approach using a potential of mean force. The system quantities are shown to fulfill the first law of thermodynamics

as a result of energy conservation, and the second law for rates in quasi-adiabatic expansion.

Finally, in Sec. 2.4, the influence of the initial state on quantum thermodynamics was studied, again using the resonant-level model as a template. After solving the equations of motion in the presence of an arbitrary driving protocol, thermodynamic quantities are established for both a factorized and a thermalized initial state of dot and lead. For a thermal initial state, the theory of stochastic thermodynamics applies, which guarantees the positivity of the mechanical work performed by a periodic drive, in accordance with the second law of thermodynamics. By comparing the analytical expressions for the work production in the resonant-level model, it was proven that this property is also exhibited by the asymptotics of a system that starts out in a factorized state and thus is never in a thermal state. Furthermore, the asymptotic properties of the dot are shown not to depend on the initial state, whereas on the other hand the correlators in the lead carry may non-transient signatures of the initial state, thus quantifying the non-equivalence of the two setups.

The results documented here show that the interplay of drive and nanoelectromechanics holds rich possibilities for further investigation and applications: By implementing the drive mechanism, for example via gate voltages in carbon nanotube quantum dots, it could be examined how the lifting of Franck-Condon blockade can be used in practice. Furthermore, our findings are not limited to carbon nanotubes, but also apply to other quantum dot architectures featuring strong electromechanical coupling. Different simulation techniques may be used to study systems beyond the paradigmatic models considered in this thesis, such as multi-dot architectures or molecular quantum dots with a complex vibrational spectrum. Work along these lines may help to identify those setups where the current response is strongest and examine the possibility of AC-gated transistors. Lastly, it would be worthwhile to consider analogous systems in the context of optomechanics and cavity quantum electrodynamics, which also involve photon degrees of freedom, opening up further further possibilities, such as the design of high-precision sensors.

An all-encompassing theory of nonequilibrium quantum thermodynamics is still far off at this point, with several issues requiring further conceptual development. The incremental progress achieved in this thesis serves to consolidate some of the approaches, by using tools from transport theory to establish the laws of thermodynamics in a model system, as well as using synergies between this approach and stochastic thermodynamics to study the long-time limit in quantum thermodynamics. This regime offers insight into questions of thermalization and could serve to establish a degree of universality among initial configurations of a system. The full thermodynamic significance of the initial state is yet to be mapped out, especially with regard to entanglement and long-range correlation in the initial configurations. Evidently, the resonant-level model offers an accessible platform to examine these questions without having to tackle the extraneous complexity inherent in other models and it is consequently far from outliving its usefulness: Bath correlators of the type studied in Sec. 2.4 can be used to obtain further quantita-

tive insight into possible nonequilibrium analogues of thermalization, and may also be used to study various definitions of entropy, with the possibility of easy comparisons with the notion of “system entropy” from Sec. 2.3. The resonant-level model furthermore holds potential for generalization: Once the thermodynamics of a single level are understood, the question of an extension to multiple levels arises naturally. Aside from the obvious appeal of describing larger systems, such an extension would also allow to use a reaction-coordinate approach for the treatment of strongly coupled dots. In a similar vein, a way to explicitly account for many-body interaction is sure to be a goal of future research.

Bibliography

- [1] M. Planck, “Zur Theorie der Wärmestrahlung,” *Annalen der Physik*, vol. 336, no. 4, pp. 758–768, 1910.
- [2] J. Park, A. N. Pasupathy, J. I. Goldsmith, C. Chang, *et al.*, “Coulomb blockade and the Kondo effect in single-atom transistors,” *Nature*, vol. 417, no. 6890, p. 722, 2002.
- [3] S. Carnot, “Réflexions sur la puissance motrice du feu et sur les machines propres à développer cette puissance,” *Annales scientifiques de l’Ecole normale*, 1872.
- [4] C. E. Shannon, “Communication theory of secrecy systems,” *Bell system technical journal*, vol. 28, no. 4, pp. 656–715, 1949.
- [5] R. Landauer, “Irreversibility and heat generation in the computing process,” *IBM journal of research and development*, vol. 5, no. 3, pp. 183–191, 1961.
- [6] J. Lin, “Divergence measures based on the Shannon entropy,” *IEEE Transactions on Information theory*, vol. 37, no. 1, pp. 145–151, 1991.
- [7] T. J. Seebeck, *Magnetische Polarisation der Metalle und Erze durch Temperatur-Differenz*. No. 70, W. Engelmann, 1895.
- [8] J. E. Geusic, E. O. Schulz-DuBios, and H. E. D. Scovil, “Quantum equivalent of the Carnot cycle,” *Phys. Rev.*, vol. 156, pp. 343–351, Apr 1967.
- [9] R. Alicki, “The quantum open system as a model of the heat engine,” *Journal of Physics A: Mathematical and General*, vol. 12, no. 5, p. L103, 1979.
- [10] Y. Shirasaki, G. J. Supran, M. G. Bawendi, and V. Bulović, “Emergence of colloidal quantum-dot light-emitting technologies,” *Nature Photonics*, vol. 7, no. 1, p. 13, 2013.
- [11] X. Michalet, F. Pinaud, L. Bentolila, J. Tsay, S. Doose, J. Li, G. Sundaresan, A. Wu, S. Gambhir, and S. Weiss, “Quantum dots for live cells, in vivo imaging, and diagnostics,” *Science*, vol. 307, no. 5709, pp. 538–544, 2005.

- [12] D. Loss and D. P. DiVincenzo, “Quantum computation with quantum dots,” *Phys. Rev. A*, vol. 57, pp. 120–126, Jan 1998.
- [13] S. W. Koch *et al.*, *Semiconductor quantum dots*, vol. 2. World Scientific, 1993.
- [14] A. P. Alivisatos, “Semiconductor clusters, nanocrystals, and quantum dots,” *Science*, vol. 271, no. 5251, pp. 933–937, 1996.
- [15] J. M. Thijssen and H. S. J. Van der Zant, “Charge transport and single-electron effects in nanoscale systems,” *physica status solidi (b)*, vol. 245, no. 8, pp. 1455–1470, 2008.
- [16] S. Datta, *Quantum transport: atom to transistor*. Cambridge university press, 2005.
- [17] C. W. J. Beenakker, “Theory of Coulomb-blockade oscillations in the conductance of a quantum dot,” *Phys. Rev. B*, vol. 44, pp. 1646–1656, Jul 1991.
- [18] H. Grabert and M. H. Devoret, *Single charge tunneling: Coulomb blockade phenomena in nanostructures*, vol. 294. Springer Science & Business Media, 2013.
- [19] Y. Alhassid, “The statistical theory of quantum dots,” *Rev. Mod. Phys.*, vol. 72, pp. 895–968, Oct 2000.
- [20] J. Koch, F. von Oppen, Y. Oreg, and E. Sela, “Thermopower of single-molecule devices,” *Phys. Rev. B*, vol. 70, p. 195107, Nov 2004.
- [21] J. Koch and F. von Oppen, “Franck-Condon blockade and giant Fano factors in transport through single molecules,” *Phys. Rev. Lett.*, vol. 94, p. 206804, May 2005.
- [22] A. Pasupathy, J. Park, C. Chang, A. Soldatov, S. Lebedkin, R. Bialczak, J. Grose, L. Donev, J. Sethna, D. Ralph, *et al.*, “Vibration-assisted electron tunneling in C140 transistors,” *Nano Letters*, vol. 5, no. 2, pp. 203–207, 2005.
- [23] J. Koch, F. von Oppen, and A. V. Andreev, “Theory of the Franck-Condon blockade regime,” *Phys. Rev. B*, vol. 74, p. 205438, Nov 2006.
- [24] S. Ilani and P. L. McEuen, “Electron transport in carbon nanotubes,” *Annual Review of Condensed Matter Physics*, vol. 1, no. 1, pp. 1–25, 2010.
- [25] E. A. Laird, F. Kuemmeth, G. A. Steele, K. Grove-Rasmussen, J. Nygård, K. Flensberg, and L. P. Kouwenhoven, “Quantum transport in carbon nanotubes,” *Rev. Mod. Phys.*, vol. 87, pp. 703–764, Jul 2015.

- [26] A. Benyamini, A. Hamo, S. V. Kusminskiy, F. von Oppen, and S. Ilani, “Real-space tailoring of the electron-phonon coupling in ultraclean nanotube mechanical resonators,” *Nature Physics*, vol. 10, no. 2, pp. 151–156, 2014.
- [27] H. G. Craighead, “Nanoelectromechanical systems,” *Science*, vol. 290, no. 5496, pp. 1532–1535, 2000.
- [28] C. S. Lau, H. Sadeghi, G. Rogers, S. Sangtarash, P. Dallas, K. Porfyrakis, J. Warner, C. J. Lambert, G. A. D. Briggs, and J. A. Mol, “Redox-dependent Franck-Condon blockade and avalanche transport in a graphene-fullerene single-molecule transistor,” *Nano letters*, vol. 16, no. 1, pp. 170–176, 2015.
- [29] E. Burzuri, Y. Yamamoto, M. Warnock, X. Zhong, K. Park, A. Cornia, and H. S. J. van der Zant, “Franck-Condon blockade in a single-molecule transistor,” *Nano Letters*, vol. 14, no. 6, pp. 3191–3196, 2014.
- [30] R. Leturcq, C. Stampfer, K. Inderbitzin, L. Durrer, C. Hierold, E. Mariani, M. G. Schultz, F. von Oppen, and K. Ensslin, “Franck-Condon blockade in suspended carbon nanotube quantum dots,” *Nature Physics*, vol. 5, no. 5, pp. 327–331, 2009.
- [31] K. Flensberg, “Electron-vibron coupling in suspended nanotubes,” *New Journal of Physics*, vol. 8, no. 1, p. 5, 2006.
- [32] W. Izumida and M. Grifoni, “Phonon-assisted tunnelling in interacting suspended single-wall carbon nanotubes,” *New Journal of Physics*, vol. 7, no. 1, p. 244, 2005.
- [33] E. Mariani and F. von Oppen, “Electron-vibron coupling in suspended carbon nanotube quantum dots,” *Phys. Rev. B*, vol. 80, p. 155411, Oct 2009.
- [34] R.-P. Riwar and T. L. Schmidt, “Transient dynamics of a molecular quantum dot with a vibrational degree of freedom,” *Phys. Rev. B*, vol. 80, p. 125109, 2009.
- [35] S. Maier, T. L. Schmidt, and A. Komnik, “Charge transfer statistics of a molecular quantum dot with strong electron-phonon interaction,” *Phys. Rev. B*, vol. 83, p. 085401, Feb 2011.
- [36] M. Esposito, R. Kawai, K. Lindenberg, and C. Van den Broeck, “Efficiency at maximum power of low-dissipation Carnot engines,” *Phys. Rev. Lett.*, vol. 105, p. 150603, Oct 2010.
- [37] M. Josefsson, A. Svilans, A. M. Burke, E. A. Hoffmann, S. Fahlvik, C. Thelander, M. Leijnse, and H. Linke, “A quantum-dot heat engine operating close to the thermodynamic efficiency limits,” *Nature Nanotechnology*, 2018.

- [38] A. V. Feshchenko, J. V. Koski, and J. P. Pekola, “Experimental realization of a Coulomb blockade refrigerator,” *Phys. Rev. B*, vol. 90, p. 201407, Nov 2014.
- [39] A. Svilans, M. Leijnse, and H. Linke, “Experiments on the thermoelectric properties of quantum dots,” *Comptes Rendus Physique*, vol. 17, no. 10, pp. 1096–1108, 2016.
- [40] H. Bruus and K. Flensberg, *Many-body quantum theory in condensed matter physics: an introduction*. Oxford University Press, 2004.
- [41] L. V. Keldysh *et al.*, “Diagram technique for nonequilibrium processes,” *Sov. Phys. JETP*, vol. 20, no. 4, pp. 1018–1026, 1965.
- [42] P. I. Arseev, “On the nonequilibrium diagram technique: derivation, some features, and applications,” *Physics-Uspexhi*, vol. 58, no. 12, p. 1159, 2015.
- [43] J. Rammer, *Quantum field theory of non-equilibrium states*. Cambridge University Press, 2007.
- [44] H. Haug and A.-P. Jauho, *Quantum kinetics in transport and optics of semi-conductors*, vol. 2. Springer, 2008.
- [45] G. D. Mahan, *Many-particle physics*. Springer Science & Business Media, 2013.
- [46] D. C. Langreth and P. Nordlander, “Derivation of a master equation for charge-transfer processes in atom-surface collisions,” *Phys. Rev. B*, vol. 43, pp. 2541–2557, Feb 1991.
- [47] A.-P. Jauho, N. S. Wingreen, and Y. Meir, “Time-dependent transport in interacting and noninteracting resonant-tunneling systems,” *Phys. Rev. B*, vol. 50, pp. 5528–5544, Aug 1994.
- [48] Y. Meir and N. S. Wingreen, “Landauer formula for the current through an interacting electron region,” *Phys. Rev. Lett.*, vol. 68, pp. 2512–2515, Apr 1992.
- [49] C. Verzijl, J. Seldenthuis, and J. Thijssen, “Applicability of the wide-band limit in DFT-based molecular transport calculations,” *The Journal of chemical physics*, vol. 138, no. 9, p. 094102, 2013.
- [50] T. Dittrich, P. Hänggi, G.-L. Ingold, B. Kramer, G. Schön, and W. Zwerger, *Quantum transport and dissipation*, vol. 3. Wiley-Vch Weinheim, 1998.
- [51] M. Grifoni and P. Hänggi, “Driven quantum tunneling,” *Physics Reports*, vol. 304, no. 5-6, pp. 229–354, 1998.

- [52] N. Goldman and J. Dalibard, “Periodically driven quantum systems: Effective hamiltonians and engineered gauge fields,” *Phys. Rev. X*, vol. 4, p. 031027, Aug 2014.
- [53] G. Floquet, “Sur les equations differentielles lineaires,” *Ann. ENS [2]*, vol. 12, no. 1883, pp. 47–88, 1883.
- [54] G. Teschl, *Ordinary differential equations and dynamical systems*, vol. 140. American Mathematical Soc., 2012.
- [55] N. Tsuji, T. Oka, and H. Aoki, “Correlated electron systems periodically driven out of equilibrium: Floquet + DMFT formalism,” *Phys. Rev. B*, vol. 78, p. 235124, Dec 2008.
- [56] A. Rivas and S. F. Huelga, *Open Quantum Systems*. Springer, 2012.
- [57] H.-P. Breuer and F. Petruccione, *The theory of open quantum systems*. Oxford University Press, 2002.
- [58] G. Schaller, *Open quantum systems far from equilibrium*, vol. 881. Springer, 2014.
- [59] G. Lindblad, “On the generators of quantum dynamical semigroups,” *Comm. Math. Phys.*, vol. 48, no. 2, pp. 119–130, 1976.
- [60] W.-M. Zhang, P.-Y. Lo, H.-N. Xiong, M. W.-Y. Tu, and F. Nori, “General non-Markovian dynamics of open quantum systems,” *Phys. Rev. Lett.*, vol. 109, p. 170402, Oct 2012.
- [61] A. Rivas, S. F. Huelga, and M. B. Plenio, “Quantum non-Markovianity: characterization, quantification and detection,” *Reports on Progress in Physics*, vol. 77, no. 9, p. 094001, 2014.
- [62] L. Li, M. J. Hall, and H. M. Wiseman, “Concepts of quantum non-markovianity: A hierarchy,” *Physics Reports*, 2018.
- [63] D. M. Carberry, J. C. Reid, G. M. Wang, E. M. Sevick, D. J. Searles, and D. J. Evans, “Fluctuations and irreversibility: An experimental demonstration of a second-law-like theorem using a colloidal particle held in an optical trap,” *Phys. Rev. Lett.*, vol. 92, p. 140601, Apr 2004.
- [64] V. Blickle, T. Speck, L. Helden, U. Seifert, and C. Bechinger, “Thermodynamics of a colloidal particle in a time-dependent nonharmonic potential,” *Phys. Rev. Lett.*, vol. 96, p. 070603, Feb 2006.
- [65] J. V. Koski, V. F. Maisi, J. P. Pekola, and D. V. Averin, “Experimental realization of a szilard engine with a single electron,” *Proceedings of the National Academy of Sciences*, vol. 111, no. 38, pp. 13786–13789, 2014.

- [66] F. Schwabl, *Statistical Mechanics*. Springer, 2006.
- [67] H. Spohn and J. L. Lebowitz, “Irreversible thermodynamics for quantum systems weakly coupled to thermal reservoirs,” *Adv. Chem. Phys.*, vol. 38, pp. 109–142, 1978.
- [68] H. Spohn, “Entropy production for quantum dynamical semigroups,” *Journal of Mathematical Physics*, vol. 19, no. 5, pp. 1227–1230, 1978.
- [69] R. Kosloff, “Quantum thermodynamics: A dynamical viewpoint,” *Entropy*, vol. 15, no. 6, pp. 2100–2128, 2013.
- [70] C. Jarzynski, “Nonequilibrium equality for free energy differences,” *Phys. Rev. Lett.*, vol. 78, pp. 2690–2693, Apr 1997.
- [71] C. B. P. Finn, *Thermal Physics*. Chapman & Hall, 1993.
- [72] G. E. Crooks, “Entropy production fluctuation theorem and the nonequilibrium work relation for free energy differences,” *Phys. Rev. E*, vol. 60, pp. 2721–2726, Sep 1999.
- [73] M. Esposito, U. Harbola, and S. Mukamel, “Nonequilibrium fluctuations, fluctuation theorems, and counting statistics in quantum systems,” *Rev. Mod. Phys.*, vol. 81, pp. 1665–1702, Dec 2009.
- [74] M. Campisi, P. Hänggi, and P. Talkner, “Quantum fluctuation relations: Foundations and applications,” *Rev. Mod. Phys.*, vol. 83, pp. 771–791, Jul 2011.
- [75] U. Seifert, “Stochastic thermodynamics, fluctuation theorems and molecular machines,” *Reports on Progress in Physics*, vol. 75, no. 12, p. 126001, 2012.
- [76] G. Watanabe, B. P. Venkatesh, P. Talkner, M. Campisi, and P. Hänggi, “Quantum fluctuation theorems and generalized measurements during the force protocol,” *Phys. Rev. E*, vol. 89, p. 032114, Mar 2014.
- [77] J. Åberg, “Fully quantum fluctuation theorems,” *Phys. Rev. X*, vol. 8, p. 011019, Feb 2018.
- [78] H. Tasaki, “Jarzynski relations for quantum systems and some applications,” *arXiv preprint cond-mat/0009244*, 2000.
- [79] J. Kurchan, “A quantum fluctuation theorem,” *arXiv preprint cond-mat/0007360*, 2000.
- [80] P. Talkner, E. Lutz, and P. Hänggi, “Fluctuation theorems: Work is not an observable,” *Phys. Rev. E*, vol. 75, p. 050102, May 2007.
- [81] P. Talkner and P. Hänggi, “Open system trajectories specify fluctuating work but not heat,” *Physical Review E*, vol. 94, no. 2, p. 022143, 2016.

- [82] P. Talkner and P. Hänggi, “Aspects of quantum work,” *Phys. Rev. E*, vol. 93, p. 022131, Feb 2016.
- [83] P. Talkner, P. Hänggi, and M. Morillo, “Microcanonical quantum fluctuation theorems,” *Phys. Rev. E*, vol. 77, p. 051131, May 2008.
- [84] P. Talkner and P. Hänggi, “The Tasaki-Crooks quantum fluctuation theorem,” *Journal of Physics A: Mathematical and Theoretical*, vol. 40, no. 26, p. F569, 2007.
- [85] C. Jarzynski, “Nonequilibrium work theorem for a system strongly coupled to a thermal environment,” *Journal of Statistical Mechanics: Theory and Experiment*, vol. 2004, no. 09, p. P09005, 2004.
- [86] C. Jarzynski, “Stochastic and macroscopic thermodynamics of strongly coupled systems,” *Phys. Rev. X*, vol. 7, p. 011008, Jan 2017.
- [87] M. F. Gelin and M. Thoss, “Thermodynamics of a subensemble of a canonical ensemble,” *Phys. Rev. E*, vol. 79, p. 051121, May 2009.
- [88] M. Campisi, P. Talkner, and P. Hänggi, “Fluctuation theorem for arbitrary open quantum systems,” *Phys. Rev. Lett.*, vol. 102, p. 210401, May 2009.
- [89] B. Roux and T. Simonson, “Implicit solvent models,” *Biophysical chemistry*, vol. 78, no. 1-2, pp. 1–20, 1999.
- [90] U. Seifert, “First and second law of thermodynamics at strong coupling,” *Phys. Rev. Lett.*, vol. 116, p. 020601, Jan 2016.
- [91] J.-T. Hsiang and B.-L. Hu, “Quantum thermodynamics at strong coupling: Operator thermodynamic functions and relations,” *Entropy*, vol. 20, p. 423, 2018.
- [92] J. Reichert, R. Ochs, D. Beckmann, H. B. Weber, M. Mayor, and H. v. Löhneysen, “Driving current through single organic molecules,” *Phys. Rev. Lett.*, vol. 88, p. 176804, Apr 2002.
- [93] J. Park, A. N. Pasupathy, J. I. Goldsmith, C. Chang, Y. Yaish, J. R. Petta, M. Rinkoski, J. P. Sethna, H. D. Abruña, P. L. McEuen, *et al.*, “Coulomb blockade and the Kondo effect in single-atom transistors,” *Nature*, vol. 417, no. 6890, p. 722, 2002.
- [94] W. Liang, M. Shores, M. Bockrath, J. Long, and H. Park, “Kondo resonance in a single-molecule transistor,” *Nature*, vol. 417, p. 725, 2002.
- [95] N. Tao, “Electron transport in molecular junctions,” *Nature nanotechnology*, vol. 1, no. 3, pp. 173–181, 2006.

- [96] A. Wallraff, D. I. Schuster, A. Blais, L. Frunzio, R.-S. Huang, J. Majer, S. Kumar, S. M. Girvin, and R. J. Schoelkopf, “Strong coupling of a single photon to a superconducting qubit using circuit quantum electrodynamics,” *Nature*, vol. 431, no. 7005, pp. 162–167, 2004.
- [97] M. Poot and H. S. van der Zant, “Mechanical systems in the quantum regime,” *Physics Reports*, vol. 511, no. 5, pp. 273 – 335, 2012. Mechanical systems in the quantum regime.
- [98] T. Frey, P. J. Leek, M. Beck, A. Blais, T. Ihn, K. Ensslin, and A. Wallraff, “Dipole coupling of a double quantum dot to a microwave resonator,” *Phys. Rev. Lett.*, vol. 108, p. 046807, Jan 2012.
- [99] Z.-L. Xiang, S. Ashhab, J. Q. You, and F. Nori, “Hybrid quantum circuits: Superconducting circuits interacting with other quantum systems,” *Rev. Mod. Phys.*, vol. 85, pp. 623–653, Apr 2013.
- [100] A. K. Hüttel, G. A. Steele, B. Witkamp, M. Poot, L. P. Kouwenhoven, and H. S. J. van der Zant, “Carbon nanotubes as ultrahigh quality factor mechanical resonators,” *Nano Letters*, vol. 9, no. 7, pp. 2547–2552, 2009.
- [101] A. K. Hüttel, H. B. Meerwaldt, G. A. Steele, M. Poot, B. Witkamp, L. P. Kouwenhoven, and H. S. J. van der Zant, “Single electron tunnelling through high-q single-wall carbon nanotube NEMS resonators,” *physica status solidi (b)*, vol. 247, no. 11-12, pp. 2974–2979, 2010.
- [102] J. Chaste, M. Sledzinska, M. Zdrojek, J. Moser, and A. Bachtold, “High-frequency nanotube mechanical resonators,” *Applied Physics Letters*, vol. 99, no. 21, p. 213502, 2011.
- [103] S. Sapmaz, P. Jarillo-Herrero, Y. M. Blanter, C. Dekker, and H. S. J. van der Zant, “Tunneling in suspended carbon nanotubes assisted by longitudinal phonons,” *Phys. Rev. Lett.*, vol. 96, p. 026801, Jan 2006.
- [104] G. A. Steele, A. K. Hüttel, B. Witkamp, M. Poot, H. B. Meerwaldt, L. P. Kouwenhoven, and H. S. J. van der Zant, “Strong coupling between single-electron tunneling and nanomechanical motion,” *Science*, vol. 325, no. 5944, pp. 1103–1107, 2009.
- [105] B. Lassagne, Y. Tarakanov, J. Kinaret, D. Garcia-Sanchez, and A. Bachtold, “Coupling mechanics to charge transport in carbon nanotube mechanical resonators,” *Science*, vol. 325, no. 5944, pp. 1107–1110, 2009.
- [106] V. Sazonova, Y. Yaish, H. Ustunel, D. Roundy, T. A. Arias, and P. L. McEuen, “A tunable carbon nanotube electromechanical oscillator,” *Nature*, 2004.

- [107] J. Paaske and K. Flensberg, “Vibrational sidebands and the Kondo effect in molecular transistors,” *Phys. Rev. Lett.*, vol. 94, p. 176801, May 2005.
- [108] I. Lang and Y. A. Firsov, “Kinetic theory of semiconductors with low mobility,” *Sov. Phys. JETP*, vol. 16, no. 5, p. 1301, 1963.
- [109] T. L. Schmidt and A. Komnik, “Charge transfer statistics of a molecular quantum dot with a vibrational degree of freedom,” *Phys. Rev. B*, vol. 80, p. 041307, Jul 2009.
- [110] G. Tang, L. Zhang, and J. Wang, “Thermal rectification in a double quantum dots system with a polaron effect,” *Phys. Rev. B*, vol. 97, p. 224311, Jun 2018.
- [111] R. Seoane Souto, A. L. Yeyati, A. Martín-Rodero, and R. C. Monreal, “Dressed tunneling approximation for electronic transport through molecular transistors,” *Phys. Rev. B*, vol. 89, p. 085412, Feb 2014.
- [112] K. F. Albrecht, A. Martín-Rodero, R. C. Monreal, L. Mühlbacher, and A. Levy Yeyati, “Long transient dynamics in the Anderson-Holstein model out of equilibrium,” *Phys. Rev. B*, vol. 87, p. 085127, Feb 2013.
- [113] C. Timm, “Tunneling through molecules and quantum dots: Master-equation approaches,” *Phys. Rev. B*, vol. 77, p. 195416, May 2008.
- [114] T. Krause, T. Brandes, M. Esposito, and G. Schaller, “Thermodynamics of the polaron master equation at finite bias,” *The Journal of Chemical Physics*, vol. 142, no. 13, 2015.
- [115] G. Schaller, T. Krause, T. Brandes, and M. Esposito, “Single-electron transistor strongly coupled to vibrations: counting statistics and fluctuation theorem,” *New Journal of Physics*, vol. 15, no. 3, p. 033032, 2013.
- [116] M. R. Bazrafkan and M. Ashrafi, “A driven damped harmonic oscillator in the ket-vector representation of the density operator,” *Journal of Russian Laser Research*, vol. 34, no. 1, pp. 41–49, 2013.
- [117] Y.-Y. Liu, K. D. Petersson, J. Stehlik, J. M. Taylor, and J. R. Petta, “Photon emission from a cavity-coupled double quantum dot,” *Phys. Rev. Lett.*, vol. 113, p. 036801, Jul 2014.
- [118] J. J. Viennot, M. C. Dartailh, A. Cottet, and T. Kontos, “Coherent coupling of a single spin to microwave cavity photons,” *Science*, vol. 349, no. 6246, pp. 408–411, 2015.
- [119] H. Pothier, P. Lafarge, C. Urbina, D. Esteve, and M. H. Devoret, “Single-electron pump based on charging effects,” *EPL (Europhysics Letters)*, vol. 17, no. 3, p. 249, 1992.

- [120] M. Switkes, C. Marcus, K. Campman, and A. Gossard, “An adiabatic quantum electron pump,” *Science*, vol. 283, no. 5409, pp. 1905–1908, 1999.
- [121] M. V. Moskalets, *Scattering matrix approach to non-stationary quantum transport*. World Scientific, 2011.
- [122] P. San-Jose, E. Prada, S. Kohler, and H. Schomerus, “Single-parameter pumping in graphene,” *Phys. Rev. B*, vol. 84, p. 155408, Oct 2011.
- [123] L. E. F. F. Torres, H. L. Calvo, C. G. Rocha, and G. Cuniberti, “Enhancing single-parameter quantum charge pumping in carbon-based devices,” *Applied Physics Letters*, vol. 99, no. 9, p. 092102, 2011.
- [124] D. Fioretto and A. Silva, “Phase coherence, inelastic scattering, and interaction corrections in pumping through quantum dots,” *Phys. Rev. Lett.*, vol. 100, p. 236803, Jun 2008.
- [125] E. Prada, P. San-Jose, and H. Schomerus, “Quantum pumping in graphene,” *Phys. Rev. B*, vol. 80, p. 245414, Dec 2009.
- [126] L. Arrachea, A. L. Yeyati, and A. Martin-Rodero, “Nonadiabatic features of electron pumping through a quantum dot in the Kondo regime,” *Phys. Rev. B*, vol. 77, p. 165326, Apr 2008.
- [127] S. J. Wright, M. D. Blumenthal, M. Pepper, D. Anderson, G. A. C. Jones, C. A. Nicoll, and D. A. Ritchie, “Parallel quantized charge pumping,” *Phys. Rev. B*, vol. 80, p. 113303, Sep 2009.
- [128] F. Stein, D. Drung, L. Fricke, H. Scherer, F. Hohls, C. Leicht, M. Götz, C. Krause, R. Behr, E. Pesel, K. Pierz, U. Siegner, F. J. Ahlers, and H. W. Schumacher, “Validation of a quantized-current source with 0.2 ppm uncertainty,” *Applied Physics Letters*, vol. 107, no. 10, p. 103501, 2015.
- [129] M. Moskalets and M. Büttiker, “Floquet scattering theory of quantum pumps,” *Phys. Rev. B*, vol. 66, p. 205320, Nov 2002.
- [130] H.-Q. Zhou, S. Y. Cho, and R. H. McKenzie, “Gauge fields, geometric phases, and quantum adiabatic pumps,” *Phys. Rev. Lett.*, vol. 91, p. 186803, Oct 2003.
- [131] M. Moskalets and M. Büttiker, “Adiabatic quantum pump in the presence of external ac voltages,” *Phys. Rev. B*, vol. 69, p. 205316, May 2004.
- [132] M. Strass, P. Hänggi, and S. Kohler, “Nonadiabatic electron pumping: Maximal current with minimal noise,” *Phys. Rev. Lett.*, vol. 95, p. 130601, Sep 2005.

- [133] B. Kaestner and V. Kashcheyevs, “Non-adiabatic quantized charge pumping with tunable-barrier quantum dots: a review of current progress,” *Reports on Progress in Physics*, vol. 78, no. 10, p. 103901, 2015.
- [134] J. Waissman, M. Honig, S. Pecker, A. Benyamini, A. Hamo, and S. Ilani, “Realization of pristine and locally tunable one-dimensional electron systems in carbon nanotubes,” *Nature nanotechnology*, vol. 8, no. 8, pp. 569–574, 2013.
- [135] P. Haughian, S. Walter, A. Nunnenkamp, and T. L. Schmidt, “Lifting the Franck-Condon blockade in driven quantum dots,” *Phys. Rev. B*, vol. 94, p. 205412, Nov. 2016.
- [136] F. Cavaliere, M. Governale, and J. König, “Nonadiabatic pumping through interacting quantum dots,” *Phys. Rev. Lett.*, vol. 103, p. 136801, Sep 2009.
- [137] B. Wang, J. Wang, and H. Guo, “Parametric pumping at finite frequency,” *Phys. Rev. B*, vol. 65, p. 073306, Jan 2002.
- [138] J. P. Pekola, “Towards quantum thermodynamics in electronic circuits,” *Nature Physics*, vol. 11, no. 2, pp. 118–123, 2015.
- [139] J. Roßnagel, S. T. Dawkins, K. N. Tolazzi, O. Abah, E. Lutz, F. Schmidt-Kaler, and K. Singer, “A single-atom heat engine,” *Science*, vol. 352, no. 6283, pp. 325–329, 2016.
- [140] A. Argun, J. Soni, L. Dabelow, S. Bo, G. Pesce, R. Eichhorn, and G. Volpe, “Experimental realization of a minimal microscopic heat engine,” *Phys. Rev. E*, vol. 96, p. 052106, Nov 2017.
- [141] P. Hänggi, G.-L. Ingold, and P. Talkner, “Finite quantum dissipation: the challenge of obtaining specific heat,” *New Journal of Physics*, vol. 10, no. 11, p. 115008, 2008.
- [142] P. Strasberg and M. Esposito, “Stochastic thermodynamics in the strong coupling regime: An unambiguous approach based on coarse graining,” *Phys. Rev. E*, vol. 95, p. 062101, Jun 2017.
- [143] P. Strasberg, G. Schaller, T. L. Schmidt, and M. Esposito, “Fermionic reaction coordinates and their application to an autonomous Maxwell demon in the strong-coupling regime,” *Phys. Rev. B*, vol. 97, p. 205405, May 2018.
- [144] P. Gaspard, “Scattering approach to the thermodynamics of quantum transport,” *New Journal of Physics*, vol. 17, no. 4, p. 045001, 2015.
- [145] M. Campisi, P. Talkner, and P. Hänggi, “Thermodynamics and fluctuation theorems for a strongly coupled open quantum system: an exactly solvable case,” *Journal of Physics A: Mathematical and Theoretical*, vol. 42, no. 39, p. 392002, 2009.

- [146] M. Esposito, K. Lindenberg, and C. V. den Broeck, “Entropy production as correlation between system and reservoir,” *New Journal of Physics*, vol. 12, no. 1, p. 013013, 2010.
- [147] A. Kato and Y. Tanimura, “Quantum heat current under non-perturbative and non-Markovian conditions: Applications to heat machines,” *The Journal of Chemical Physics*, vol. 145, no. 22, p. 224105, 2016.
- [148] P. Strasberg, G. Schaller, N. Lambert, and T. Brandes, “Nonequilibrium thermodynamics in the strong coupling and non-Markovian regime based on a reaction coordinate mapping,” *New Journal of Physics*, vol. 18, no. 7, p. 073007, 2016.
- [149] D. Xu, C. Wang, Y. Zhao, and J. Cao, “Polaron effects on the performance of light-harvesting systems: a quantum heat engine perspective,” *New Journal of Physics*, vol. 18, no. 2, p. 023003, 2016.
- [150] G. Katz and R. Kosloff, “Quantum thermodynamics in strong coupling: heat transport and refrigeration,” *Entropy*, vol. 18, no. 5, p. 186, 2016.
- [151] G. B. Cuetara, A. Engel, and M. Esposito, “Stochastic thermodynamics of rapidly driven systems,” *New Journal of Physics*, vol. 17, no. 5, p. 055002, 2015.
- [152] T. Kita, “Introduction to nonequilibrium statistical mechanics with quantum field theory,” *Progress of Theoretical Physics*, vol. 123, no. 4, pp. 581–658, 2010.
- [153] J. Keeling, A. V. Shytov, and L. S. Levitov, “Coherent particle transfer in an on-demand single-electron source,” *Phys. Rev. Lett.*, vol. 101, p. 196404, Nov. 2008.
- [154] T. L. Schmidt, P. Werner, L. Mühlbacher, and A. Komnik, “Transient dynamics of the Anderson impurity model out of equilibrium,” *Phys. Rev. B*, vol. 78, p. 235110, 2008.
- [155] P. Haughian, H. H. Yap, J. Gong, and T. L. Schmidt, “Charge pumping in strongly coupled molecular quantum dots,” *Phys. Rev. B*, vol. 96, p. 195432, Nov 2017.
- [156] M. F. Ludovico, J. S. Lim, M. Moskalets, L. Arrachea, and D. Sánchez, “Dynamical energy transfer in ac-driven quantum systems,” *Phys. Rev. B*, vol. 89, p. 161306, Apr 2014.
- [157] M. Esposito, M. A. Ochoa, and M. Galperin, “Nature of heat in strongly coupled open quantum systems,” *Phys. Rev. B*, vol. 92, p. 235440, Dec 2015.

- [158] M. Esposito, M. A. Ochoa, and M. Galperin, “Quantum thermodynamics: A nonequilibrium Green’s function approach,” *Phys. Rev. Lett.*, vol. 114, p. 080602, Feb 2015.
- [159] M. F. Ludovico, F. Battista, F. von Oppen, and L. Arrachea, “Adiabatic response and quantum thermoelectrics for ac-driven quantum systems,” *Phys. Rev. B*, vol. 93, p. 075136, Feb 2016.
- [160] A. Bruch, M. Thomas, S. V. Kusminskiy, F. von Oppen, and A. Nitzan, “Quantum thermodynamics of the driven resonant level model,” *Physical Review B*, vol. 93, no. 11, p. 115318, 2016.
- [161] M. A. Ochoa, A. Bruch, and A. Nitzan, “Energy distribution and local fluctuations in strongly coupled open quantum systems: The extended resonant level model,” *Phys. Rev. B*, vol. 94, p. 035420, Jul 2016.
- [162] M. F. Ludovico, M. Moskalets, D. Sánchez, and L. Arrachea, “Dynamics of energy transport and entropy production in ac-driven quantum electron systems,” *Phys. Rev. B*, vol. 94, p. 035436, Jul 2016.
- [163] M. F. Ludovico, L. Arrachea, M. Moskalets, and D. Sánchez, “Periodic energy transport and entropy production in quantum electronics,” *Entropy*, vol. 18, no. 11, 2016.
- [164] A. Bruch, C. Lewenkopf, and F. von Oppen, “Landauer-Büttiker approach to strongly coupled quantum thermodynamics: inside-outside duality of entropy evolution,” *Phys. Rev. Lett.*, vol. 120, p. 107701, Mar 2018.
- [165] B. Dutta, J. T. Peltonen, D. S. Antonenko, M. Meschke, M. A. Skvortsov, B. Kubala, J. König, C. B. Winkelmann, H. Courtois, and J. P. Pekola, “Thermal conductance of a single-electron transistor,” *Phys. Rev. Lett.*, vol. 119, p. 077701, Aug 2017.
- [166] G. Wei, K.-T. Shiu, N. C. Giebink, and S. R. Forrest, “Thermodynamic limits of quantum photovoltaic cell efficiency,” *Applied Physics Letters*, vol. 91, no. 22, p. 223507, 2007.
- [167] J. M. Horowitz and M. Esposito, “Thermodynamics with continuous information flow,” *Phys. Rev. X*, vol. 4, p. 031015, Jul 2014.
- [168] R. Rao and M. Esposito, “Nonequilibrium thermodynamics of chemical reaction networks: Wisdom from stochastic thermodynamics,” *Phys. Rev. X*, vol. 6, p. 041064, Dec 2016.
- [169] P. Haughian, M. Esposito, and T. L. Schmidt, “Quantum thermodynamics of the resonant-level model with driven system-bath coupling,” *Phys. Rev. B*, vol. 97, p. 085435, Feb 2018.

- [170] F. Brandão, M. Horodecki, N. Ng, J. Oppenheim, and S. Wehner, “The second laws of quantum thermodynamics,” *Proceedings of the National Academy of Sciences*, vol. 112, no. 11, pp. 3275–3279, 2015.
- [171] A. Bruch, C. Lewenkopf, and F. von Oppen, “Landauer-Büttiker approach to strongly coupled quantum thermodynamics: Inside-outside duality of entropy evolution,” *Phys. Rev. Lett.*, vol. 120, p. 107701, Mar 2018.

Acknowledgments

Science is a collaborative endeavor, and many together may achieve what is outside of the reach of the individual. Even though only my name appears on the cover of this thesis, the work documented here would not have been possible without the efforts of my colleagues and co-authors. In particular, I am indebted to my advisor, Prof. Thomas Schmidt, for more than three years of scientific guidance, encouragement and patience. During my time in Luxembourg, I had the pleasure of working with a bunch of talented, helpful, and entertaining colleagues: Many thanks to Alexia, Chris, Edvin, Giacomo, Hugo, Johan, Kristof, and Solofo from my group, and others from all around the department. Furthermore, I am grateful for the hospitality of Prof. Jiangbin Gong in Singapore and his group, who took me in for half a year, leading to a successful collaboration and nice memories. I also thank the members of my thesis committee for the advice and criticism that helped my work move forward. Thanks also go to my mom for trusting and encouraging me in all of my plans, even though these led me to visit home less often than I wanted to. Finally, thanks to Jing for her company during the last two years. I could not have wished for someone better to share the joys and struggles of academia with me.

List of publications

1. P. Haughian, S. Walter, A. Nunnenkamp, and T. L. Schmidt, “Lifting the Franck-Condon blockade in driven quantum dots,” *Phys. Rev. B*, vol. 94, p. 205412, Nov 2016
2. P. Haughian, H. H. Yap, J. Gong, and T. L. Schmidt, “Charge pumping in strongly coupled molecular quantum dots,” *Phys. Rev. B*, vol. 96, p. 195432, Nov 2017
3. P. Haughian, M. Esposito, and T. L. Schmidt, “Quantum thermodynamics of the resonant-level model with driven system-bath coupling,” *Phys. Rev. B*, vol. 97, p. 085435, Feb 2018